OPEN ACCESS

Original research

Neutrophils prevent rectal bleeding in ulcerative colitis by peptidyl-arginine deiminase-4-dependent immunothrombosis

Moritz Leppkes ,[1,2] Aylin Lindemann,[1] Stefanie Gößwein,[1] Susanne Paulus,[1] Dominik Roth,[1] Anne Hartung,[1] Eva Liebing,[1] Sebastian Zundler ,[1,2] Miguel Gonzalez-Acera,[1] Jay V Patankar,[1] Fabrizio Mascia,[1] Kristina Scheibe,[1] Markus Hoffmann,[3] Stefan Uderhardt,[2,3] Christine Schauer,[3] Sebastian Foersch,[4] Clemens Neufert ,[1,2] Michael Vieth,[5] Georg Schett,[2,3] Raja Atreya,[1,2] Anja A Kühl,[6] Andre Bleich,[7] Christoph Becker ,[1] Martin Herrmann,[3] Markus F Neurath [1,2]

► Additional supplemental material is published online only. To view, please visit the journal online (http://dx.doi.org/10.1136/gutjnl-2021-324725).

For numbered affiliations see end of article.

Correspondence to
Dr Moritz Leppkes, Department of Medicine 1, University Clinic, Friedrich-Alexander-University Erlangen-Nuremberg, Erlangen, Germany;
moritz.leppkes@uk-erlangen.de

ML and AL are joint first authors.

Received 22 March 2021
Accepted 2 November 2021
Published Online First
3 December 2021

Linked

► http://dx.doi.org/10.1136/gutjnl-2021-326484

Check for updates

To cite: Leppkes M, Lindemann A, Gößwein S, *et al*. *Gut* 2022;**71**:2414–2429.

ABSTRACT

Objective Bleeding ulcers and erosions are hallmarks of active ulcerative colitis (UC). However, the mechanisms controlling bleeding and mucosal haemostasis remain elusive.

Design We used high-resolution endoscopy and colon tissue samples of active UC (n = 36) as well as experimental models of physical and chemical mucosal damage in mice deficient for peptidyl-arginine deiminase-4 (PAD4), gnotobiotic mice and controls. We employed endoscopy, histochemistry, live-cell microscopy and flow cytometry to study eroded mucosal surfaces during mucosal haemostasis.

Results Erosions and ulcerations in UC were covered by fresh blood, haematin or fibrin visible by endoscopy. Fibrin layers rather than fresh blood or haematin on erosions were inversely correlated with rectal bleeding in UC. Fibrin layers contained ample amounts of neutrophils coaggregated with neutrophil extracellular traps (NETs) with detectable activity of PAD. Transcriptome analyses showed significantly elevated *PAD4* expression in active UC. In experimentally inflicted wounds, we found that neutrophils underwent NET formation in a PAD4-dependent manner hours after formation of primary blood clots, and remodelled clots to immunothrombi containing citrullinated histones, even in the absence of microbiota. PAD4-deficient mice experienced an exacerbated course of dextrane sodium sulfate-induced colitis with markedly increased rectal bleeding (96 % vs 10 %) as compared with controls. PAD4-deficient mice failed to remodel blood clots on mucosal wounds eliciting impaired healing. Thus, NET-associated immunothrombi are protective in acute colitis, while insufficient immunothrombosis is associated with rectal bleeding.

Conclusion Our findings uncover that neutrophils induce secondary immunothrombosis by PAD4-dependent mechanisms. Insufficient immunothrombosis may favour rectal bleeding in UC.

Summary box

What is already known about the subject?

⇒ Rectal bleeding is a significant and worrisome feature of active ulcerative colitis (UC) and is present in many cases. Here we study the role of neutrophil-mediated immunothrombosis and extracellular trap formation in damaged intestinal mucosae and describe their beneficial haemostatic function during flares of UC.

What are the new findings?

⇒ Activated neutrophils migrate to sites denuded of intestinal epithelium, aggregate and extrude decondensed chromatin as neutrophil extracellular traps (NETs) in a peptidyl-arginine deiminase-4 (PAD4)-dependent manner.

⇒ PAD4-dependent NET formation is closely linked to the remodelling of blood clots to secondary immunothrombi. PAD4-dependent immunothrombosis achieves successful mucosal haemostasis and limits rectal bleeding in UC and in experimental models of disease.

How might it impact on clinical practice in the foreseeable future?

⇒ The concept of a beneficial role of immunothrombosis and extracellular trap formation at mucosal surfaces challenges the prevailing view of harmful NETs. Therapeutic approaches in active UC need to carefully balance rather than abrogate the neutrophil response.

INTRODUCTION

Ever since the initial therapeutic studies of Truelove and Witts,[1] rectal bleeding has been considered as an important component of the clinical features of patients suffering from severe ulcerative colitis (UC). Increased rectal bleeding may require hospitalisation and rarely emergency surgical interventions.[2 3] In UC, the epithelial lining is breached and emergency barriers are immediately required before epithelial restitution can be achieved.[4] Emergency barriers need to provide provisional control of microbial invasion, avoid loss of blood and mucosal tissue fluids and support a timely restitution of mucosal epithelial integrity.[5] Colitis can

be caused by various infectious microorganisms. Additionally, non-infectious causes of mucosal damage exist, ranging from drug-induced to diet-induced mucosal stress.[6] Failure to clear instigating factors or repeated challenges in a structurally vulnerable microenvironment[7] favour sustained chronic inflammation in UC and the development of flares of acute inflammation. Flares often feature rectal bleeding and the presence of large numbers of polymorphonuclear granulocytes.[8]

Neutrophil granulocytes may trespass epithelial layers, phagocytise and serve as a first line of defense.[9 10] Neutrophil granulocytes may further extrude decondensed chromatin decorated with granular and nuclear constituents termed neutrophil extracellular traps (NETs).[11] Peptidyl arginine deiminase-4 (PAD4) contributes to chromatin decondensation in the course of NET formation in response to select triggers.[12–15] NETs tend to aggregate,[16] contribute to host defense[13] and are increasingly appreciated as a prothrombotic element.[17 18] We observed that granulocytes and NETs represent a dominant element of the mucosal surface in UC, especially in areas of erosions and ulcerations. In experimental models, we noticed NET formation in direct proximity of blood clots and hypothesised a role of neutrophils and NETs in the remodelling of blood clots, mucosal haemostasis and control of rectal bleeding. In this study, we, thus, closely characterised surface remodelling and NET formation on mucosal erosions in both UC and experimental models, determined its functional role in mucosal wound healing and acute colitis and its dependence on PAD4.

MATERIALS AND METHODS

Patient and public involvement

Patients suffering from acute UC (n = 36) were recruited from the academic IBD centre of the University Hospital Erlangen, Germany. Partial Mayo scoring of rectal bleeding was performed on a clinical visit. Routine colonoscopy was performed in accordance to standard clinical practice and colon tissue biopsies were collected after informed consent in agreement to the approval granted by the Ethics Committee of the Friedrich-Alexander-University Erlangen-Nürnberg. Further clinical information on localisation and extent of disease, severity, age, sex and past or current therapies are included in the online supplemental table S1 and S2. Patients or the public were not involved in the design of this study. No additional burden was inflicted to study patients as interventions were planned for diagnostic and therapeutic reasons.

Endoscopic grading

A total of at least five images per patient derived from different areas of the colon were assessed by an experienced endoscopist in a blinded fashion for a graded assessment of the frequency of mucosal erosions and ulcerations inspired by the Blackstone score (0: no visible erosions, 1: less than 10 erosions (< 5 mm in size) per 10 cm section, 2: more than 10 erosions (< 5 mm in size) per 10 cm section to 3: more than 10 erosions (< 5 mm in size) and ulcerations (> 5 mm in size) per 10 cm section).[19] The section most strongly affected, almost exclusively the rectum and sigmoid colon, determined the grading result. Additionally, the morphology of all mucosal erosions was analysed and the frequency of either fibrin coverage or persistence of fresh blood or haematin was assessed in these images. These findings were correlated to the clinically assessed partial Mayo score indicating the frequency of rectal bleeding. Of initially evaluated 41 patients, 36 patients were included. Three were excluded, as no endoscopy was performed. Two patients were excluded due to regular anticoagulant medication.

Human tissue samples

Colonoscopy was performed according to clinical guidelines after informed consent of the patient. Paraffin-embedded tissues (10 colon ulcers (including UC and diverticulitis) and 22 samples of eroded surface in active UC) were subjected to staining by immunofluorescence. All samples were derived from routine clinical practice after informed consent in Mainz, Bayreuth and Erlangen and a positive ethical review of the local authorities.

Transcriptomic analyses

The Predicting Response to Standardized Pediatric Colitis Therapy (PROTECT) study was a multicentre inception cohort study based at 29 centres in the USA and Canada providing RNAseq analyses of 206 patients with UC. Additionally, RNAseq analyses of an independent cohort of the RISK study encompassing 55 non-IBD controls, 43 patients with UC and 92 patients with Crohn's disease (CD) was analysed based on publicly available datasets (PROTECT (GSE109142), RISK (GSE117993)).[20] Additionally, RNA sequencing was performed in-house on murine colon wound tissues as described before.[21] In short, a total amount of 1 µg RNA per sample was used as input material for the RNA sample preparations. Sequencing libraries were generated using NEBNext Ultra RNA Library Prep Kit for Illumina (New England Biolabs) following the manufacturer's recommendations and index codes were added to attribute sequences to each sample. polymerase chain reaction (PCR) was performed with Phusion High-Fidelity DNA polymerase (New England Biolabs), Universal PCR primers and Index (X) Primer. PCR products were purified (AMPure XP system) and library quality was assessed on the Agilent Bioanalyzer 2100 system. The clustering of the index-coded samples was performed on a cBot Cluster Generation System using PE Cluster Kit cBot-HS (Illumina) according to the manufacturer's instructions. After cluster generation, the library preparations were sequenced on an Illumina platform and paired-end reads were generated followed by data analyses as described.[21] The newly developed dataset is publicly available at the European Bioinformatics Institute ArrayExpress website (https://www.ebi.ac.uk/arrayexpress/) under the accession number (E-MTAB-10824).[22] Genes related to each topic (clot remodelling, neutrophils, myeloid cells, lymphocytes, fibroblasts) were individually selected inspired by published studies and gene ontology terms. For cell-related genes, specificity of expression was analysed using data assembled by the ImmGen consortium.[23]

Mice

PAD4$^{-/-}$ mice were kindly provided by K Mowen, Scripps Institute, La Jolla, California, USA and have been described previously.[15] All mice used were on the C57BL/6 background. For each individual experiment, age-matched and sex-matched mice were used. Mice aged 6–14 weeks were used for experimental procedures. In experiments comparing PAD4-deficient mice to wild-type, PAD4-proficient littermates were used as controls. All mice were kept under specific pathogen-free (SPF) conditions at the animal facility of the University of Erlangen. C57BL/6 mice raised under gnotobiotic conditions were provided by A Bleich and kept in isolators for the course of the experiment performed under sterile conditions with control C57BL/6 mice kept under SPF conditions in separate cages. Experimental procedures were

approved by the local committees of Lower Franconia (AZ 55.2 2532-2-358).

Experimental models of disease

Acute colitis was induced by the administration of 3–4 % dextran sodium sulfate (DSS, 36-50 kD) (MP Biotech, Santa Ana, California, USA) to the drinking water of mice. Weight and clinical features were documented throughout the experiment. If scheduled by the experiment, deoxyribonuclease I (DNase I) (5 U/g body weight) (Sigma-Aldrich) was injected intravenously each day. Endoscopic analysis of the colonic mucosa was performed on day 7 of DSS administration. Mice were euthanised if a weight loss of 20 % occurred during the course of the disease or sacrificed at day 9 for further examinations. COLOVIEW high-resolution mouse video endoscopic system (Karl Storz, Tuttlingen, Germany) was used for mouse colonoscopy. Colonic wounds were inflicted using an endoscopic forceps during mouse colonoscopy (size: 3 Fr.) as described previously.[24] Colonoscopy was performed on a daily basis in order to kinetically evaluate the development of the wound area. Wound area calculation was performed on screen shots as described.[25] Mice were sacrificed at the indicated time points and colon tissue was dissected and wounds were recovered using a punch biopsy. Samples were subjected to further analysis using RNA and protein isolation techniques as well as analyses by histochemistry.

Cell isolation procedures

Murine lamina propria mononuclear cells were isolated as previously described.[26] In brief, colonic tissue was mechanically dissected, and intestinal epithelial cells were removed by incubation in ethylenediaminetetraacetic acid (EDTA). Remaining tissue was digested in collagenase D (Roche Diagnostics, Mannheim, Germany), DNase I (Sigma-Aldrich, Munich, Germany), and dispase II (Roche Diagnostics). Digested tissue was passed through a 100 µm cell strainer, and the remaining cellular content was prepared for flow cytometry using fluorescently labelled antibodies directed against CD45, CD11b, Siglec F, Ly6C and Ly6G (BioLegend). Human peripheral blood neutrophils were isolated from healthy donors after informed written consent in agreement with local ethical regulations and separated using PanColl (PanBiotech, Germany) density gradient centrifugation. Granulocytes were enriched from the erythrocyte pellet by consequent dextrane sedimentation (60 min, 1 %, Carl Roth, Germany). The purity of neutrophil isolations was routinely above 90 %. Murine myeloid cells were sorted by flow cytometry from thioglycolate-induced peritoneal cells. These were harvested from the peritoneal cavity by peritoneal lavage of a Hank's balanced salt solution (HBSS)-EDTA solution 18 hours after thioglycolate instillation (3 %) into the peritoneal cavity. Cell suspensions were sorted directly into RNA lysis buffer.

Real-time quantitative PCR

Tissue RNA was isolated by directly freezing tissue samples in liquid nitrogen in lysis buffer of the peqGOLD Total RNA Kit (Peqlab, Erlangen, Germany). RNA quantification was performed using Nanodrop technology (Thermo Scientific, Wilmington, Delaware, USA). Reverse transcription into complementary DNA (cDNA) was performed using the BioRad iScript cDNA synthesis Kit (Bio-Rad Laboratories, Munich, Germany). Real-time quantitative PCR (qPCR) was performed using QuantiTect Primer Assays for *Actb, Aqp9*, *Csf2*, *Csf3*, *Cxcl5*, *Cxcr2*, *Hprt*, *Il1b*, *Il6*, *Nos2*, *Tnfa, Pad2, Pad4, S100a9* (Qiagen, Hilden, Germany) and QuantiTect SYBR Green qPCR Kit (Qiagen) on the Roche LightCycler system (Roche, Penzberg, Germany). Expression was calculated relative to the housekeeping gene *Hprt* using the deltadelta threshold cycle (ΔΔCt) algorithm. Fold difference to control treated animals or unstimulated control, respectively, was calculated as a ratio to the respective control mean.

Immunofluorescence and blotting techniques

Histological staining was performed on paraffin-embedded sections with the classical haematoxylin-eosin (H&E) staining procedure. Immunofluorescence of cryosections or paraffin-embedded slides was performed as described below and recorded on either a confocal laser scanning-microscope or a standard fluorescence microscope (Leica, Germany) using overnight hybridisation with primary Abs specific for α-smooth muscle actin (Abcam, Cambridge, UK, 1:500), Beta-Catenin (Cell Signalling, 1:500), E-Cadherin (BD, 1:100), EpCAM (BioLegend, 1:100), citrullinated histone H3 (Abcam, 1:200), MPO (Abcam, 1:200), C3d (R&D Systems, 1:100). Detection was performed using either biotinylated secondary Abs (goat anti-rabbit or anti-rat, Abcam, 1:1000) and TSA Fluorescein/Cy3 kits (PerkinElmer, Waltham, Massachusetts, USA) or directly labelled Alexa 488 or Alexa 555-conjugated goat anti-rat antibodies (Abcam, 1:200–1:1000). Before examination, the nuclei were counterstained with either Hoechst 33342, propidium iodide or SYTOX Green (Invitrogen Molecular Probes, Karlsruhe, Germany; BD, Heidelberg, Germany). Autofluorescence of blood clots in paraffin-fixed sections was determined at excitation 488 nm and emission 525 nm in the absence of Alexa 488/fluorescein isothiocyanate (FITC)-based immunofluorescence. Tissue-derived proteins were isolated from snap frozen samples using Mammalian Protein Extraction Reagent (MPER) complete buffer (Thermo Scientific) and mechanical disruption using a ball mill. Protein quantification was performed using Bradford reagent (Carl Roth). For dot blots, protein lysates were directly administered to nitrocellulose membranes. For further analysis, Western blots were performed after sodium dodecyl sulphate-polyacrylamide gel electrophoresis (SDS-PAGE) using ready-made gels (Bio-Rad).

Calculation of ulcerated area

Tissue sections stained with H&E were used for a blinded morphometric analysis calculating the area affected by ulceration relative to the total sectional mucosal surface.

Assessment of fecal bacterial load

Stool samples of gnotobiotic and SPF mice were collected before and 18 hours after wound infliction. Stool samples were suspended in a weight-normalised amount of sterile phosphate-buffered saline (PBS). Filtrates were plated on sterile LB agar plates without antibiotics, incubated at 37 °C for 24 hours and bacterial colonies were counted.

PAD4-dependent plasmin activity assay

Various concentrations of human α_2-antiplasmin (Merck Millipore, Darmstadt, Germany) were preincubated with or without active PAD4 enzyme (Cayman Chem, Ann Arbor) for 2 hours at 37 °C in a buffer containing 100 mM Tris-HCl, 160 mM lysine and 10 mM $CaCl_2$. Afterwards, human active plasmin enzyme was added and incubated for 30 min at 37 °C. The fluorescent plasmin substrate N-Succinyl-Ala-Phe-Lys-AMC (Merck Millipore) was then added to each well and the fluorescence intensity measured in a Tecan Infinite M200 microplate reader (Tecan, Männedorf, Switzerland) with ex/em 345/465 nm at 37 °C over

a period of 60 min. Results were analysed using Microsoft Excel (Microsoft, Redmond, Washington, USA).

Assessment of transglutaminase activity in colon wounds

The transglutaminase substrate 5-(Biotinamido)pentylamine (Merck Millipore) was dissolved in sterile PBS and injected intraperitoneally at a concentration of 100 mg/kg body weight in wild-type and PAD4$^{-/-}$ mice immediately before colon wound infliction.[27] After 6 hours, the tissue was harvested, frozen and cut. Wound sections were fixed and stained with a fluorescent streptavidin conjugate (Dylight 488, Thermo Fisher). After counterstaining with Hoechst, imaging was performed using a standard fluorescence microscope (Leica, Germany). Relative fluorescence intensity in the wound clot area was assessed by digital image analyses. D-dimer concentration in colon wound homogenates was measured using the Abbexa D-dimer ELISA kit (Cambridge, UK) according to manufacturer's instructions.

Flow cytometric analysis of the cellular composition of colon wounds

Three to four colonic wounds per mouse were inflicted using an endoscopic forceps during mouse colonoscopy and colon tissue was isolated after 18 hours. The wound area was punched out using a 3 mm biopsy punch and wounds and the residual non-wounded colon tissue were retained in separate tubes. Lamina propria leukocytes (LPL) and intraepithelial leukocytes (IEL) were isolated separately from both tissue fractions using the Lamina Propria Dissociation Kit for mouse (Miltenyi Biotec, order no. 130-097-410). Briefly, the tissue was cut into small pieces, incubated with predigestion solution at 37 °C for 2×20 min with vigorous shaking and then filtered through a 100 µm cell strainer. The filtrate containing the IEL fraction was kept on ice while the remaining tissue pieces were incubated with HBSS without Ca^{2+} and Mg^{2+} + 10 mM 4-(2-hydroxyethyl)-1-piperazineethanesulfonic acid (HEPES) at 37 °C for 20 min with vigorous shaking. After repeated filtration, the tissue pieces were enzymatically digested for 30 min at 37 °C and subsequently shredded using the gentleMACS Dissociator (Miltenyi Biotec). The remaining LPLs were transferred into a fresh tube and centrifuged in parallel with the IEL filtrate to pelletise the cells. The pelletised LPL and IEL fractions were purified using a Percoll Cytiva density gradient and washed with flow cytometry buffer in a final step. After staining with fluorophore-coupled antibodies, flow cytometric analysis was performed using a LSRFortessa Cell Analyzer and FlowJo software (BD Biosciences, Franklin Lakes, New Jersey, USA).

DNase-mediated digestion of wound clots in-vitro

Colon wounds were inflicted on wild-type mice as described above. After 18 hours, mice were sacrificed and wound clots were picked from the excised colon. The clots were transferred into chamber slide wells containing PBS and stained with Hoechst and SYTOX Green for 30 min at room temperature. Subsequently, DNase I (1 U/mL) was added to the wound clots and incubated at 37 °C for 20 hours. Microscopic imaging was performed at three time points before and after addition of DNase.

Assessment of neutrophil–blood clot interactions in vitro

Citrated human whole blood was recalcified on glass cover slips using 10 mM $CaCl_2$ in accordance with standard protocols. After 1 hour of incubation at 37 °C, a well of a defined size was punched in the centre of the blood clot. Neutrophil suspensions (5×10^5 cells per well) were seeded in this well in the presence of 5 mM SYTOX Green in autologous serum. After 180 min, samples were fixed in 4 % paraformaldehyde (1 hour or over night) and stained according to the following protocol. Samples were carefully washed with PBS and subjected to a blocking solution (PBS + 10 % fetal calf serum (FCS) + 1 % bovine serum albumine (BSA)). Overnight-incubation with primary antibody in blocking solution ensued. A directly labelled secondary antibody 1:200 in PBS was incubated for 2 hours. Hoechst and/or SYTOX Green (5 mM) was used for chromatin staining.

Live-cell imaging

Human neutrophil suspensions in a HEPES-buffered Roswell Park Memorial Institute (RPMI)-based medium supplemented with 2 % autologous human serum and nucleic acid stains were incubated for 1.5 hours at 37 °C with selected inhibitors or solvent controls. Cells were then seeded in 48-well plates and imaged using a Keyence microscope with temperature and gas-control at 37 °C and 5 % CO_2. Wells were previously prepared to contain a mixture of high-melting and low-melting agarose gels in the centre of the well mixed with human autologous serum (20 %) of the respective donor. Serum was used either native or heat-inactivated (30 min, 56 °C). Repetitive automated imaging using the Keyence microscope allowed the study of the kinetics of NET formation at the edge of the agarose gel.

Confocal laser-scanning microscopic analysis of colon tissues and mucosal ulcers

Immunothrombi formed on top of mucosal wounds were manually picked and put on glass slides followed by immunostaining as presented above. Wounded areas were excised from the colon of sacrificed mice using a punch biopsy. The samples were mounted as a whole on top of glass slides, fixed and subjected to immunostaining as presented above. Stained samples were subjected to confocal laser-scanning microscopy (Leica SP5) and z-stacks were acquired. Further image processing was achieved by Leica and Image J software.

Statistical analysis

Data were analysed as indicated in the figure legends using the unpaired Student t-test using Microsoft Excel (Microsoft, Redmond, Washington, USA) or an analysis of variance with post-hoc Tukey honestly significant difference (HSD) tests, as well as Fisher's exact test for 2×2 contingency tables and Wilcoxon rank-sum test, as indicated. Correlation of ordinal and metrically scaled parameters was performed using non-parametric Spearman rank-order correlation test.

RESULTS

Bleeding in active UC is controlled by successful formation of fibrin on mucosal erosions

Epithelial barrier dysfunction characterises UC, especially during flares of disease. In this setting, many patients experience marked rectal bleedings. We observed that patients with endoscopically active UC exhibit abundant mucosal erosions, while intensity of rectal bleeding strongly varies (figure 1A and B). We assessed both rectal bleeding as reported on clinical visits (partial Mayo score) as well as endoscopic features of disease. There was an increased frequency of mucosal erosions and ulcerations in patients suffering from rectal bleeding (figure 1B). However, the presence of erosions did not necessarily prompt rectal bleeding. Mucosal haemostasis was successfully established even in active UC, when the erosions were completely covered by fibrin (figure 1C). However, incomplete coverage by fibrin correlated

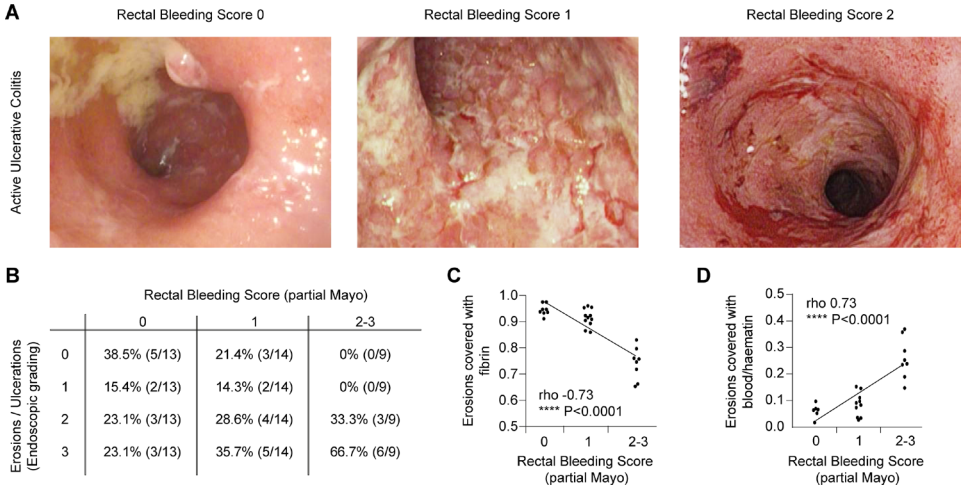

Figure 1 Bleeding in active UC is controlled by successful formation of fibrin on mucosal erosions. (A) Patients experiencing flares of UC often suffer from rectal bleeding, typically assessed by the partial Mayo score (0: none, 1: visible blood with stool (< 50 %), 2: visible blood with stool (> 50 %), 3: passing blood alone). Patients suffering from flares of UC underwent routine endoscopy. Representative endoscopic images of patients with various degrees of rectal bleeding are depicted. (B) Clinically observed rectal bleeding coincided with the enhanced presence of mucosal erosions on endoscopy as graded by an experienced endoscopist in a blinded fashion inspired by the Blackstone score (0: no visible erosions, 1: less than 10 erosions (< 5 mm in size) per 10 cm section, 2: more than 10 erosions (< 5 mm in size) per 10 cm section to 3: more than 10 erosions (< 5 mm in size) and ulcerations (> 5 mm in size) per 10 cm section). The section most strongly affected determined the grading result (Spearman's rho: 0.38, * $p < 0.05$). additionally, the morphology of mucosal erosions was analysed and the frequency of either fibrin coverage or persistence of fresh blood or haematin was assessed in these images supported by digital image analysis. (C) Presence of erosions did not necessarily prompt rectal bleeding, rather complete coverage by fibrin on all mucosal erosions achieved haemostasis. Less efficient fibrin coverage was observed in patients suffering from rectal bleeding as assessed by partial Mayo score (spearman Rho: 0.73, **** $p < 0.0001$). (D) Persistent presence of blood or haematin on erosions was associated with clinical rectal bleeding (spearman Rho: 0.73, **** $p < 0.0001$). The study cohort included 36 patients suffering from active UC with varying degrees of rectal bleeding. UC, ulcerative colitis.

with increased rectal bleeding. Increased occurrence of fresh blood or haematin on the surface of mucosal erosions correlated with clinical rectal bleeding (figure 1D). These findings suggested a haemostatic function of fibrin layers in active UC.

Eroded colonic mucosa features blood clots which are remodelled to a fibrin layer rich in aggregated granulocytes and NETs

As the mechanisms controlling mucosal haemostasis in UC are incompletely understood, we assessed the morphology of mucosal erosions by microscopy in subsequent studies. We studied erosions covered with blood or haematin and those covered with whitish fibrin (figure 2A and D). The surface of blood-covered erosions featured homogenous blood clots. Invasion of neutrophils from the edge of the blood clot was observed (figure 2B). MPO^+ neutrophils at the edge of the autofluorescent blood clot were present in aggregates showing interspersed decondensed chromatin and featured citrullinated histone H3 (H3cit) as evidence for PAD activity (figure 2C). We speculated that infiltrating neutrophils and the associated PAD activity might be directly involved in the remodelling of the clot to a haematoxylin-affine amorphous fibrin layer. Fibrin-covered erosions also showed ample amounts of infiltrating neutrophils (figure 2D). We identified fibrin layers in active UC and on colonic ulcers to be rich in $CD15^+$ neutrophils and myeloperoxidase (figure 2D–E, online supplemental figure 1A). Moreover, the fibrin layer on eroded surfaces was characterised by extracellular chromatin devoid of nuclear morphology displaying citrullinated histone H3 (H3cit), typical of NETs (figure 2F, online supplemental figure 1B). At the edge of blood clots on blood-covered erosions, single neutrophils were observed which also displayed H3cit. While H3cit was largely absent in MPO^+ cells in the lamina propria (online supplemental figure 1A,B), strong H3cit immunopositivity and hence PAD activity was found within fibrin layers in direct proximity to aggregated granulocytes (figure 2F). Transcriptomes showed the increased presence of *PAD4* in the inflamed mucosa of colonic CD, ileocolonic CD and UC in two independent patient cohorts in both male and female patients alike, whereas *PAD2* was reduced in active disease (figure 2F and G). Subsequent studies revealed that *Padi4* expression is restricted mostly to innate immune cells of the myeloid lineage, especially neutrophil and eosinophil granulocytes (online supplemental figure 2A), while it is not detected in intestinal epithelial cells. Taken together, histone citrullination and formation of NETs is associated with increased presence of *PAD4* in severe intestinal inflammation in IBD and occurs mostly in fibrin layers which cover mucosal ulcerations.

Mucosal damage leads to the formation of red blood clots subject to remodelling to neutrophil-rich fibrin layers characterised by marked PAD4-activity

Based on these findings, we hypothesised that neutrophils take part in the remodelling of red blood clots on mucosal erosions to fibrin layers. In order to dynamically model healing of mucosal ulcers *in vivo*, we inflicted colonic wounds in mice by endoscopy using a grasping forceps (figure 3A): directly after wounding, a red blood clot forms on the mucosal wound, which was remodelled to a whitish fibrin layer hours after wounding (figure 3A). 18 hours after wounding, a breach of the epithelial lining was still appreciated on the microscopic level (figure 3B). As observed previously in humans, the wound bed was covered by both amorphous material and aggregated MPO^+ neutrophils (figure 3B and C). The fibrin layer was further intensely fibrinogen-positive, indicative of fibrin polymerisation (figure 3D), featured PAD activity as evidenced by

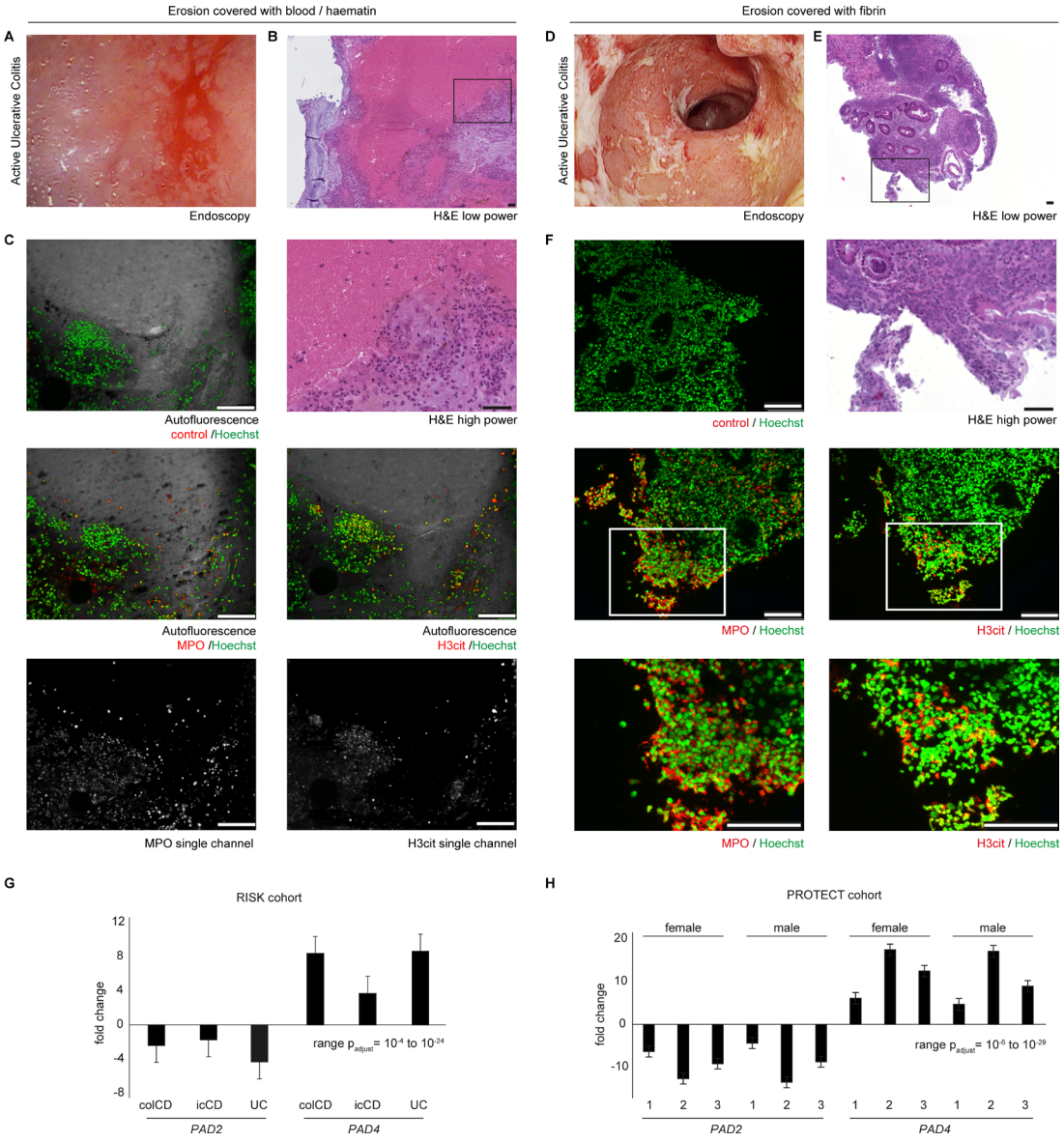

Figure 2 Eroded colonic mucosa features blood clots which are remodelled to a fibrin layer rich in aggregated granulocytes and NETs. During colonoscopy of active UC, biopsies were taken specifically from either (A–C) blood clot-covered or (D–F) fibrin-covered erosions and analysed by endoscopy and microscopy as indicated. Representative endoscopic images of (A) blood/haematin-covered and (D) fibrin-covered colon erosions of patients suffering from active UC are shown. (B) Representative low-power and high-power images are provided (scale bars: 100 µm). We identified marked infiltration of neutrophils into the blood clot and adjacent amorphous haematoxyline-affine material. Samples from (E) fibrin-covered erosions showed a strong abundance of aggregated neutrophils (scale bars = 100 µm). (C, F) Immunofluorescence of such biopsies is shown using either MPO or H3cit-directed primary antibodies. (C) Aggregates of MPO^+ neutrophils were present at the edge of the autofluorescent primary blood clot (488/525 nm). In this area, decondensed chromatin and H3cit was detected. Combined and single channel analyses are presented (scale bars = 100 µm). (F) Fibrin visible on the endoscopic level is rich in H3cit and aggregated MPO^+ neutrophils. As depicted, H3cit is rather restricted to the fibrin layer (representative of n = 22 biopsies studied). (G–H) Publicly available datasets of RNAseq-based transcriptomics of large cohorts of patients suffering from icCD (1), colCD (2) or UC (3) were reanalysed for expression of *PAD2* and *PAD4*, respectively. Fold change as compared with non-diseased controls is depicted. colCD, colonic Crohn's disease; H3cit, citrullinated histone H3; icCD, ileocolonic Crohn's disease; MPO, myeloperoxidase; NETs, neutrophil extracellular traps; PAD, peptidyl-arginine deiminase; UC, ulcerative colitis.

H3cit (figure 3E) and displayed the presence of C3d, indicating complement activity (figure 3F). By flow cytometry, we assessed the relative amounts of various immune cells to both wound surface and lamina propria. Both surface and lamina propria showed a strikingly increased infiltration of $CD11b^+$ myeloid cells as compared with adjacent healthy mucosa. Both surface and lamina propria showed significant increases of $CD11b^+Ly6G^+$ neutrophils: especially the wound surface showed a striking enrichment of up to 73 % of all infiltrating $CD11b^+$ myeloid cells being neutrophils (figure 3G), while $CD11b^+Ly6C^{int}Ly6G^-SiglecF^+$ eosinophils were scarce (figure 3H). The wound surface of both blood-covered and fibrin covered-erosions was additionally analysed in a top view perspective by confocal microscopy. Aggregated neutrophils and NETs were observed in direct proximity to blood clots. Ultimately, the blood clots were completely remodelled to H3cit-positive layers (figure 3I). We further quantified PAD activity in colonic wounds and detected markedly elevated H3cit in wounds (figure 3J and K). Remodelling of the blood clot on eroded surfaces thus leads to a fibrin layer,

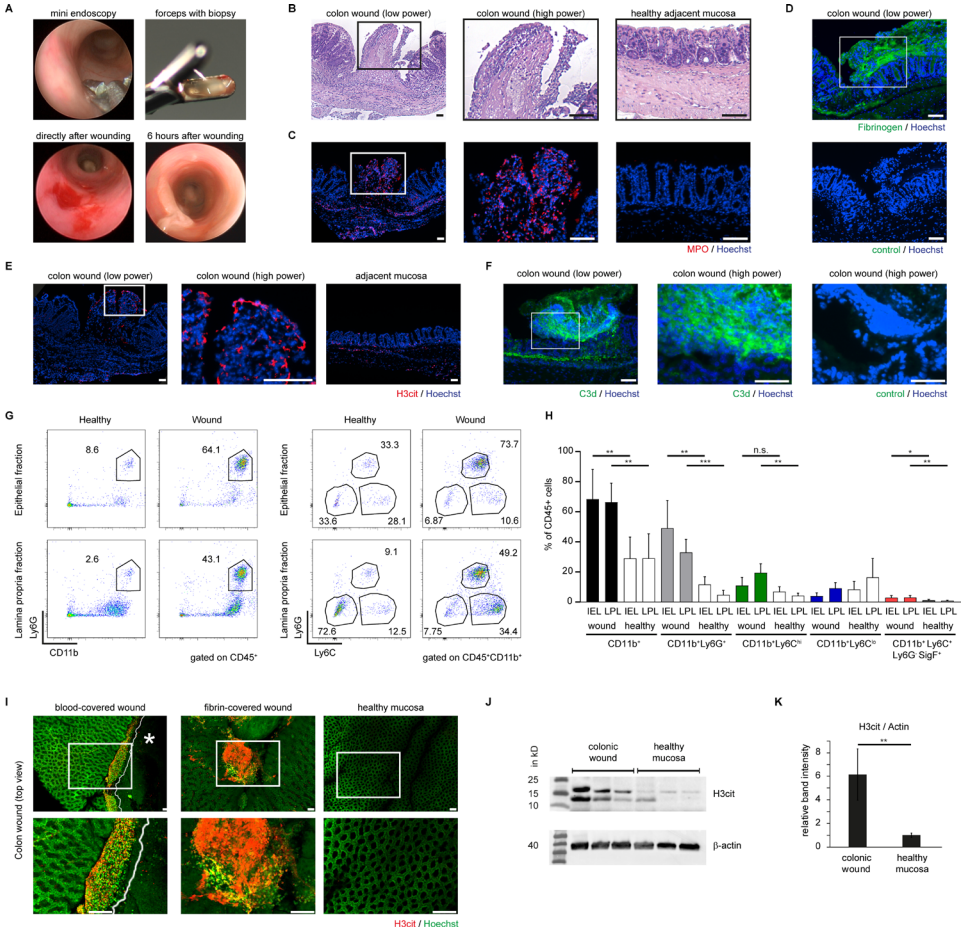

Figure 3 Mucosal damage leads to the formation of red blood clots subject to remodelling to neutrophil-rich fibrin layers characterised by marked PAD-activity. Colonoscopy was performed in mice and mucosal wounds were induced using an endoscopic forceps. (A) *Top Left*: forceps during endoscopy; *top right*: forceps with biopsy; *bottom right*: red blood clot on the mucosal wound directly after wounding; *bottom left*: whitish fibrin covers the mucosal wound 6 hours after wounding. The red blood clot was remodelled. (B) H&E staining of sections of mucosal ulcers (18 hours after injury) display an amorphous layer rich in granulocytes at the surface of the mucosal ulceration. An overview of a cross-section (*left*) and a high-power magnification (centre) is presented, as well as an image of healthy mucosa (*right*). (C) The remodelled layer covering the wound bed is positive for MPO as evidenced by immunofluorescence. MPO staining shows fiber-like constitution, indicative of a partially extracellular localisation, colocalised to DNA. (D) The remodelled layer is also characterised by fibrin deposition, as evidenced by fibrinogen immunofluorescence (*top*) as compared with control (*bottom*) (scale bars = 100 µm). (E) H3cit is preferentially detected in the wound surface, also featuring (F) cleaved complement C3d. (G) Flow cytometric analysis of healthy and wound tissue 18 hours after wounding. Both the LPL fractions and the IEL fractions of wounds were analysed. In wound tissues, $CD11b^+Ly6G^+$ neutrophils are the dominant cell type in the IEL fraction, whereas the lamina propria features large populations of both $CD11b^+Ly6G^+$ neutrophils and $CD11b^+Ly6C^{hi}$ monocytes. (H) Quantification of the cellular composition of colon wounds and adjacent healthy colon tissue (n = 18 wounds studied, *** $p < 0.001$, Student's t-test, ** $p < 0.01$, Student's t-test, * $p < 0.05$, Student's t-test). (I) Colonic wounds were mounted on glass slides as a whole and subjected to epifluorescence analysis after immunostaining of H3cit (in red) and Hoechst (in green) staining. The wound surface of two different wounds both derived from wild-type mice is presented. *Left*: a wound with persistent presence of the primary blood clot. A cell-rich layer in proximity to the blood clot characterised by H3cit-positive chromatin threads separates the blood clot from the adjacent mucosa. *Centre:* a remodelled colonic ulcer surface, covered by $H3cit^+$ chromatin. *Right*: no H3cit is detectable on healthy mucosa. Images are representative of > 10 colonic wounds studied. (J) Western blot analyses of colonic wounds and healthy mucosa collected 18 hours after wounding were performed. (K) Densitometry of Western blots as in (J) shows increased presence of H3cit in the wound bed as compared with healthy control tissues (** $p < 0.001$, Student's t-test, 3 independent experiments performed). Loading control: β-Actin. All scale bars = 100 µm. H3cit, citrullinated histone H3; IEL, intraepithelial lymphocyte; LPL, lamina propria leucocyte; MPO, myeloperoxidase; PAD, peptidyl-arginine deiminase.

characterised not only by fibrin polymerisation but also by the activity of complement and a significant contribution of neutrophil granulocytes, which aggregate, form NETs and show marked PAD activity.

To underline this crucial contribution of innate immune cells to the remodelling of the wound surface, we introduced the term immunothrombus to define a primary blood clot, which has been remodelled by innate immune cells.[17]

An increased neutrophil-related transcriptional signature coincides with the increase of clot remodelling-associated transcripts

To further characterise the dynamic process of wound healing and wound-bed remodelling on a transcriptional level, we performed RNA sequencing of colon wounds at defined time points of 6, 24 and 48 hours after wounding as compared with healthy tissue. Specifically, we assessed dynamic changes in expression over time

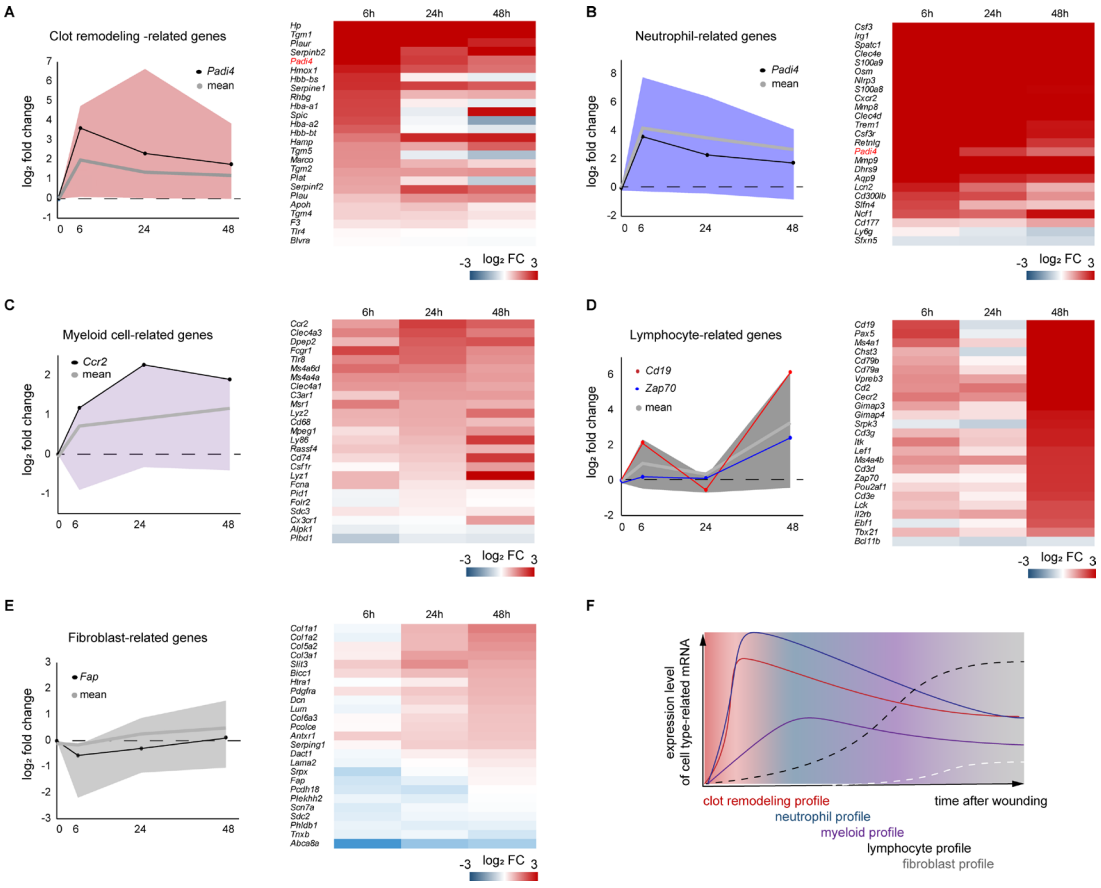

Figure 4 An increased neutrophil-related transcriptional signature coincides with the increase of clot remodelling-associated transcripts. RNA-sequencing was performed studying the transcriptome of healthy colon and wound tissue from three defined time points after wounding (6 hours, 24 hours, 48 hours after wounding, n = 3 wounds per time point). Expression was analysed as a fold-change in relation to the healthy state. An expression time course for each gene set (clot remodelling-related, neutrophil-related, myeloid cell-related, lymphocyte-related, fibroblast-related) is provided. The area between the minimal and maximal differentially expressed genes of each gene set is coloured. Additionally, the mean of each gene set and exemplary single gene time courses are depicted for the genes indicated. A heat map of the entire topic-related gene set studied is provided visualising the $\log_2$ fold change in colour (increase in red, decrease in blue). (A) Expression of clot remodelling-related genes is most strongly increased 6 hours after wound infliction. (B) Neutrophil-related genes – among these *Padi4* – are also most strongly increased 6 hours after wound infliction. (C) Expression of myeloid cell-related genes show a slower increase within the first day of healing peaking at 24–48 hours. (D) The profile of lymphocyte-related genes peaks at 48 hours after damage. (E) Expression of fibroblast-related genes shows only a moderate increase over time. (F) Summarised depiction of the expression profiles shown in (A)–(E) over time. Please appreciate the sequential dynamics of the designated profiles.

of preselected genes functionally associated to haemolysis and fibrinolysis, clot remodelling, as well as immune cell-associated signatures related to neutrophils, myeloid cells, lymphocytes and fibroblasts. Clot remodelling-associated transcripts, for example, *Hp*, *Tgm1*, *Plaur*, *Serpine1*, *Serpinf2* and *Hmox1* showed strongly increased abundance as soon as 6 hours after wounding (figure 4A). Interestingly, increased abundance of neutrophil-related transcripts, for example, *Csf3*, *Clec4e*, *S100a9*, *Cxcr2* and *Padi4* coincided with clot remodelling-associated transcripts (figure 4B). A myeloid cell-related gene set reached its maximum in abundance at 24 hours after wounding (figure 4C), whereas lymphocyte-related transcripts peaked at 48 hours (figure 4D). Fibroblast-related transcripts showed less marked alterations in abundance as compared with the aforementioned immune cell compartments (figure 4E). Taken together, abundance in clot remodelling-related genes coincides with a neutrophil-related gene signature, whereas myeloid and lymphocyte-related signatures increase at later time points after wounding (figure 4F). Findings from RNA sequencing studies were corroborated by selective qPCR analyses of colon wounds and adjacent healthy mucosa at 24 hours post wounding. Specifically, *Padi4* mRNA was increased in colonic wounds, while *Padi2* mRNA was not (online supplemental figure 2B).

Deficiency of PAD4 disturbs blood clot remodelling on mucosal ulcerations and delays mucosal wound healing

Next, we assessed the functional contribution of immunothrombi *in vivo*. We made use of PAD4-deficient mice. We observed striking morphological differences in the wound healing process in PAD4-deficient mice as compared with controls. In the absence of PAD4, H3cit was strongly reduced in the wound surface (online supplemental figure 3A) and less decondensed chromatin was present. Functionally, the remodelling of the ulcerated surface was disturbed (figure 5A, video 1): red blood clots persisted more often as analysed 6 hours after wounding and led to a continued sanguinary appearance on endoscopy (figure 5B). Following the delayed remodelling of the wound surfaces, the timely restitution of the mucosal integrity was delayed in the absence of PAD4 as compared with wild-type controls. This was evidenced by repeated endoscopy and morphometry (figure 5C and D). H&E staining of colon wound

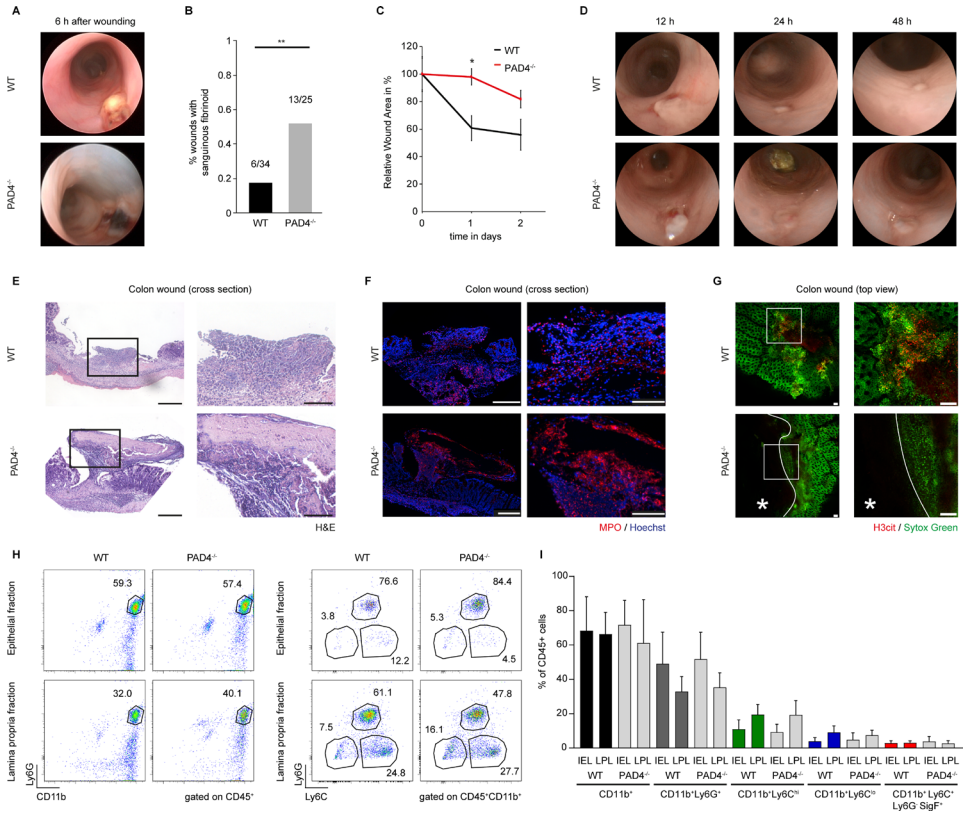

Figure 5 Deficiency of PAD4 disturbs blood clot remodelling on mucosal ulcerations and delays mucosal wound healing. Mini-colonoscopy was repetitively performed after physical wounding of the colon mucosa. (A) Representative endoscopic imaging of colon wounds 6 hours after wounding performed in PAD4$^{-/-}$ and wild-type (WT) mice display the disturbed remodelling of the blood clot on the ulcer surface in PAD4$^{-/-}$ mice. Please appreciate the persistent sanguinous appearance of wounds in PAD4$^{-/-}$ mice. (B) Quantification of the fraction of wounds displaying a sanguinous morphology covering the wounds (** $p < 0.05$, Fisher's exact test for 2×2 contingency tables). (C) Wound bed size was measured on repeated endoscopic examinations. Wounds in PAD4-deficient mice had a delayed kinetic of wound healing (* $p < 0.05$, Student's t-test). (D) Time course of mucosal healing as evidenced by representative endoscopic images of colon wounds performed in PAD4$^{-/-}$ and WT mice (n = 24 wounds per group (* $p < 0.05$, Student's t-test)). (E) H&E staining of colonic wound sections from WT and PAD4$^{-/-}$ mice after 18 hours shows a remodelled blood clot in the WT colon, characterised by a high abundance of invading granulocytes throughout the fibrin layer. In contrast, the PAD4$^{-/-}$ wound clot still contains the primary blood clot with granulocytes only present at the clot edge (scale bars: low power = 200 µm, high power = 100 µm). The same wound as in (E) was subjected to immunofluorescence. (F) Staining of MPO shows neutrophil infiltration throughout the clot in WT mice. The wound from PAD4$^{-/-}$ mice features MPO^{+} cells surrounding the unstained sanguinous core (scale bars: low power = 200 µm, high power = 100 µm). (G) Epifluorescence analyses of the colon ulcer surface of PAD4$^{-/-}$ and WT mice displayed the reduced presence of H3cit in PAD4$^{-/-}$ mice as well as the persistence of the primary blood clot (marked by the asterisk). High-power insets are presented on the right. Counterstaining with sytox green. (H) Flow cytometric analyses of cellular infiltrates of wound tissues from WT and PAD4$^{-/-}$ mice 18 hours after wounding are presented. Both genotypes exhibit a marked infiltration of CD11b^{+}Ly6G^{+} neutrophils to the wound site. Especially in the epithelial fraction representing the ulcer surface, CD11b^{+}Ly6G^{+} neutrophils are strongly enriched in both groups. (I) Comparative quantification of the cellular composition of WT and PAD4$^{-/-}$ wound tissue as assessed in (H) shows no significant differences in the cellular composition with regard to the examined leucocyte populations (n = 18 wounds from two independent experiments evaluated). H3cit, citrullinated histone H3; MPO, myeloperoxidase; PAD, peptidyl-arginine deiminase; WT, wild-type.

sections evidenced the persistence of blood clots on the wound in the absence of PAD4 (figure 5E), whereas in wild-type controls remodelling to a neutrophil-rich immunothrombus occurred regularly. Neutrophil chemoattraction to the wound surface was not disturbed as evidenced by MPO staining (figure 5F). Further whole mount immunofluorescence demonstrated that neutrophil chemoattraction persisted in the absence of PAD4, while histone citrullination and chromatin decondensation was markedly disturbed (figure 5G, online supplemental figure 3A). Flow cytometric analyses corroborated the strong and equally effective chemoattraction of neutrophils to the wounds in the absence of PAD4 (figure 5H). Additionally, no significant alterations in the influx of other myeloid cells were observed (figure 5I).

Immunothrombosis occurs on mucosal erosions even in the absence of bacteria

Immunothrombi on colonic wounds were subject to bacterial invasion in mice: both in wild-type and PAD4-deficient mice invasion of the wound surface by bacteria was detected using 16s-rRNA eubacteria-directed fluorescent probes. Obvious tissue infiltration into deeper layers of the intestinal mucosa by bacteria was not observed (online supplemental figure 3B). We aimed to understand, whether microbial invasion was important for NET formation in immunothrombi. Gnotobiotic C57BL/6 mice were used and wounds were inflicted under sterile conditions. Bacteria could not be detected in the murine faeces of treated mice even 18 hours after the endoscopic procedure

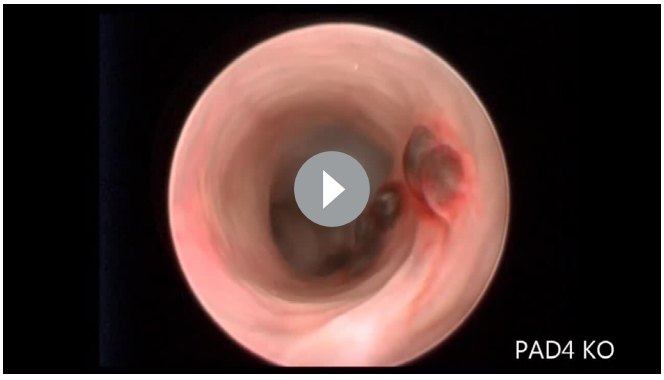

Video 1 Proctoscopy was performed in PAD4$^{-/-}$ and wild-type littermates 6 hours after inducing wounds with an endoscopic forceps and the morphology of the ulcer surface was studied by video mini-endoscopy. Note the remodelling of the clot to whitish fibrin in wild-type mice, whereas a sanguinous morphology persists in PAD4$^{-/-}$ mice.

(figure 6A). We compared the course of wound healing in gnotobiotic C57BL/6 mice and mice raised under SPF conditions. We detected regular formation of blood clots and successful remodelling to immunothrombi on colonic wounds, even in the absence of microbiota (figure 6B). Neutrophils infiltrated the colonic wound surface in both gnotobiotic C57BL/6 mice and in SPF mice as evidenced by H&E staining (figure 6C) and formed immunothrombi. However, submucosal oedema and submucosal leucocyte infiltration were significantly reduced in gnotobiotic mice as compared with SPF mice (figure 6D and E). MPO$^+$ cells infiltrated the wound surface in both gnotobiotic and SPF mice alike, whereas submucosal MPO$^+$ cells were significantly reduced in gnotobiotic mice (figure 6F1). Both PAD (H3cit) activity (figure 6G and J) and complement (C3d) activity (figure 6H and K) persisted in immunothrombi, even under gnotobiotic conditions. Thus, neutrophil recruitment to wound surfaces, PAD activity and complement activity persist in the absence of microbiota.

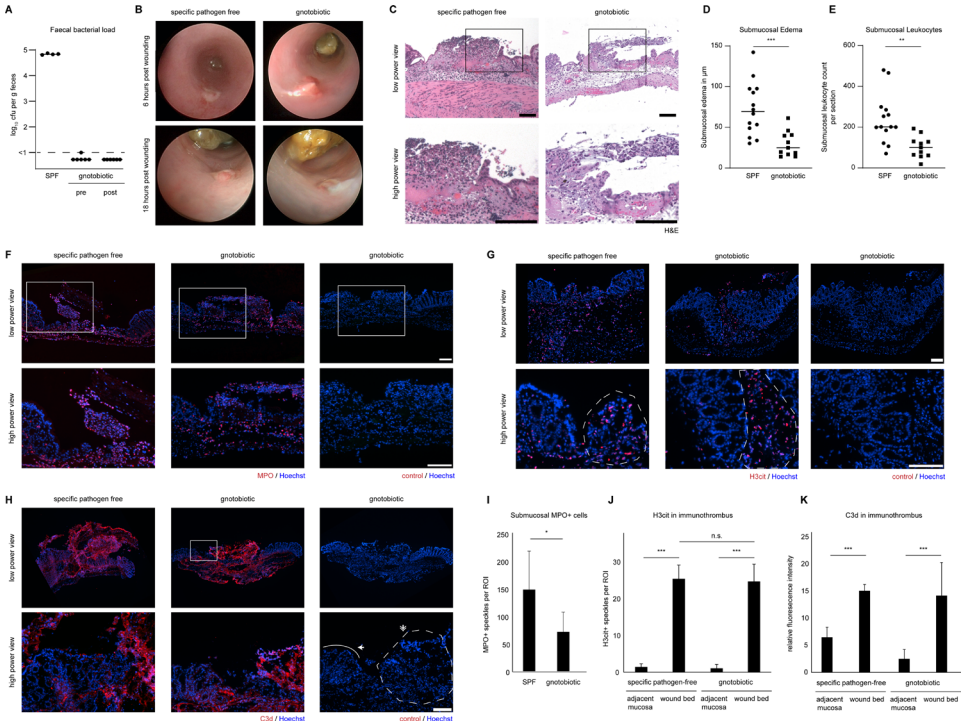

Figure 6 Immunothrombosis occurs on mucosal erosions even in the absence of bacteria. Colonoscopy was performed in mice and mucosal wounds were induced using an endoscopic forceps system in SPF and gnotobiotic wild-type C57BL/6 mice under sterile conditions. (A) Faecal bacterial load was assessed by 24 h-culture of faecal homogenates on lb agar plates. Gnotobiotic mice remained sterile throughout the experiment. (B) Mini-colonoscopy was performed 6 and 18 hours after wounding. Representative endoscopic images of colon wounds show that remodelling of the wound bed surface occurs in a similar fashion independently of the colonic microbiota. (C) H&E staining of wounded colon tissue sections shows infiltration of leucocytes to the wounded colon and submucosal oedema in both SPF and gnotobiotic mice. (D) Submucosal oedema thickness was quantified in cross sections in SPF and gnotobiotic mice (N: 11–14 wounds per group, *** $p < 0.001$, Student's t-test, bars represent the means) (E) scatter plots of leucocyte numbers infiltrating the submucosa quantified in cross sections in SPF and gnotobiotic mice (** $p < 0.01$, Student's t-test, bars represent the means). (F) Marked infiltration of MPO$^+$ neutrophils to both wound bed and submucosa in SPF and gnotobiotic mice was observed by immunofluorescence, (G) H3cit was preferentially detected in wound beds of SPF and gnotobiotic mice as compared with the adjacent mucosa as studied by immunofluorescence. Dashed lines indicate the ROI of the immunothrombus area. (H) Complement activation as studied by C3d staining in both SPF and gnotobiotic mice was prominent in the wound bed area in both groups. (I) MPO$^+$ cells in the submucosa were quantified in images as in (F) (N: 8–10 wounds per group, * $p < 0.05$, Student's t-test, mean ± SD are depicted). Dashed lines indicate the ROI of the immunothrombus area. The solid line indicates the intact border of the wound (J) H3cit$^+$ speckles per ROI in the wound bed and adjacent mucosa were quantified in images as in (G) (N: 3–7 wounds per group, *** $p < 0.001$, Student's t-test, mean ± SD are depicted) (K) C3d relative fluorescence intensity per ROI in the wound bed and adjacent mucosa was quantified in images as in (H) (N: 5–10 wounds per group, *** $p < 0.001$, Student's t-test, mean ± SD are depicted, scale bars = 100 µm). H3cit, citrullinated histone H3; MPO, myeloperoxidase; ROI, region of interest; SPF, specific pathogen-free.

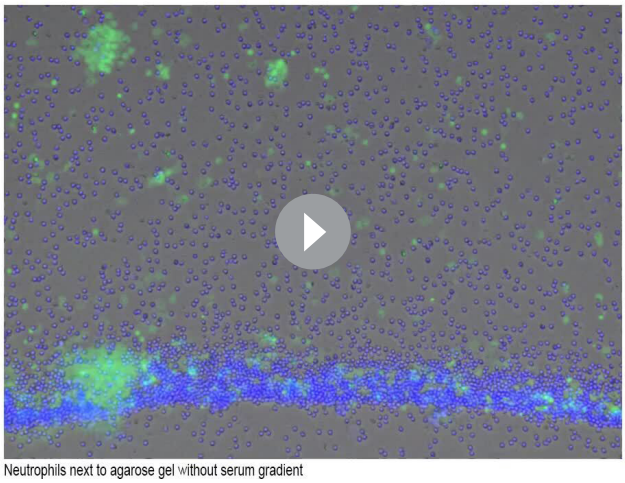
Neutrophils next to agarose gel without serum gradient

Video 2 Neutrophils were cultured in RPMI supplemented with 2 % autologous serum in culture dishes previously prepared with an agarose gel in the centre prepared without autologous serum as control. The edge of the gel was imaged by live-cell microscopy (37 °C, 5 % CO_2). This video displays high cellular densities at the gel edge, with only low amount of NET formation. Video time course 12 hours.

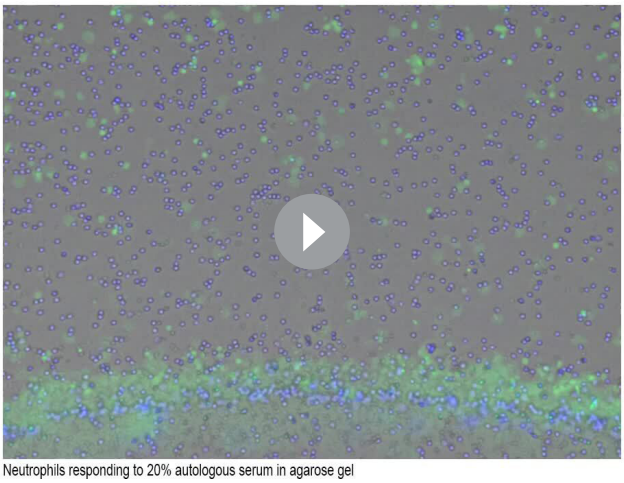
Neutrophils responding to 20% autologous serum in agarose gel

Video 3 Neutrophils were cultured in RPMI supplemented with 2 % autologous serum in culture dishes previously prepared with an agarose gel in the centre containing 20 % autologous serum. The edge of the gel was imaged by live-cell microscopy (37 °C, 5 % CO_2). This video displays neutrophils in high cellular densities at the edge of the serum-containing agarose gel which preferentially form NETs at the edge of the gel. Video time course 12 hours.

We then devised *in vitro* systems to assess the interaction of neutrophils with preformed blood clots. First, we induced a blood clot on glass cover slips (online supplemental figure 4A, B). We then applied neutrophil suspensions to a punched hole. Interestingly, neutrophils accumulated at the edge of the sterile blood clot and formed NETs as evidenced by decondensed chromatin and H3cit (online supplemental figure 4B), even in the absence of microorganisms. Over time, the blood clot destabilised and hampered further functional analyses and imaging. We asked whether soluble factors might activate this neutrophil response. Thus, an agarose gel loaded with 20 % autologous serum was created in culture dishes (online supplemental figure 4C). Addition of neutrophil suspensions led to an accumulation of neutrophils at the edge of the agarose gel. At the edge, neutrophils in high cellular densities extruded decondensed chromatin (online supplemental figure 4D) in response to autologous serum (videos 2 and 3). Inhibition of PADs by BB-Cl-amidine did not hamper accumulation of neutrophils at the edge of the agarose gel (online supplemental figure 4DE, video 4). However, NET formation was abrogated, when PADs were inhibited, irrespective of the use of native or heat-inactivated serum (online supplemental figure 4FG, videos 3–6). Hence, neutrophils respond to coagulated blood and form PAD-dependent NETs at high cellular densities in response to soluble factors, even in the absence of microbiota.

PAD4-mediated immunothrombosis controls mucosal haemostasis in acute DSS-induced colitis

The formation of immunothrombi is not limited to physically inflicted mucosal wounds. We also observed neutrophil aggregation and NETs in the course of chemical damage to the colonic mucosa. We employed the acute DSS-induced model of colitis, which features epithelial erosions and bleeding. H&E staining of colon sections shows the marked infiltration of leucocytes to the bowel wall and an abundance of granulocytes in the lumen (figure 7A). Specifically, in the lumen in direct proximity to blood, large amounts of MPO^+ neutrophils can be detected (figure 7B). Immunoblots were performed, which detected the increased presence of H3cit in the inflamed colon on day 8 of acute DSS-induced colitis (figure 7C and D). In line with analyses of human tissues, we found MPO^+ neutrophil aggregates and H3cit preferentially on the surfaces of ulcerated mucosae (figure 7E). To assess the functional role of PAD4-mediated immunothrombosis in this model, we again made use of PAD4-deficient mice. PAD4-deficient mice featured an aggravated, accelerated course of acute DSS-induced colitis: PAD4-deficient mice suffered from an increased weight loss (figure 7F) and enhanced lethality (figure 7G). Additionally, colon length was reduced (figure 7H). Strikingly, PAD4-deficient mice displayed increased bleeding mucosal ulcerations compared with wild-type counterparts as assessed by endoscopy (figure 7I, video 7). In fact, 96 % of PAD4-deficient mice displayed

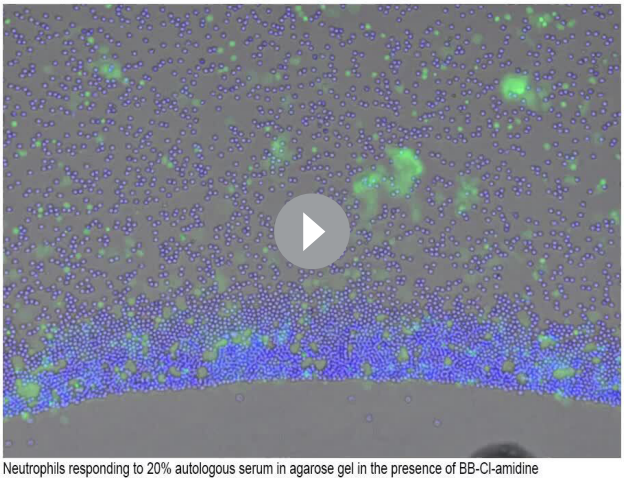
Neutrophils responding to 20% autologous serum in agarose gel in the presence of BB-Cl-amidine

Video 4 Neutrophils were cultured in RPMI supplemented with 2 % autologous serum in culture dishes previously prepared with an agarose gel in the centre containing 20 % autologous serum in the presence of the PAD-inhibitor BB-Cl-amidine (20 µM). The edge of the gel was imaged by live-cell microscopy (37 °C, 5 % CO_2). This video displays neutrophils in high-cellular densities at the clot edge. BB-Cl-amidine blocks NET formation at the edge of the gel. Video time course 12 hours.

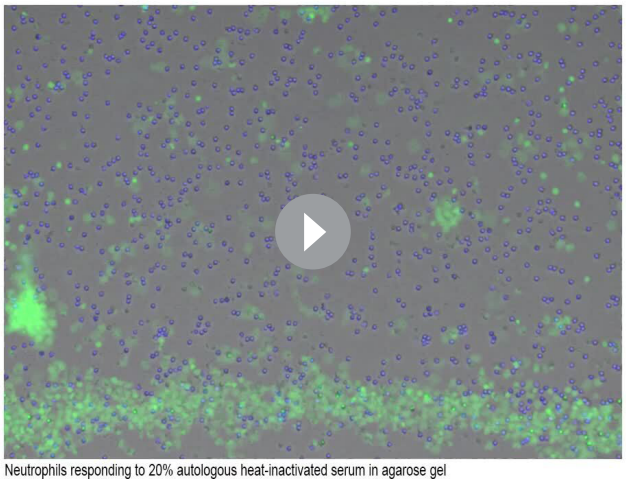

Video 5 Neutrophils were cultured in RPMI supplemented with 2 % autologous serum in culture dishes previously prepared with an agarose gel in the centre containing 20 % heat-inactivated autologous serum. The edge of the gel was imaged by live-cell microscopy (37 °C, 5 % CO_2). This video displays neutrophils in high cellular densities forming NETs at the edge of the gel. Video time course 12 hours.

continued rectal bleeding as compared with 10 % in wild-type littermates (figure 7J). This was also corroborated by complete blood counts: DSS induced a significantly more pronounced reduction in haematocrit (figure 7K) and haemoglobin levels in PAD4-deficient mice as compared with wild-type controls (figure 7L). Analyses of sections of the distal colon demonstrated that DSS treatment led to a severe disruption of the epithelial surface and often a complete loss of the crypt architecture of the mucosa. These severe mucosal changes were more extensive in colons of PAD4-deficient mice as compared with wild-type (online supplemental figure 5AB). In analyses by immunofluorescence, we observed that wild-type mice mostly showed intact

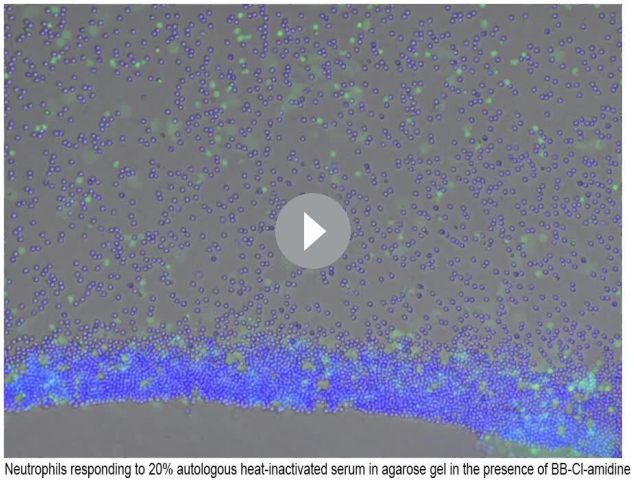

Video 6 Neutrophils were cultured in RPMI supplemented with 2 % autologous serum in culture dishes previously prepared with an agarose gel in the centre containing 20 % heat-inactivated autologous serum in the presence of the PAD-inhibitor BB-Cl-amidine (20 µM). The edge of the gel was imaged by live-cell microscopy (37 °C, 5 % CO_2). This video displays neutrophils in high cellular densities at the edge of the gel. BB-Cl-amidine blocks NET formation at the edge of the gel. Video time course 12 hours.

mucosal surfaces. PAD4-deficient samples, however, showed more areas denuded of epithelium as visualised by β-catenin and E-cadherin staining (online supplemental figure 5C). In acute DSS-induced colitis, we noted that wound-associated epithelia begin to cover areas with crypt loss. Interestingly, the disturbed remodelling of the ulcerated surface and disrupted immunothrombosis in PAD4-deficient mice hampered epithelial restitution by wound-associated epithelial cells (online supplemental figure 5DE): Significantly less distorted mucosa was covered by wound-associated epithelia in the absence of PAD4. Specified wound-associated epithelial cells characterised by the elevated expression of claudin-4 form at the edge of the residual epithelial lining and bridge the ulcerated surface over time. The length of the claudin-4-positive layer of wound-associated epithelia at the edge of forceps-induced colonic wounds was reduced in PAD4-deficient mice as compared with wild-type (online supplemental figure 5F, G). Additionally, we assessed the composition of myeloid cells which infiltrate the bowel wall in the course of DSS-induced colitis by flow cytometry and immunofluorescence. Here, $CD11b^{+}Ly6C^{hi}$ and $CD11b^{+}Ly6C^{lo}$ myeloid cells, eosinophils and neutrophils characterise the inflammatory infiltrate. However, this approach misses neutrophils in the colon lumen (figure 7A and B, online supplemental figure 6A, B). Both PAD4-deficient and wild-type neutrophils robustly migrate to the intestinal lamina propria and are abundant in the colon lumen in the course of DSS-induced colitis. MPO immunofluorescence of cross-sections takes luminal neutrophils into account and demonstrated a significant increase of infiltrating neutrophils in $PAD4^{-/-}$ mice (online supplemental figure 6C) versus wild-type control. Overall, $PAD4^{-/-}$ mice displayed more infiltrating neutrophils as a consequence of increased mucosal ulcerations in these mice.

PAD4 affects clot remodelling by reducing serpin activity resulting in a mature immunothrombus covalently cross-linked by transglutaminases

The effect of PAD4 on enhanced stability of immunothrombi may be attributed in part to chromatin of NETs. We thus asked whether DNase I-treatment might recapitulate the observations of PAD4-deficiency in DSS-induced colitis. Daily administration of DNase I in the course of acute DSS-induced colitis did not significantly alter clinical parameters of disease severity: Weight loss (online supplemental figure 7A), colon length (online supplemental figure 7B) and the fraction of mice with rectal bleeding were unaffected by this intervention (online supplemental figure 7C). On the microscopic level, a slight protection from colonic ulceration was observed in DNase I-treated mice (online supplemental figure 7DE). We further characterised the kinetics of DNase I-mediated digestion of colonic immunothrombi. Colonic immunothrombi picked from colonic wounds and NETs generated from isolated neutrophils were subjected to DNase I treatment *in vitro* (online supplemental figure 6F): While NETs generated from isolated neutrophils were quickly dismantled by DNase I in the course of 90 min, DNase I-mediated digestion of colonic immunothrombi was less efficient. After 20 hours, a reduction in DNA^{SYTOX} was noted in DNase I-treated immunothrombi. However, DNase I did not dismantle the clot and Hoechst could still bind the immunothrombus. Thus, DNase I treatment does not phenocopy PAD4-deficient mice in the DSS-induced colitis model and only inefficiently digests colonic immunothrombi.

We further assessed PAD4-mediated functions beyond chromatin decondensation in our models. PAD4 has been shown to

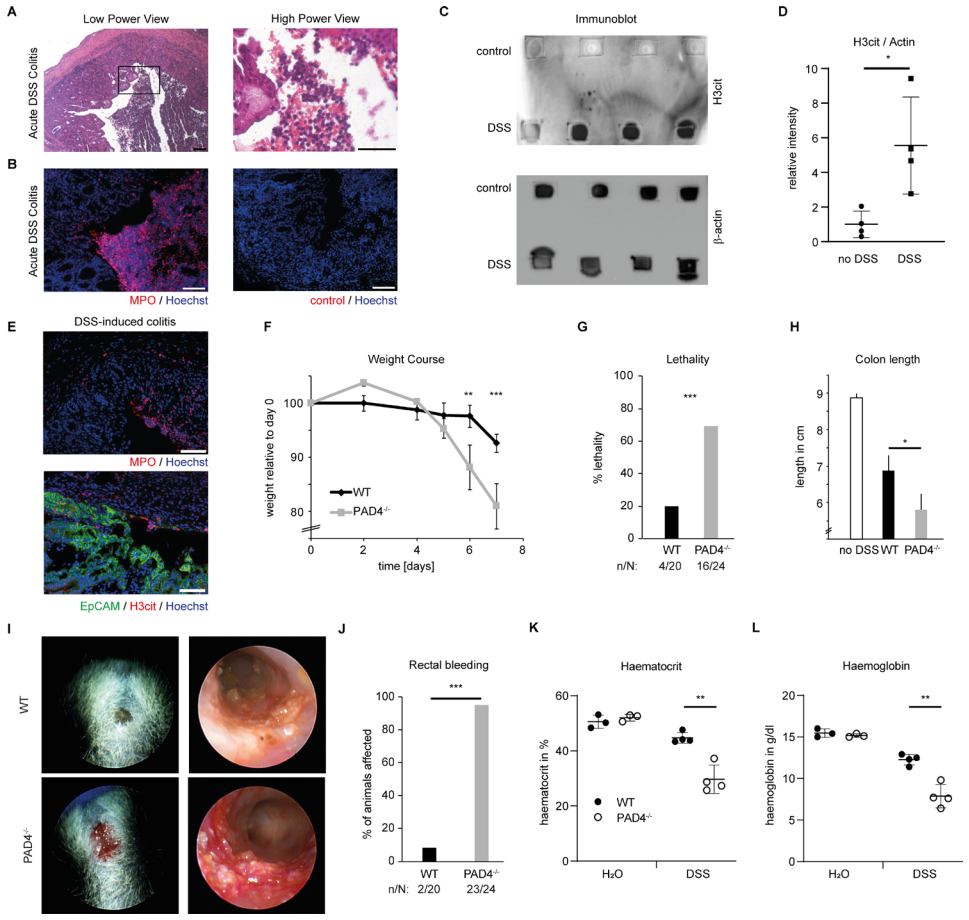

Figure 7 PAD4-mediated immunothrombosis controls mucosal haemostasis in acute DSS-induced colitis. Acute colitis was induced in mice by 4 % DSS in the drinking water for 7 days. (A) H&E staining and (B) immunofluorescence of MPO of murine colonic wounds at day 9 shows a massive destruction of the epithelial cell layer with abundant neutrophils in the colon lumen (scale bars = 100 µm). (C) Colon tissue lysates from day 9 of acute DSS-induced colitis and untreated controls were analysed by an immuno-dot blot technique. The amount of citrullinated histone H3 and hence PAD activity is markedly increased under inflammatory conditions. β–actin immunoblot serves as a loading control (representative of 3 independent experiments with a total of n = 12 samples). (D) Semiquantitative image density analyses of immuno-dot blots as in (C) reveal a significantly higher H3cit expression in DSS-colitis tissue compared with healthy tissue (* $p < 0.05$, Student's t test). (E) Immunofluorescence of MPO (top), EpCAM and H3cit (bottom) performed on cryosections of colonic tissue samples derived from day 9 of acute DSS-induced colitis (4 %) shows the increased presence of MPO in the inflamed mucosa with H3cit restricted to the eroded area with a breached epithelial lining (as seen by lack of EpCAM staining (top part of the lower micrograph)) (representative of n > 10 samples, scale bar = 100 µm). (F) Weight (in %) of mice subjected to 4 % DSS in the drinking water was measured during the course of the experiments comparing PAD4-deficient ($PAD4^{-/-}$) mice and PAD4-proficient littermates (WT). Please appreciate the accelerated weight loss in $PAD4^{-/-}$ mice. (G) Lethality of mice, interpreted by the number of mice suffering a weight loss of > 20 %, was strongly increased in the $PAD4^{-/-}$ group (*** $p < 0.001$, Fisher's two-tailed exact test). (H) At the time of sacrifice, colon length of mice was measured. A reduced length is typical of increased inflammation. A reduced colon length was observed in $PAD4^{-/-}$ mice as compared with WT littermates after DSS treatment. (I) Rectal bleeding is a typical hallmark of severe acute DSS-induced colitis, detectable on both clinical assessment (left) and on analyses by endoscopy of affected mice (right). This was evident more often in $PAD4^{-/-}$ mice. (J) The number of mice suffering from persistent rectal bleeding was strongly increased in $PAD4^{-/-}$ mice subjected to DSS as compared with wild-type littermates (*** $p < 0.001$, Fisher's two tailed exact test, n: number of mice suffering from rectal bleeding, N: total number of mice studied). Complete blood count was performed on day 10 of DSS-induced colitis. (K) Haematocrit and (L) haemoglobin were measured in the blood of WT and $PAD4^{-/-}$ mice subjected to drinking water containing DSS or not (H_2O). when subjected to DSS, $PAD4^{-/-}$ mice exhibited significantly more blood loss than WT mice, whereas untreated mice showed no differences (** $p < 0.01$, Student's t test). DSS, dextrane sodium sulfate; MPO, myeloperoxidase; PAD, peptidyl-arginine deiminase; WT, wild-type.

inhibit serine protease inhibitors by inactivating core P1 arginine residues in the reactive centre loop of multiple serpins[28] with complex theoretical consequences to the coagulation and fibrinolysis cascade (online supplemental figure 8A). Indeed, *in vitro* studies showed the inhibition of α2-antiplasmin and increased plasmin activity in the presence of PAD4 (online supplemental figure 8B). We analysed the net effect of PAD4 downstream of coagulation and fibrinolysis by assessment of D-dimers in colonic wounds. Interestingly, the relative amount of D-dimers was significantly reduced in PAD4-deficient wounds as compared with wild-type controls (online supplemental figure 8C). D-dimer formation requires cross-linking of fibrin by transglutaminases, for example, FXIIIa (online supplemental figure 8D). We thus assessed, whether PAD4 alters the amount of transglutaminase activity in colonic wounds. We injected a biotin-labelled transglutaminase substrate prior to wounding in both

Video 7 Proctoscopy was performed in mice on day 7 of acute DSS-induced colitis (4 %) and monitored by video-endoscopy. Please appreciate the increased rectal bleeding and increased amount of ulcerations in PAD4$^{-/-}$ mice as compared with controls.

wild-type and PAD4-deficient mice and assessed transglutaminase activity in immunothrombi by streptavidin-linked fluorescence microscopy. Transglutaminase activity in immunothrombi on colon wounds was significantly reduced in the absence of PAD4 (online supplemental figure 8E, F).

Taken together, neutrophils make use of PAD4 to stabilise the eroded surface in part by NETs and by the remodelling and maturation of the fibrin clot and thus favour epithelial restitution.

DISCUSSION

Rectal bleeding and bloody diarrhoea are major hallmarks of acute flares of UC.[29] Early mucosal healing is a valuable goal to improve long-term clinical outcomes[30] but initiation of mucosal healing in ulcerative lesions remains elusive. In this study, we uncovered a role for neutrophils and PAD4 in controlling rectal bleeding and regulating mucosal haemostasis in human IBD and experimental models of disease. Our endoscopic and microscopic studies in human UC show that successful haemostasis is associated with remodelling of blood clots[31] to fibrin layers as an important step towards mucosal healing. Remodelling of the wound surface is guided by innate immune cells, mostly neutrophils. We thus propose the term immunothrombus to define a blood clot which has been remodelled by innate immune cells.[17] We identified extracellular chromatin, aggregated neutrophils and PAD4 activity in immunothrombi, which cover mucosal ulcerations and erosions in UC. Erosions, ulcerations, blood, neutrophils and fibrin are positively associated with severe disease.[32 33] However, we observed that blood/haematin coverage of erosions rather than fibrin coverage is associated with rectal bleeding, consistent with the role of fibrin as a protective emergency barrier. This reconciles these seemingly paradox observations: fibrin and neutrophil-rich immunothrombi occur in severe disease, yet provide protection in this setting by stabilising the damaged mucosa and successfully achieving haemostasis before epithelial restitution can occur.

We closely studied the kinetics of mucosal injury over time in mice.[25 34] We detected that blood clots are remodelled in the course of hours to whitish immunothrombi by innate immune cells with highly prevalent neutrophils and PAD4-dependent NETs. In line with a protective function of PAD4-mediated NETs and immunothrombosis, PAD4-deficient mice suffered from an aggravated course of acute DSS-induced colitis with marked rectal bleeding and consecutively reduced haematocrit and haemoglobin levels. This further corroborated the role of PAD4 to support mucosal haemostasis and control rectal bleeding in colitis. Commensal bacteria are capable of infiltrating immunothrombi to a certain extent, as observed by fluorescent in-situ hybridisation. While microorganisms may stimulate neutrophils to undergo NET formation under specific settings,[11] especially with regard to possible UC-related pathobionts,[35] our study shows that PAD4 activity and complement activation persist in immunothrombi on colonic wounds, even in the absence of microbiota. In fact, neutrophils were strongly stimulated by coagulated blood and heat-insensitive components of serum to aggregate and form NETs. Neutrophils formed marked PAD4-dependent NETs in high cellular densities[36] at the edges of the clots. Inhibition of PAD enzymes inhibited NET formation in high cellular densities at the edge of serum-containing agarose gels. These observations are in line with previous studies on the role of NETs in various diseases. While initial studies of NETs focused on their role in host defence against microorganisms,[11 13] following studies highlighted the role of NETs in the course of thrombotic diseases[18 37] and noninfectious inflammation.[38–41] In our experiments, deficiency of PAD4 led to a failure to remodel blood clots on the mucosal surface, delayed colonic wound healing and aggravated colitis with a failure to control rectal bleeding. What is the mechanistic role of PAD4 in the remodelling of the blood clot to a stable immunothrombus? PAD4 mediates chromatin decondensation of neutrophils in the course of NET formation as observed in direct proximity to blood clots. Extracellular chromatin of NETs can occlude vessels[42] and may serve as a scaffold for further platelet aggregation[37] and activation of Factor XII.[43] In our experiments, however, DNase I-treatment did not favour rectal bleeding as might have been expected if extracellular chromatin alone was responsible for clot stability. However, DNase I only inefficiently dismantled colonic immunothrombi *in vitro*. As large size, limited penetration of the large immunothrombus as well as DNase-insensitive sodium or calcium salts of DNA[44] might limit DNase I efficacy in this model, an important role of extracellular chromatin in immunothrombi cannot be excluded or suggested by these experiments. Nonetheless, we chose to look for additional effects of PAD4 beyond NET formation. On a molecular level, PAD4 mediates the modification of peptide-bound arginine to citrulline. Apart from effects on the structure of chromatin,[14] the function of various proteases and their inhibitors including serine proteases,[28] metalloproteases[45 46] and calpains[47] is modified by PAD4 and might be of relevance in the process of immunothrombosis.[17 18] In line with findings by Tilvawala *et al*[28] we detected that serine proteases with a central P1 arginine in the reactive centre loop, for example, α2-antiplasmin, were inactivated by PAD4 *in vitro*. Inhibition of multiple serpins of the coagulation/fibrinolysis balance resulted in an overall reduced amount of fibrin turnover in the absence of PAD4. Reduced levels of D-dimers in colonic wounds were detected in PAD4-deficient mice. Interestingly, in the absence of PAD4 transglutaminase activity and thus covalent cross-linking of the immunothrombus by transglutaminases was reduced. This is in line with a model, in which PAD4-mediated inhibition of serpins, for example, antithrombin, is required for effective thrombin-mediated activation of the transglutaminase Factor XIIIa and subsequent stabilisation of the immunothrombus. Analyses of the colon mucosa during DSS-induced colitis demonstrate that epithelial restitution of eroded surfaces is disturbed in the absence of PAD4. Gene expression analyses did not detect *Padi4* in intestinal epithelial cells arguing for an indirect effect of reduced stability of the immunothrombus and the eroded surface in the absence of PAD4 which thus hampers epithelial restitution.

Neutrophils have been observed and studied in colitis for many years: neutrophils have been implicated as drivers of

mucosal inflammation in IBD.[8] Specifically, it has been proposed that NET formation should be therapeutically inhibited.[32 48 49] Infection-induced or autoimmunity-induced overabundance of NET formation or defective clearance may, indeed, damage the host, especially small vessels,[42 50–52] in particular in the presence of UC-associated pathobionts.[35 53] In contrast, mixed results were reported in experimental models studying neutrophil depletion approaches in colitis in the past.[54 55] Phagocyte dysfunction is implicated in the setting of monogenic IBD in childhood.[56] Moreover, neutropenia of diverse origin may result in the development of neutropenic enterocolitis.[57] In the setting of glycogen storage disease type Ib, chronic enteritis may develop that can be successfully treated by G-CSF infusions.[58] This further highlights the protective potential of neutrophils in mucosal inflammation. We provide a novel perspective to this topic by describing the haemostatic function of neutrophils, NETs and immunothrombosis on ulcerations and erosions in active colitis. Our study provides an explanation for the increased bleeding as a consequence of granulocyte depletion, which has been reported previously.[54]

Taken together, we have shown that neutrophils make use of PAD4 to remodel blood clots to immunothrombi on mucosal ulcerations rich in NETs. Immunothrombi function as an emergency barrier in the setting of epithelial disruption. Our findings indicate that PAD4-dependent immunothrombi support mucosal wound healing and prevent bleeding of ulcers in severe IBD. Thus, these data suggest that the neutrophil response in active UC should be carefully balanced, rather than completely abrogated.

Author affiliations
[1]Medical Clinic 1, University Clinic, Friedrich Alexander University, Erlangen, Germany
[2]Deutsches Zentrum Immuntherapie, Erlangen, Germany
[3]Medical Clinic 3, University Clinic, Friedrich Alexander University, Erlangen, Germany
[4]Institute of Pathology, University Medical Center, Mainz, Germany
[5]Friedrich Alexander University, Institute of Pathology, Klinikum Bayreuth, Erlangen, Germany
[6]Charité - Universitätsmedizin Berlin, Corporate Member of Freie Universität Berlin and Humboldt-Universität zu Berlin, Berlin, Germany
[7]Institute for Laboratory Animal Science, Hannover Medical School, Hannover, Germany

Contributors ML, AL, SG, SP, DR, CS, FM and EL performed experiments. ML drafted the manuscript. SF, SZ, RA, AAK, AB and MV provided valuable samples and advice for this study. ML, MFN and MH designed the study and all authors edited the manuscript. ML serves as the guarantor responsible for the overall content of this manuscript.

Funding This work has been supported by the Deutsche Forschungsgemeinschaft (BE3686/2-1, KFO 257 CEDER, FOR 2438, TRR241 (A03, B04, C04, INF), CRC 1181 (B02, C02, C03, C05), SPP1656, SCHA 2040/1-1), the German Bundeswirtschaftsministerium (Grant-No. ZF4010106MD9) and the Interdisciplinary Center for Clinical Research (IZKF) of the University Erlangen-Nuremberg (J63, J68).

Competing interests None declared.

Patient consent for publication Not applicable.

Provenance and peer review Not commissioned; externally peer reviewed.

Data availability statement Data are available in a public, open access repository. Data sharing not applicable as no datasets generated and/or analysed for this study. Data are available upon reasonable request. All data relevant to the study are included in the article or uploaded as supplementary information. All data relevant to the study are included in the article or uploaded as supplementary information.RNAseq studies are made available in a public, open access repository (Accession: E-MTAB-10824). Additional data are available upon reasonable request.

ORCID iDs
Moritz Leppkes http://orcid.org/0000-0003-2311-090X
Sebastian Zundler http://orcid.org/0000-0003-0888-2784
Clemens Neufert http://orcid.org/0000-0003-1418-7921
Christoph Becker http://orcid.org/0000-0002-1388-1041
Markus F Neurath http://orcid.org/0000-0003-4344-1474

REFERENCES

1 Truelove SC, Witts LJ. Cortisone in ulcerative colitis; preliminary report on a therapeutic trial. *Br Med J* 1954;2:375–8.
2 Samuel S, Ingle SB, Dhillon S, *et al*. Cumulative incidence and risk factors for hospitalization and surgery in a population-based cohort of ulcerative colitis. *Inflamm Bowel Dis* 2013;19:1858–66.
3 Robert JH, Sachar DB, Aufses AH, *et al*. Management of severe hemorrhage in ulcerative colitis. *Am J Surg* 1990;159:550–5.
4 Kaser A, Zeissig S, Blumberg RS. Inflammatory bowel disease. *Annu Rev Immunol* 2010;28:573–621.
5 Neurath MF, Leppkes M. Resolution of ulcerative colitis. *Semin Immunopathol* 2019;41:747–56.
6 Ananthakrishnan AN, Bernstein CN, Iliopoulos D, *et al*. Environmental triggers in IBD: a review of progress and evidence. *Nat Rev Gastroenterol Hepatol* 2018;15:39–49.
7 Schroeder BO, Birchenough GMH, Ståhlman M, *et al*. Bifidobacteria or fiber protects against diet-induced Microbiota-Mediated colonic mucus deterioration. *Cell Host Microbe* 2018;23:27–40.
8 Fournier BM, Parkos CA. The role of neutrophils during intestinal inflammation. *Mucosal Immunol* 2012;5:354–66.
9 Chin AC, Lee WY, Nusrat A, *et al*. Neutrophil-mediated activation of epithelial protease-activated receptors-1 and -2 regulates barrier function and transepithelial migration. *J Immunol* 2008;181:5702–10.
10 Bennike TB, Carlsen TG, Ellingsen T, *et al*. Neutrophil extracellular traps in ulcerative colitis: a proteome analysis of intestinal biopsies. *Inflamm Bowel Dis* 2015;21:2052–67.
11 Brinkmann V, Reichard U, Goosmann C, *et al*. Neutrophil extracellular traps kill bacteria. *Science* 2004;303:1532–5.
12 Neeli I, Khan SN, Radic M. Histone deimination as a response to inflammatory stimuli in neutrophils. *J Immunol* 2008;180:1895–902.
13 Li P, Li M, Lindberg MR, *et al*. PAD4 is essential for antibacterial innate immunity mediated by neutrophil extracellular traps. *J Exp Med* 2010;207:1853–62.
14 Wang Y, Li M, Stadler S, *et al*. Histone hypercitrullination mediates chromatin decondensation and neutrophil extracellular trap formation. *J Cell Biol* 2009;184:205–13.
15 Hemmers S, Teijaro JR, Arandjelovic S, *et al*. PAD4-mediated neutrophil extracellular trap formation is not required for immunity against influenza infection. *PLoS One* 2011;6:e22043.
16 Knopf J, Leppkes M, Schett G, *et al*. Aggregated nets sequester and detoxify extracellular histones. *Front Immunol* 2019;10:2176.
17 Engelmann B, Massberg S. Thrombosis as an intravascular effector of innate immunity. *Nat Rev Immunol* 2013;13:34–45.
18 Martinod K, Demers M, Fuchs TA, *et al*. Neutrophil histone modification by peptidylarginine deiminase 4 is critical for deep vein thrombosis in mice. *Proc Natl Acad Sci U S A* 2013;110:8674–9.
19 Paine ER. Colonoscopic evaluation in ulcerative colitis. *Gastroenterol Rep* 2014;2:161–8.
20 Haberman Y, Karns R, Dexheimer PJ, *et al*. Ulcerative colitis mucosal transcriptomes reveal mitochondriopathy and personalized mechanisms underlying disease severity and treatment response. *Nat Commun* 2019;10:38.
21 Patankar JV, Müller TM, Kantham S, *et al*. E-type prostanoid receptor 4 drives resolution of intestinal inflammation by blocking epithelial necroptosis. *Nat Cell Biol* 2021;23:796–807.
22 Leppkes M, Lindemann A. Temporal changes in the transcriptome of mouse colonic tissues post biopsy-induced wound generation using RNA seq, 2021. ArrayExpress. Available: http://www.ebi.ac.uk/arrayexpress/experiments/E-MTAB-10824
23 Heng TSP, Painter MW, Immunological Genome Project Consortium. The immunological genome Project: networks of gene expression in immune cells. *Nat Immunol* 2008;9:1091–4.

24 Neurath MF, Wittkopf N, Wlodarski A, *et al*. Assessment of tumor development and wound healing using endoscopic techniques in mice. *Gastroenterology* 2010;139:1837–43.
25 Pickert G, Neufert C, Leppkes M, *et al*. Stat3 links IL-22 signaling in intestinal epithelial cells to mucosal wound healing. *J Exp Med* 2009;206:1465–72.
26 Weigmann B, Tubbe I, Seidel D, *et al*. Isolation and subsequent analysis of murine lamina propria mononuclear cells from colonic tissue. *Nat Protoc* 2007;2:2307–11.
27 Jeong EM, Son YH, Choi Y, *et al*. Transglutaminase 2 is dispensable but required for the survival of mice in dextran sulfate sodium-induced colitis. *Exp Mol Med* 2016;48:e267.
28 Tilvawala R, Nguyen SH, Maurais AJ, *et al*. The rheumatoid arthritis-associated Citrullinome. *Cell Chem Biol* 2018;25:691–704.
29 Lewis JD, Chuai S, Nessel L, *et al*. Use of the noninvasive components of the Mayo score to assess clinical response in ulcerative colitis. *Inflamm Bowel Dis* 2008;14:1660–6.
30 Colombel JF, Rutgeerts P, Reinisch W, *et al*. Early mucosal healing with infliximab is associated with improved long-term clinical outcomes in ulcerative colitis. *Gastroenterology* 2011;141:1194–201.
31 Paul G, Bataille F, Obermeier F, *et al*. Analysis of intestinal haem-oxygenase-1 (HO-1) in clinical and experimental colitis. *Clin Exp Immunol* 2005;140:547–55.
32 Dinallo V, Marafini I, Di Fusco D, *et al*. Neutrophil extracellular traps sustain inflammatory signals in ulcerative colitis. *J Crohns Colitis* 2019;13:772–84.
33 Abd El Hafez A, Mohamed AS, Shehta A, *et al*. Neutrophil extracellular traps-associated protein peptidyl arginine deaminase 4 immunohistochemical expression in ulcerative colitis and its association with the prognostic predictors. *Pathol Res Pract* 2020;216:153102.
34 Leoni G, Neumann P-A, Sumagin R, *et al*. Wound repair: role of immune-epithelial interactions. *Mucosal Immunol* 2015;8:959–68.
35 Saha P, Yeoh BS, Xiao X, *et al*. PAD4-dependent nets generation are indispensable for intestinal clearance of Citrobacter rodentium. *Mucosal Immunol* 2019;12:761–71.
36 Schauer C, Janko C, Munoz LE, *et al*. Aggregated neutrophil extracellular traps limit inflammation by degrading cytokines and chemokines. *Nat Med* 2014;20:511–7.
37 Fuchs TA, Brill A, Duerschmied D, *et al*. Extracellular DNA traps promote thrombosis. *Proc Natl Acad Sci U S A* 2010;107:15880–5.
38 Leppkes M, Maueröder C, Hirth S, *et al*. Externalized decondensed neutrophil chromatin occludes pancreatic ducts and drives pancreatitis. *Nat Commun* 2016;7:10973.
39 Jorch SK, Kubes P. An emerging role for neutrophil extracellular traps in noninfectious disease. *Nat Med* 2017;23:279–87.
40 Guglietta S, Chiavelli A, Zagato E, *et al*. Coagulation induced by C3aR-dependent NETosis drives protumorigenic neutrophils during small intestinal tumorigenesis. *Nat Commun* 2016;7:11037.
41 Muñoz LE, Boeltz S, Bilyy R, *et al*. Neutrophil extracellular traps initiate gallstone formation. *Immunity* 2019;51:443–50.
42 Jiménez-Alcázar M, Rangaswamy C, Panda R, *et al*. Host DNases prevent vascular occlusion by neutrophil extracellular traps. *Science* 2017;358:1202–6.
43 von Brühl M-L, Stark K, Steinhart A, *et al*. Monocytes, neutrophils, and platelets cooperate to initiate and propagate venous thrombosis in mice in vivo. *J Exp Med* 2012;209:819–35.
44 Douvas A, Price PA. Some effects of calcium and magnesium ions on the activity of bovine pancreatic deoxyribonuclease a. *Biochim Biophys Acta* 1975;395:201–12.
45 Boon L, Ugarte-Berzal E, Martens E, *et al*. Citrullination as a novel posttranslational modification of matrix metalloproteinases. *Matrix Biol* 2021;95:68-83.
46 Sorvillo N, Mizurini DM, Coxon C, *et al*. Plasma peptidylarginine deiminase IV promotes VWF-platelet string formation and accelerates thrombosis after vessel injury. *Circ Res* 2019;125:507–19.
47 Göβwein S, Lindemann A, Mahajan A, *et al*. Citrullination licenses calpain to decondense nuclei in neutrophil extracellular trap formation. *Front Immunol* 2019;10:2481.
48 Li T, Wang C, Liu Y, *et al*. Neutrophil extracellular traps induce intestinal damage and thrombotic tendency in inflammatory bowel disease. *J Crohns Colitis* 2020;14:240–53.
49 Chumanevich AA, Causey CP, Knuckley BA, *et al*. Suppression of colitis in mice by Cl-amidine: a novel peptidylarginine deiminase inhibitor. *Am J Physiol Gastrointest Liver Physiol* 2011;300:G929–38.
50 Leppkes M, Knopf J, Naschberger E, *et al*. Vascular occlusion by neutrophil extracellular traps in COVID-19. *EBioMedicine* 2020;58:102925.
51 Zuo Y, Yalavarthi S, Shi H, *et al*. Neutrophil extracellular traps in COVID-19. *JCI Insight* 2020;5.
52 Meng H, Yalavarthi S, Kanthi Y, *et al*. In vivo role of neutrophil extracellular traps in antiphospholipid antibody-mediated venous thrombosis. *Arthritis Rheumatol* 2017;69:655–67.
53 Bücker R, Schulz E, Günzel D, *et al*. α-Haemolysin of escherichia coli in IBD: a potentiator of inflammatory activity in the colon. *Gut* 2014;63:1893–901.
54 Kühl AA, Kakirman H, Janotta M, *et al*. Aggravation of different types of experimental colitis by depletion or adhesion blockade of neutrophils. *Gastroenterology* 2007;133:1882–92.
55 Natsui M, Kawasaki K, Takizawa H, *et al*. Selective depletion of neutrophils by a monoclonal antibody, RP-3, suppresses dextran sulphate sodium-induced colitis in rats. *J Gastroenterol Hepatol* 1997;12:801–8.
56 Uhlig HH, Schwerd T, Koletzko S, *et al*. The diagnostic approach to monogenic very early onset inflammatory bowel disease. *Gastroenterology* 2014;147:990–1007.
57 Gorschlüter M, Mey U, Strehl J, *et al*. Neutropenic enterocolitis in adults: systematic analysis of evidence quality. *Eur J Haematol* 2005;75:1–13.
58 Volz MS, Nassir M, Treese C, *et al*. Inflammatory bowel disease (IBD)-like disease in a case of a 33-year old man with glycogenosis 1b. *BMC Gastroenterol* 2015;15:45.

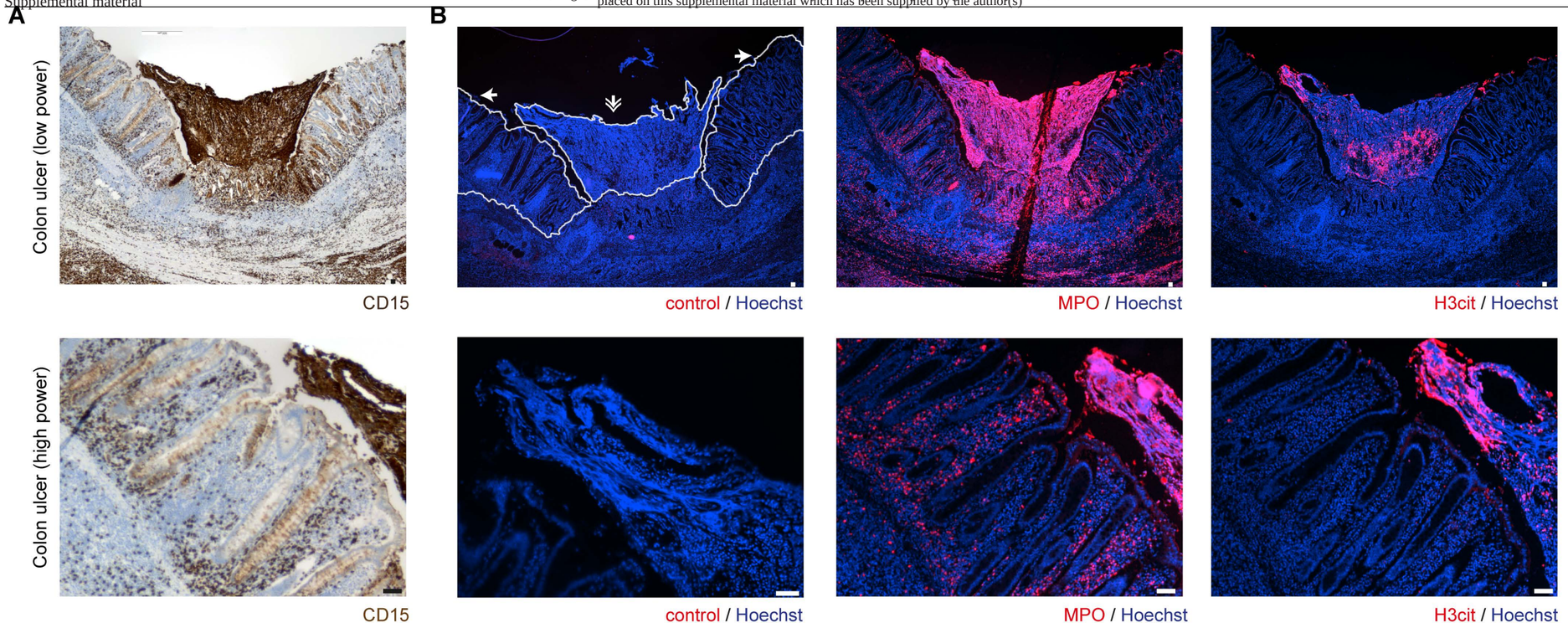

Supplementary Figure 1: Intercryptal lamina propria neutrophils mostly do not display PAD activity

(A) Low power (top) and high power (bottom) view of a human colon ulcer analysed for the presence of CD15 (DAB) and **(B)** myeloperoxidase (MPO), citrullinated histone H3 (H3cit) and. Note the broadly dispersed MPO in the fibrin layer, while MPO is also present in singly dispersed cells in the lamina propria. H3cit is strongly present in the fibrin layer whereas neutrophils in the intercryptal lamina propria are rather H3cit-negative. Please appreciate the decondensed chromatin in immunothrombi (scale bars = 100 µm) **(C)** Immunopositive cells in the intercryptal lamina propria as in (A–B) were quantified, displaying significantly less H3cit-positive cells in the intercryptal space, while MPO^+ and $CD15^+$ cells can be found in ample amounts (n = 10 samples, ** $p < 0.01$, Student's t-test).

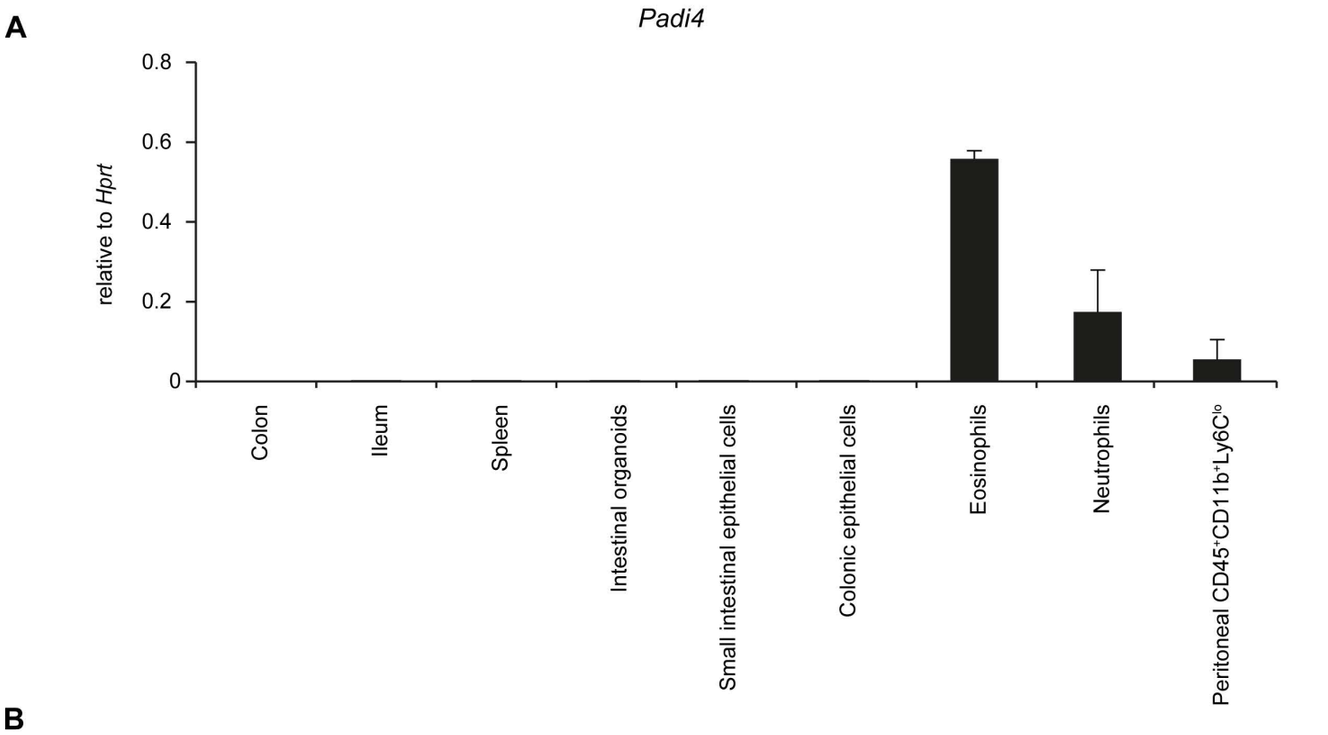
A
Padi4
relative to Hprt
0.8
0.6
0.4
0.2
0
Colon
Ileum
Spleen
Intestinal organoids
Small intestinal epithelial cells
Colonic epithelial cells
Eosinophils
Neutrophils
Peritoneal CD45+CD11b+Ly6Clo

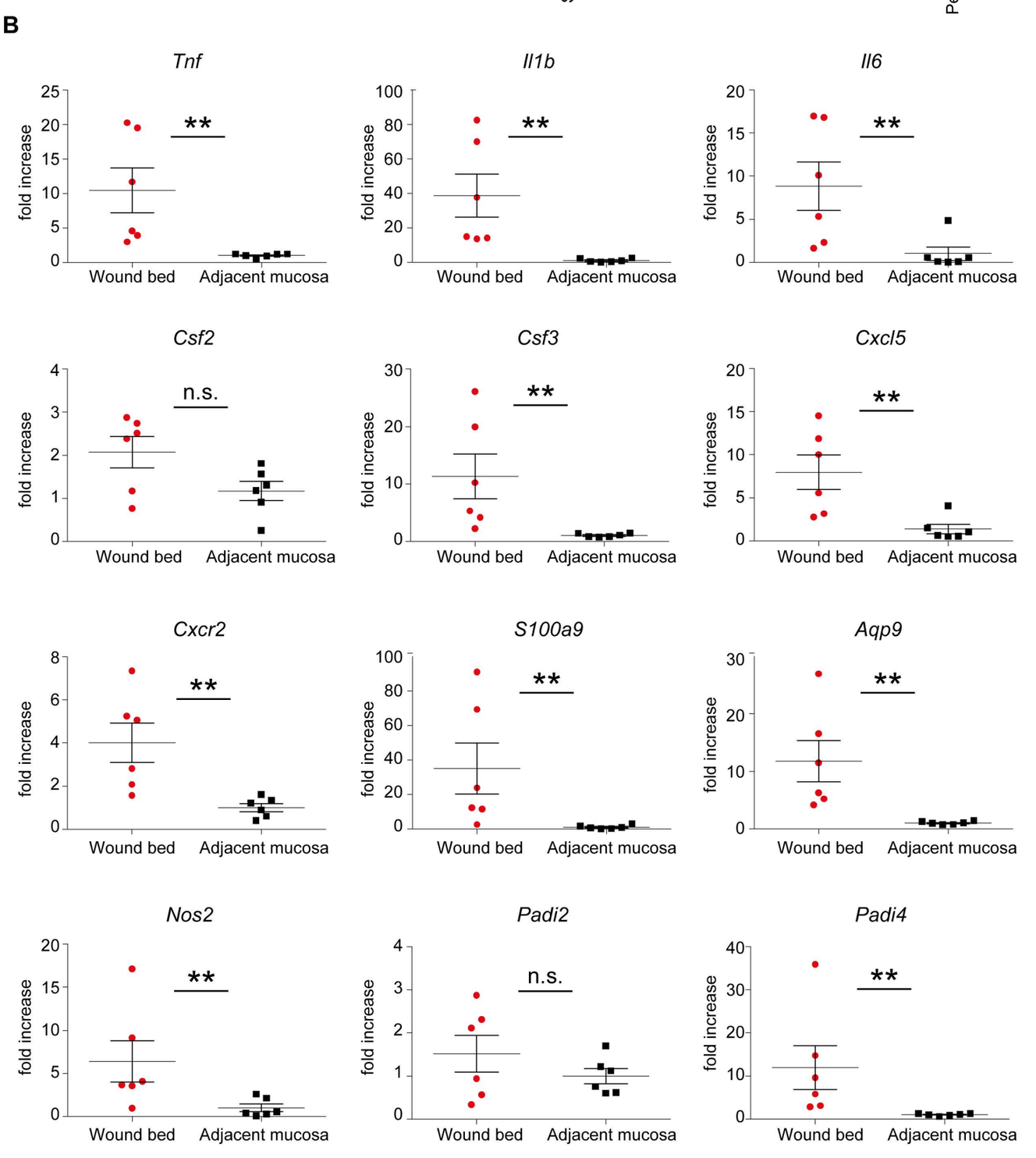
B
Tnf
Il1b
Il6
Csf2
Csf3
Cxcl5
Cxcr2
S100a9
Aqp9
Nos2
Padi2
Padi4
fold increase
Wound bed
Adjacent mucosa
**
n.s.

Supplementary Figure 2: *Padi4* is expressed in myeloid cells, predominantly granulocytes and is significantly increased in the colon wound bed

(A) RT-PCR analyses show a prevailing expression of *Padi4* in neutrophils and eosinophils and to a smaller extent in peritoneal Ly6C-low monocytes, whereas no expression of *Padi4* was detected in whole colon or ileum, isolated epithelial cells, spleen or intestinal organoids. **(B)** Analysis of mRNA expression of selected neutrophil- and inflammation-related genes in forceps-induced colonic wound beds and adjacent healthy mucosa was performed at 24 hours post-injury, displaying markedly increased abundance of neutrophil- and inflammation-related transcripts (at least n = 6 samples per group (** $p < 0.01$, Student's t-test, mean + SEM are depicted).

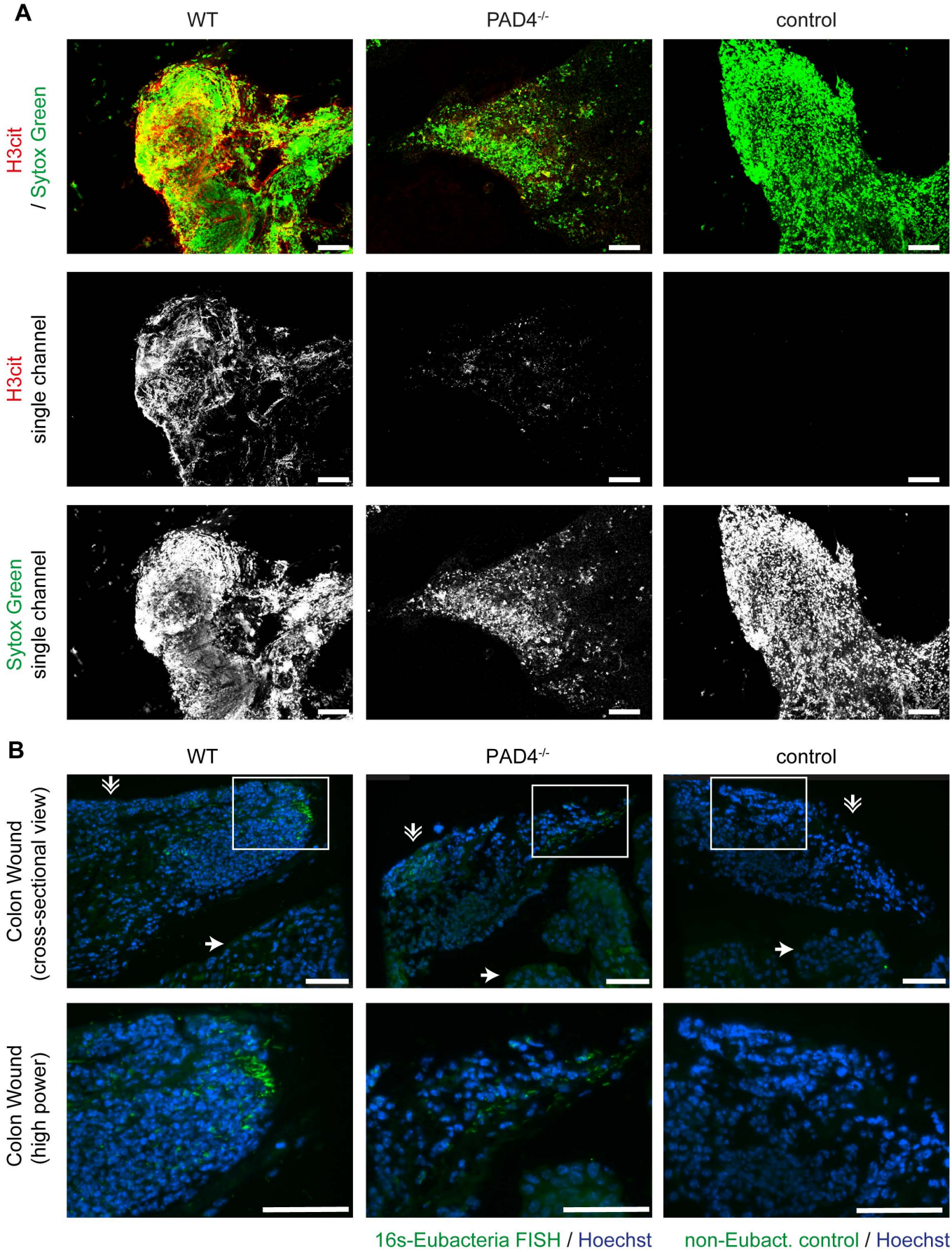
A
WT
PAD4-/-
control
H3cit / Sytox Green
H3cit single channel
Sytox Green single channel
B
WT
PAD4-/-
control
Colon Wound (cross-sectional view)
Colon Wound (high power)
16s-Eubacteria FISH / Hoechst
non-Eubact. control / Hoechst

Supplementary Figure 3: PAD4-deficient mice fail to adequately decondense neutrophil chromatin in immunothrombi on mucosal wounds

(A) Manually grasped immunothrombi from colon wounds were subjected to immunofluorescence. Decondensed chromatin is a striking feature in immunothrombi as evidenced by SYTOX Green staining. We detected H3cit throughout the immunothrombus, which is strongly diminished in fibrinoid derived from PAD4$^{-/-}$ mice. **(B)** Cross-sections of colon wounds were subjected to fluorescent *in-situ* hybridisation using 16S-rRNA-Eubacteria directed probes. The immunothrombi of both wild-type and PAD4$^{-/-}$ mice (indicated by the double-head arrow) was infiltrated by bacteria, while none were detected in deeper layers of the mucosa (the ulcer edge is highlighted by a single head arrow). Low power and high power magnification are presented. (Scale bars = 100 µm).

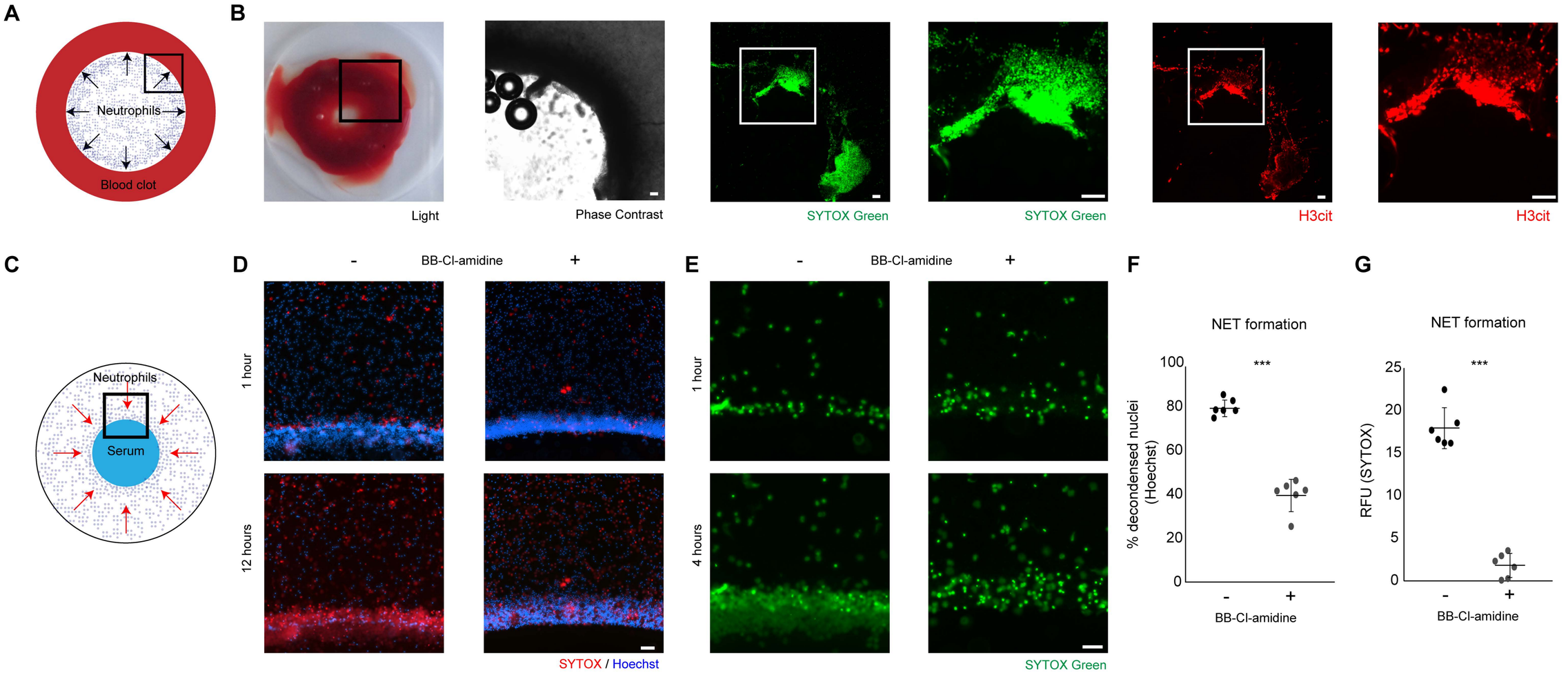

Supplementary Figure 4: PAD4-mediated NET formation is instigated in high cellular densities at the edge of a blood clot in the absence of bacteria

(A) Human citrated whole blood was clotted by recalcification. 2×10^5 isolated human neutrophils were cultured in autologous serum and added to the punched-out center of the clot (31 mm², scale bar = 2 mm). **(B)** This setup was analysed by brightfield (left) and immunofluorescence: Decondensed SYTOX Green$^+$ (center) and H3cit$^+$ chromatin (right) was preferentially formed at the edge of the blood clot as depicted in representative photomicrographs. Scale bars = 100 µm. **(C–G)** Human neutrophils were cultured in RPMI medium supplemented with 2 % autologous serum in the presence and absence of the pan-PAD inhibitor BB-Cl-amidine (20 µM) or solute control in a well prepared with an agarose gel in the center containing 20 % autologous serum. **(C)** A graphic model of this experimental setup is presented. The black box represents a typical field of view as presented in D, E. **(D)** The edge of the surrogate clot is presented at two different time points after stimulation in the presence and absence of the PAD inhibitor BB-Cl-amidine. Hoechst shows all nucleated cells in blue, while SYTOX Green staining of extracellular DNA and permeable cells is depicted in red, representative images of three independent experiments. Please appreciate the increased presence of condensed chromatin at the edge of the clot in the presence of the pan-PAD inhibitor, whereas more chromatin is decondensed in its absence. Scale bars = 100 µm. **(E)** The SYTOX Green channel of this experimental setup is displayed after 1 and 4 hours. Please appreciate the strongly reduced chromatin decondensation at the edge of the clot in the presence of BB-Cl-amidine. Scale bars = 100 µm. **(F)** NET formation was quantified in images as depicted in (D, E) by quantification of decondensed nuclei at the clot edge using the Hoechst signal and **(G)** by use of fluorescence intensity quantification of the SYTOX signal (*** $p < 0.001$, Student's t-test, three independent experiments reported). Scale bars = 100 µm.

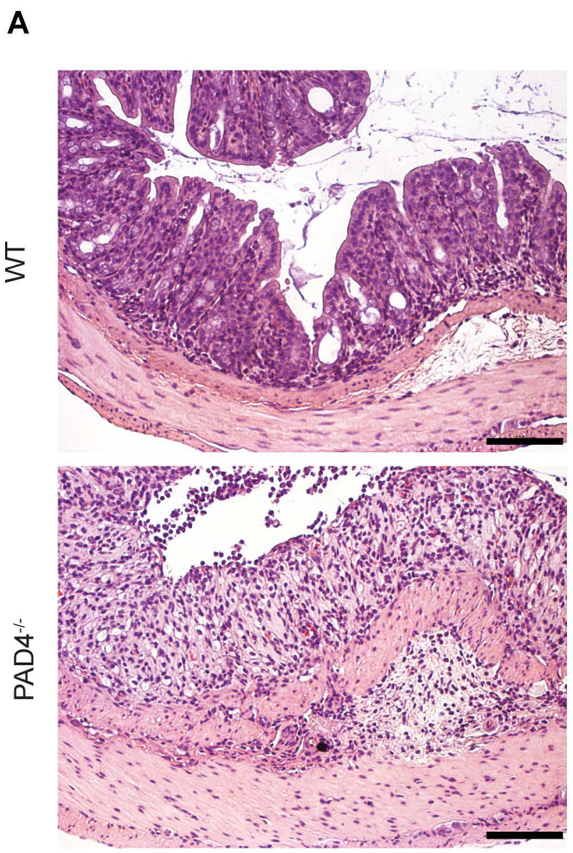
A
WT
PAD4-/-
H&E

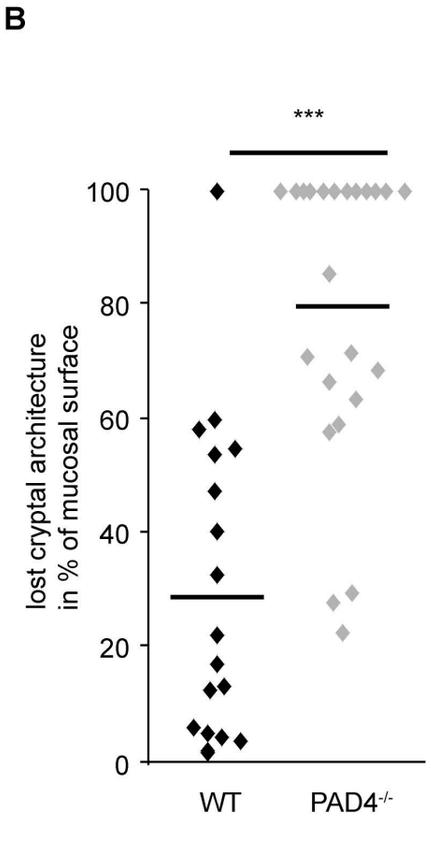
B
***
lost cryptal architecture in % of mucosal surface
100
80
60
40
20
0
WT
PAD4-/-

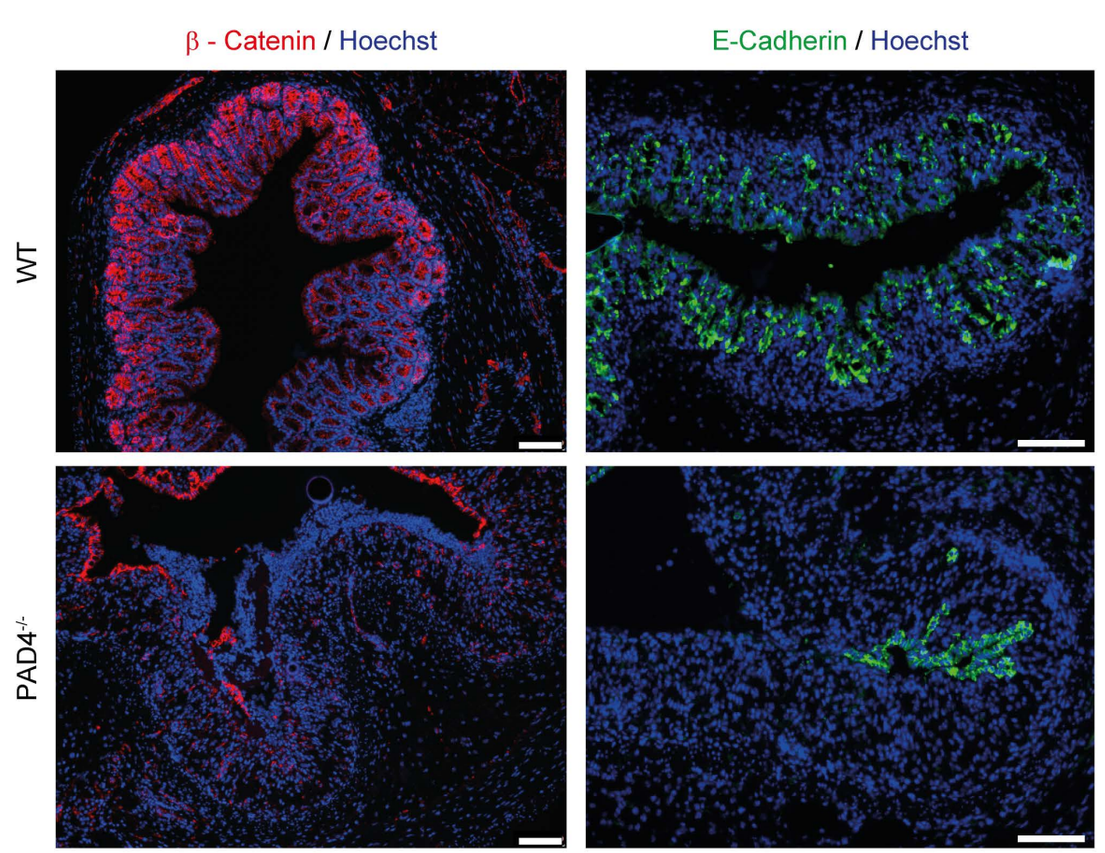
C
β - Catenin / Hoechst
E-Cadherin / Hoechst
WT
PAD4-/-

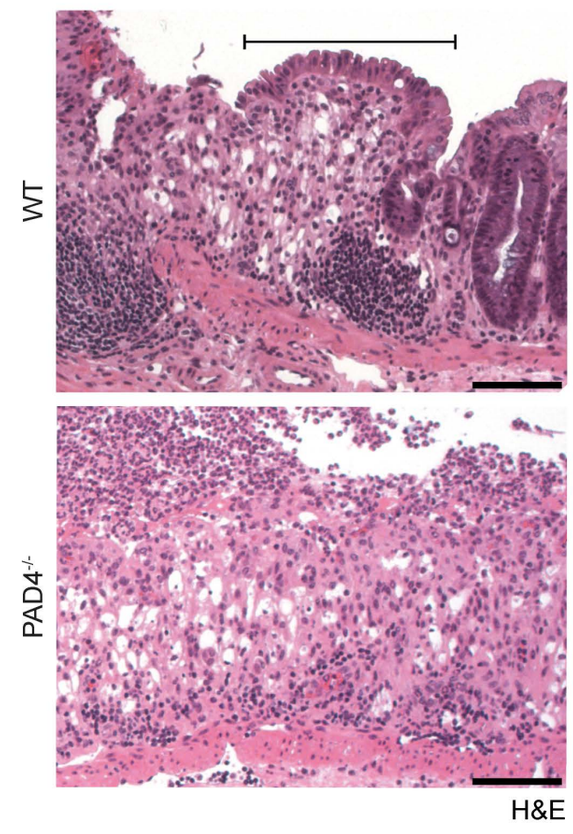
D
WT
PAD4-/-
H&E

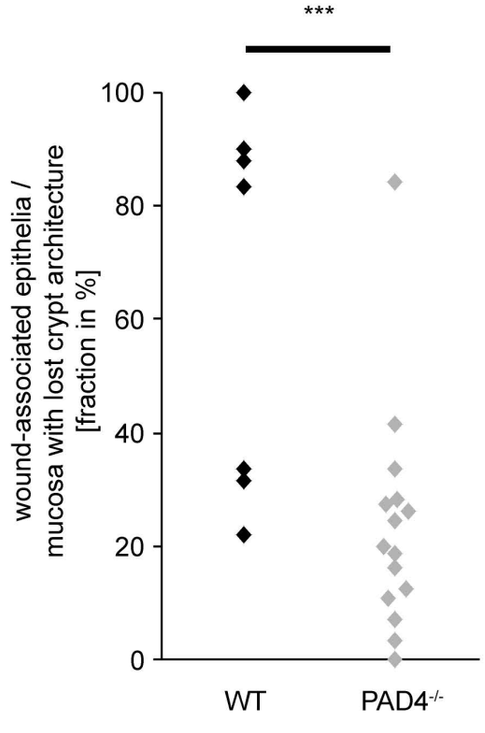
E
***
wound-associated epithelia / mucosa with lost crypt architecture [fraction in %]
100
80
60
40
20
0
WT
PAD4-/-

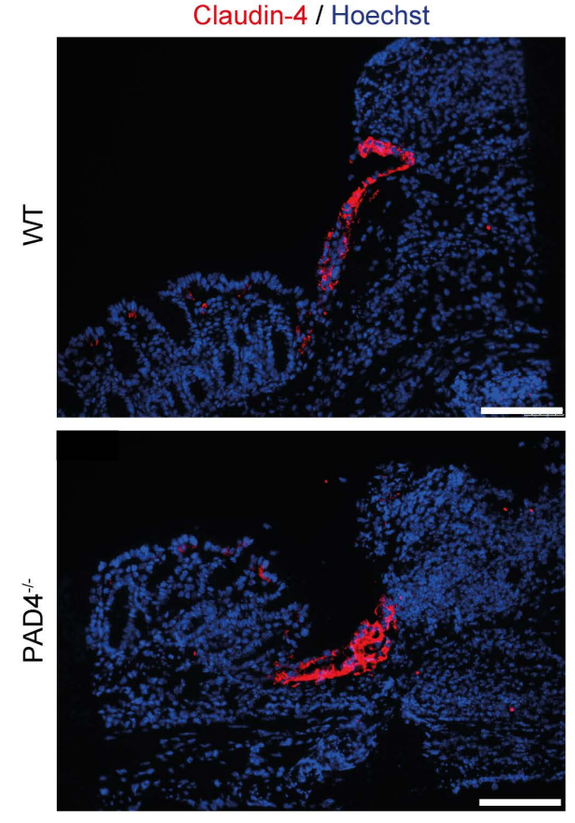
F
Claudin-4 / Hoechst
WT
PAD4-/-

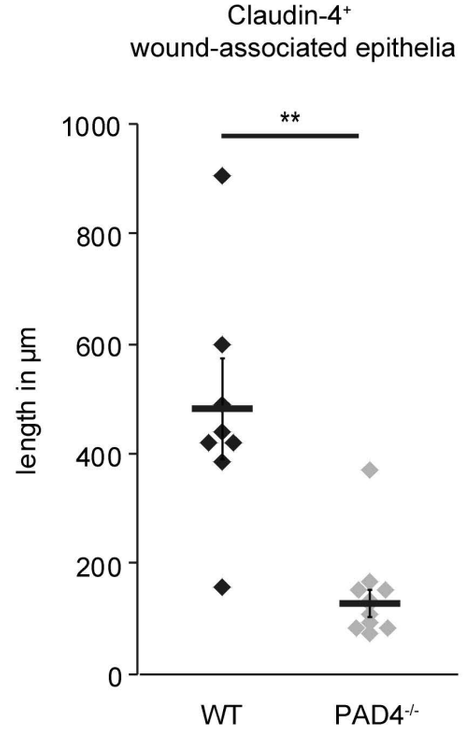
G
Claudin-4+ wound-associated epithelia
**
length in µm
1000
800
600
400
200
0
WT
PAD4-/-

Supplementary Figure 5: Epithelial restitution by wound-associated epithelial cells is improved in the presence of PAD4-dependent immunothrombi

(A) Colon sections of DSS-treated mice were stained by haematoxylin and eosin (H&E) on day 9 after DSS. Here, a completely eroded mucosa was noted in PAD4-/- mice, whereas in WT mice, the mucosa was mildly inflamed with nearly intact crypt architecture. **(B)** The eroded surface of the colon as related to the complete mucosal surface was measured on random cross-sections of the distal colon as in (A). The quantitative analysis supports the increased presence of erosions in $PAD4^{-/-}$ mice. (*** $p < 0.001$, Student's t test) **(C)** β-catenin and E-cadherin staining corroborates the increased proportion of eroded mucosa in $PAD4^{-/-}$ mice. **(D)** Colon sections of DSS-treated mice were stained by haematoxylin and eosin (H&E) as in (A). While less frequent in WT mice, areas of crypt loss were detected in both experimental groups. Please note, that in wild-type mice, adjacent wound-associated epithelia repopulate the area with a lost crypt architecture (black line), whereas this response is disturbed in $PAD4^{-/-}$ mice. (n 20–24 mice per group studied, respectively). **(E)** The fraction of the mucosal surface with lost crypt architecture, which is covered by wound-associated epithelia as in (D) was quantified (*** $p < 0.001$, Student's t test) **(F)** The edge of forceps-induced colon wounds was studied regarding the presence and length of the layer of claudin-4^{+} wound-associated epithelia employing immunofluorescence. Representative images are shown displaying a shorter layer of wound-associated epithelia in $PAD4^{-/-}$ mice. **(G)** The length of the layer of wound-associated epithelia as presented in (E) was quantified (n = 8 samples per group studied) (** $p < 0.01$ Student's t test). Scale bars equal 100 µm throughout the figure.

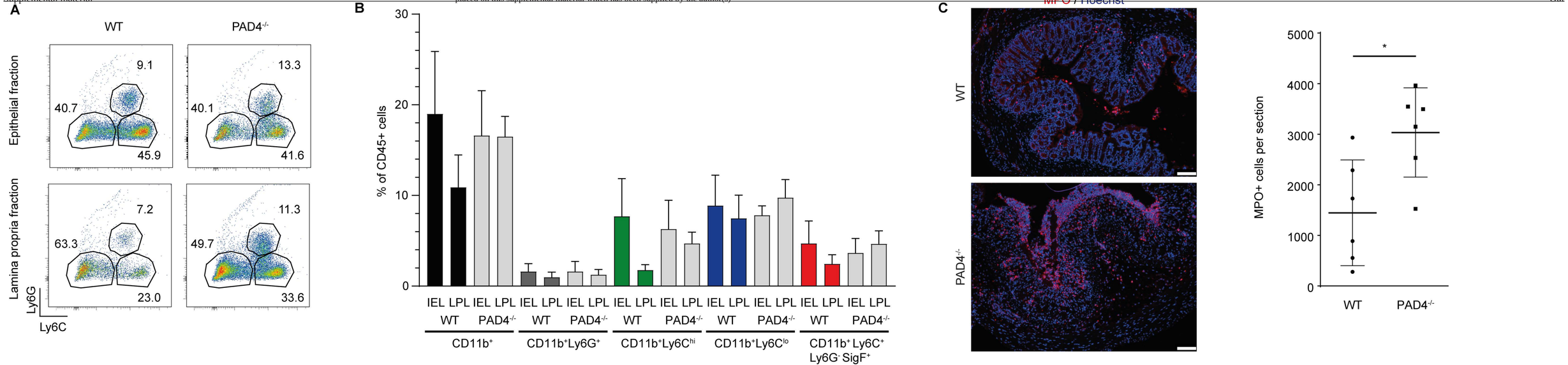

Supplementary Figure 6: Analyses of immune cell populations in colon tissue in the course of DSS-induced colitis in wild-type and PAD4$^{-/-}$ mice

(A, B) Flow cytometric analysis of colon tissue from wild-type and PAD4$^{-/-}$ mice subjected to 3 % DSS in the drinking water for 7 days. Both mouse strains exhibit ample infiltration of various myeloid cell populations to the bowel wall. Both the intraepithelial and lamina propria fraction are depicted (n = 6 samples per group), while luminal leukocytes are not represented in these analyses. **(C)** Immunofluorescence (left) of colon sections of DSS-treated mice show the marked infiltration of MPO^{+} granulocytes to the eroded mucosa in both groups. The eroded area in PAD4$^{-/-}$ mice is covered by a layer of myeloperoxidase (MPO)-positive neutrophils. Quantification (right) of MPO-positive cells in cross-sections of DSS-induced colitis reveals a significantly higher invasion of neutrophils in PAD4$^{-/-}$ mice compared to wild-type, when luminal neutrophils are accounted for (sections of n = 6 mice evaluated).

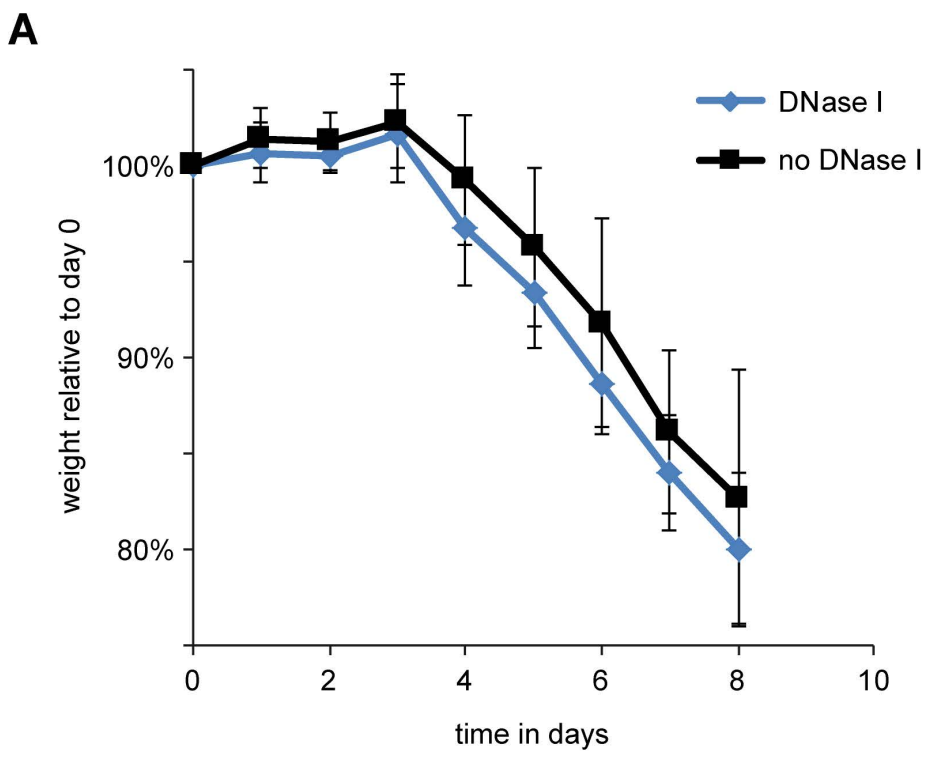
A
DNase I
no DNase I
100%
90%
80%
weight relative to day 0
0
2
4
6
8
10
time in days

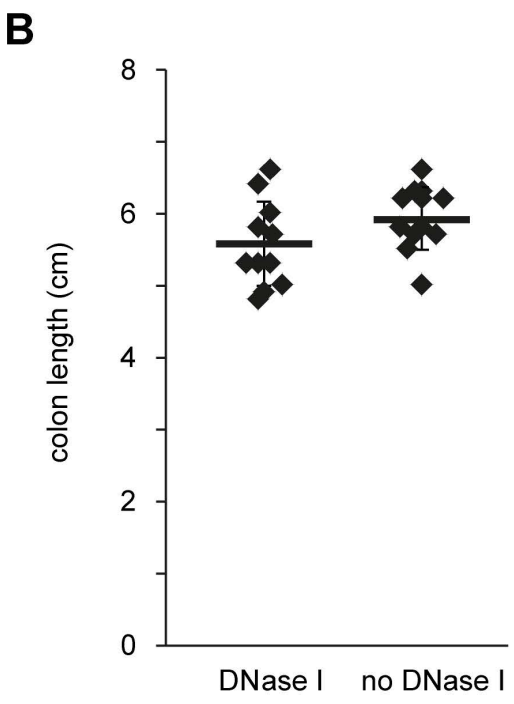
B
8
6
4
2
0
colon length (cm)
DNase I
no DNase I

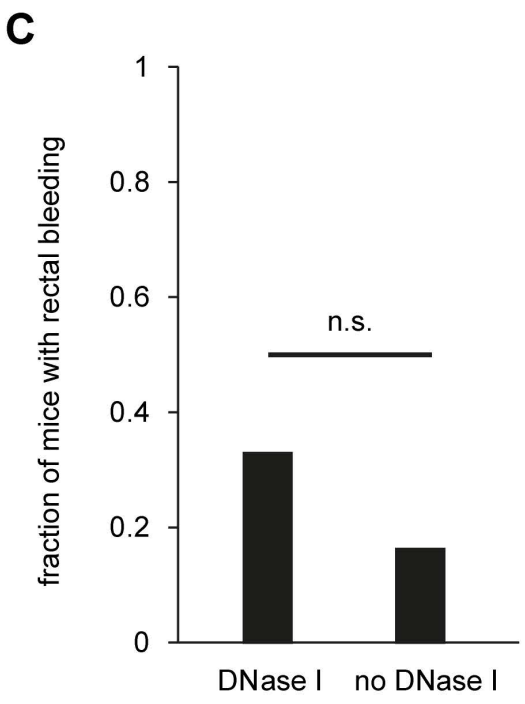
C
1
0.8
0.6
0.4
0.2
0
fraction of mice with rectal bleeding
n.s.
DNase I
no DNase I

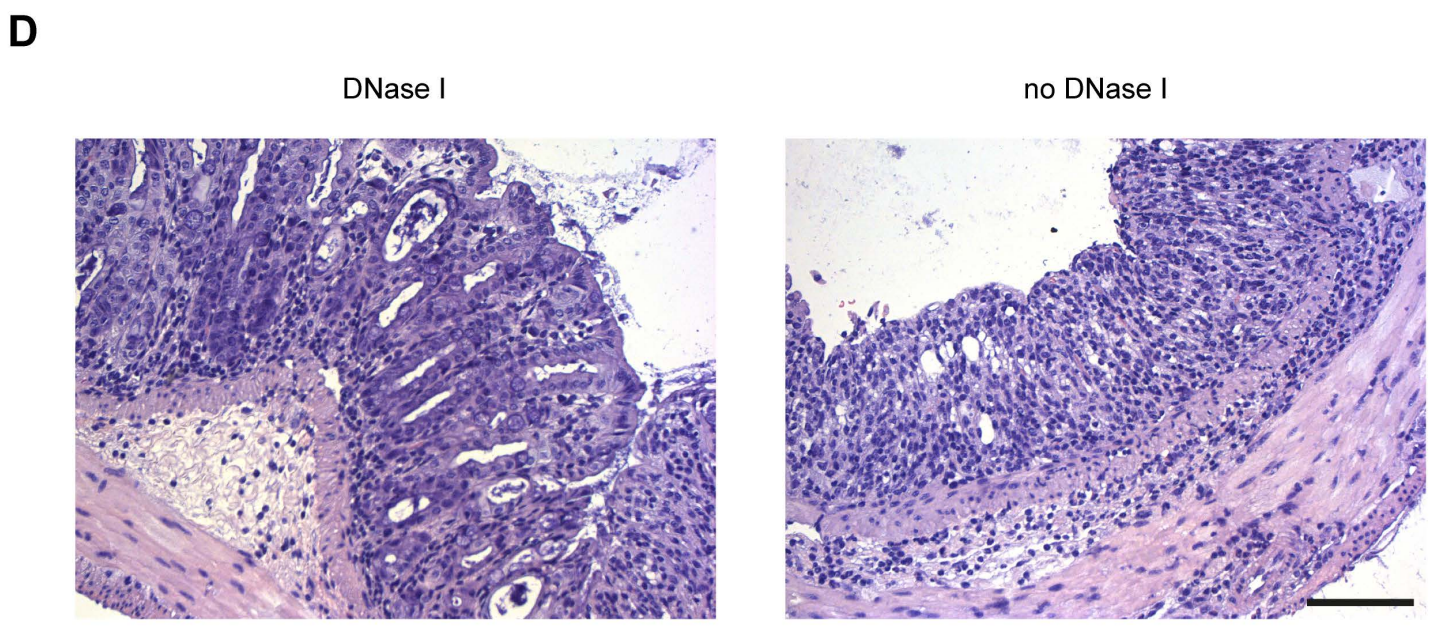
D
DNase I
no DNase I

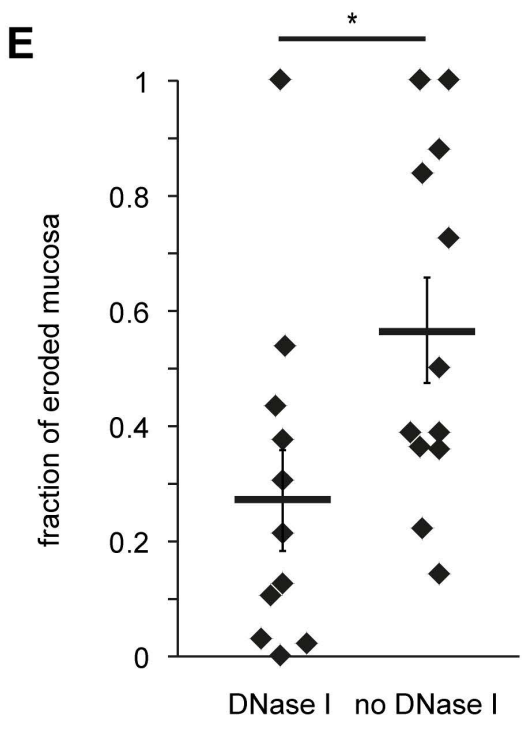
E
*
1
0.8
0.6
0.4
0.2
0
fraction of eroded mucosa
DNase I
no DNase I

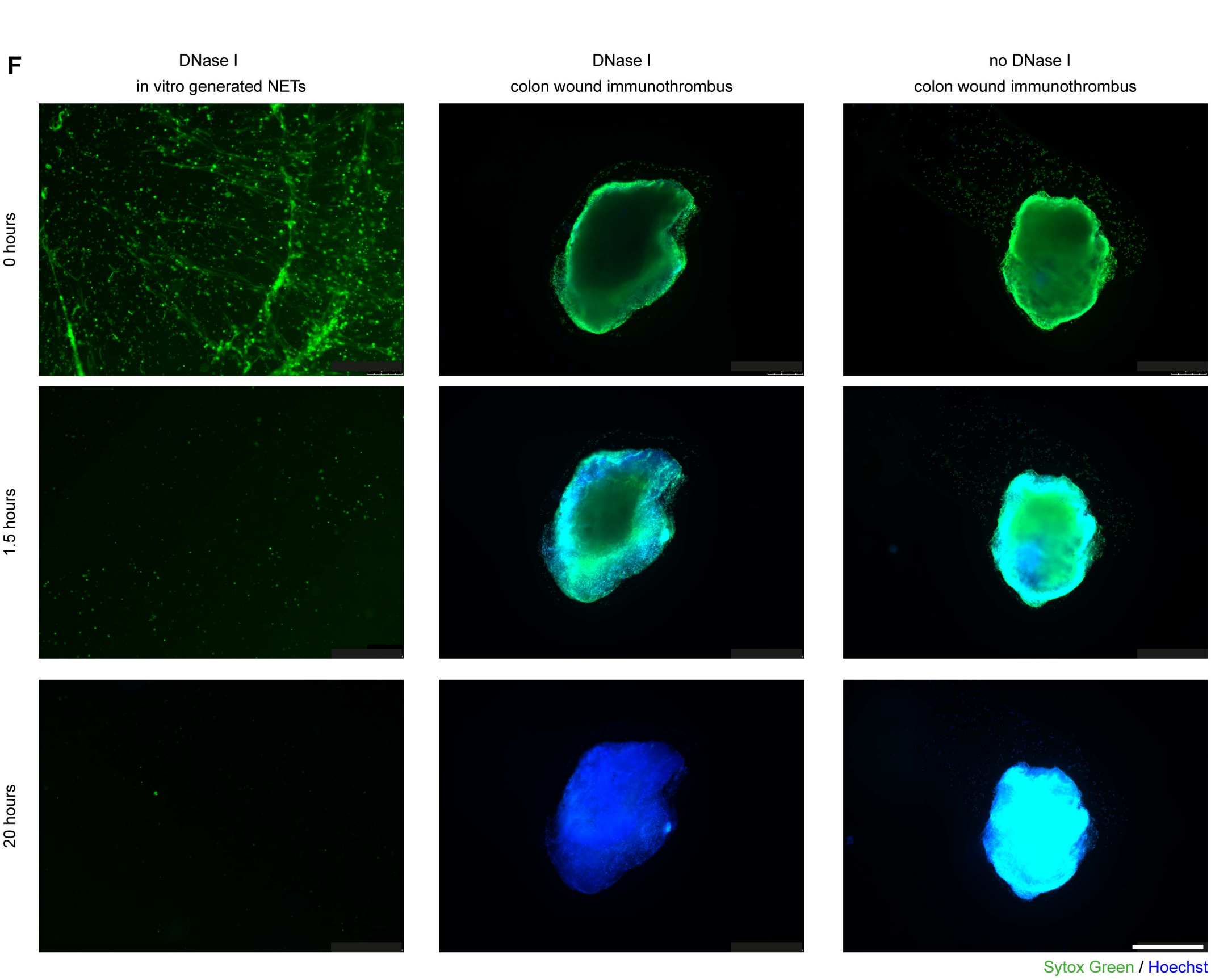
F
DNase I
in vitro generated NETs
DNase I
colon wound immunothrombus
no DNase I
colon wound immunothrombus
0 hours
1.5 hours
20 hours
Sytox Green / Hoechst

Supplementary Figure 7: DNase I does not facilitate rectal bleeding in DSS-induced colitis

Wild-type mice were treated with 3% DSS in drinking water for 7 days and injected intravenously with DNase I (5U/g) or control every day. **(A)** DNase I treatment did not affect weight loss, **(B)** colon length or **(C)** rectal bleeding frequency induced by DSS treatment. **(D)** Histological stainings of colon sections revealed reduced erosions in mice treated with DNase I (scale bar = 100 µm). **(E)** The fraction of eroded mucosa was reduced in DNase-I-treated animals as determined from images as in (D) (* $p < 0.05$, Student's t test, n: 12 mice per group). **(F)** *In-vitro* generated NETs (stimulus: 50mM $NaHCO_3$) can be effectively digested by DNase I (1U/ml). In contrast, ex-vivo colon wound immunothrombi incubated with DNase I (1U/ml) exhibit a markedly slower reduction of intercalating SYTOX Green staining over time and retained major grove-binding Hoechst signal, but are not disintegrated among enzymatic treatment (scale bar = 500 µm, representative of 3 independent experiments).

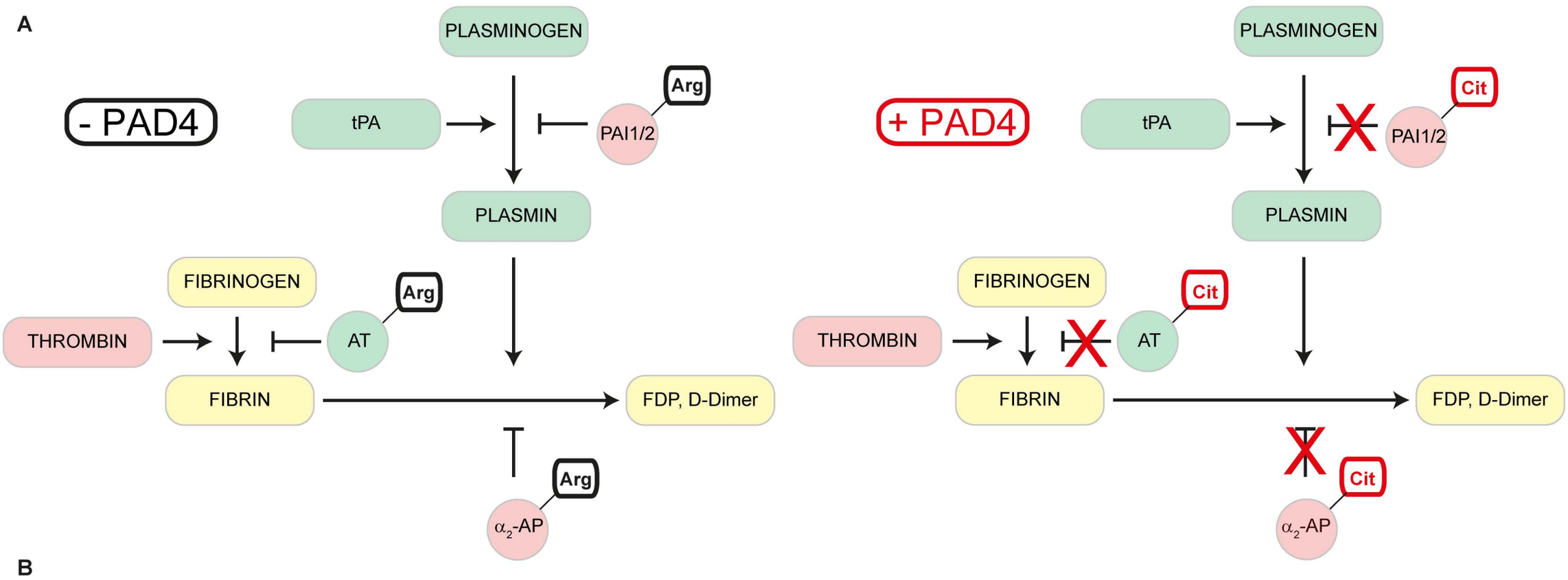
A
- PAD4
PLASMINOGEN
tPA
PAI1/2
Arg
PLASMIN
FIBRINOGEN
THROMBIN
AT
Arg
FIBRIN
FDP, D-Dimer
α2-AP
Arg
+ PAD4
PLASMINOGEN
tPA
PAI1/2
Cit
PLASMIN
FIBRINOGEN
THROMBIN
AT
Cit
FIBRIN
FDP, D-Dimer
α2-AP
Cit

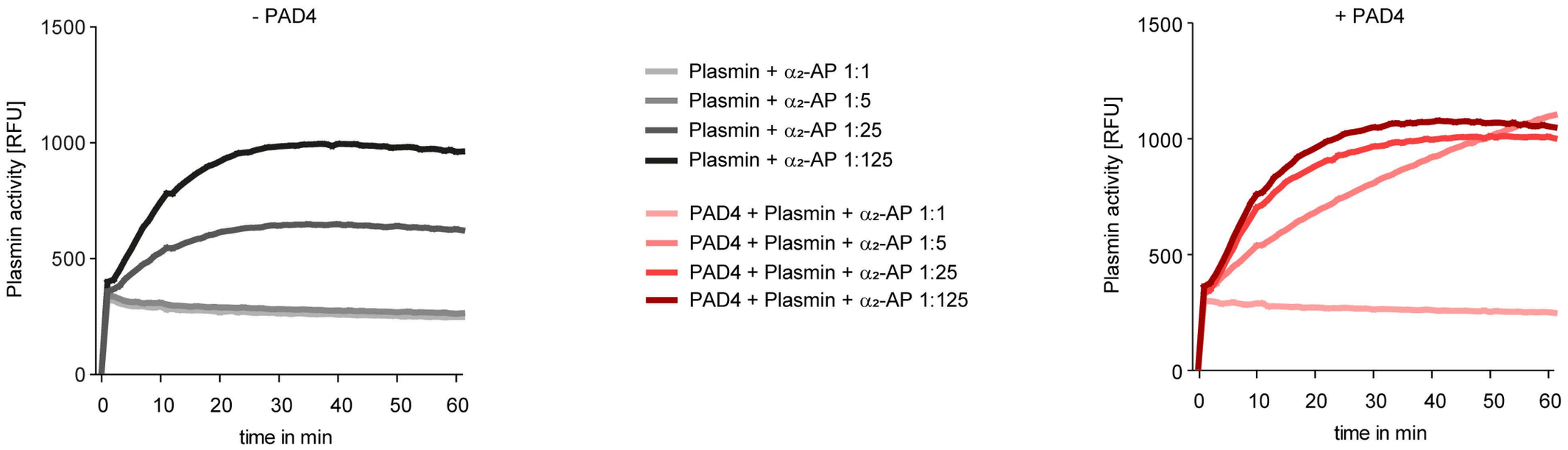
B
- PAD4
Plasmin activity [RFU]
1500
1000
500
0
0 10 20 30 40 50 60
time in min
Plasmin + α2-AP 1:1
Plasmin + α2-AP 1:5
Plasmin + α2-AP 1:25
Plasmin + α2-AP 1:125
PAD4 + Plasmin + α2-AP 1:1
PAD4 + Plasmin + α2-AP 1:5
PAD4 + Plasmin + α2-AP 1:25
PAD4 + Plasmin + α2-AP 1:125
+ PAD4
Plasmin activity [RFU]
1500
1000
500
0
0 10 20 30 40 50 60
time in min

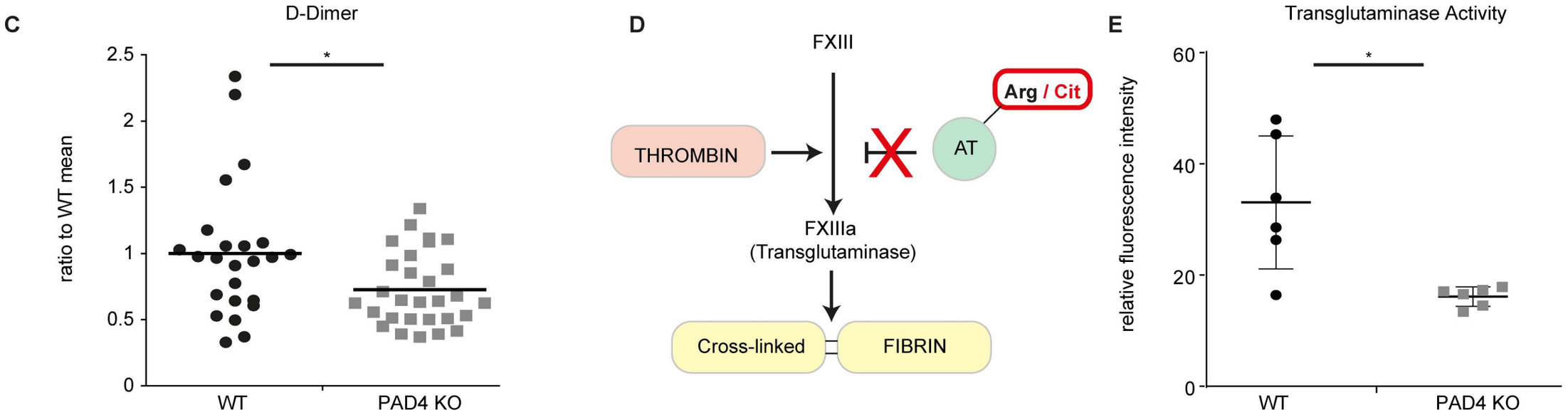
C
D-Dimer
ratio to WT mean
2.5
2
1.5
1
0.5
0
*
WT
PAD4 KO
D
FXIII
THROMBIN
AT
Arg / Cit
FXIIIa
(Transglutaminase)
Cross-linked
FIBRIN
E
Transglutaminase Activity
relative fluorescence intensity
60
40
20
0
*
WT
PAD4 KO

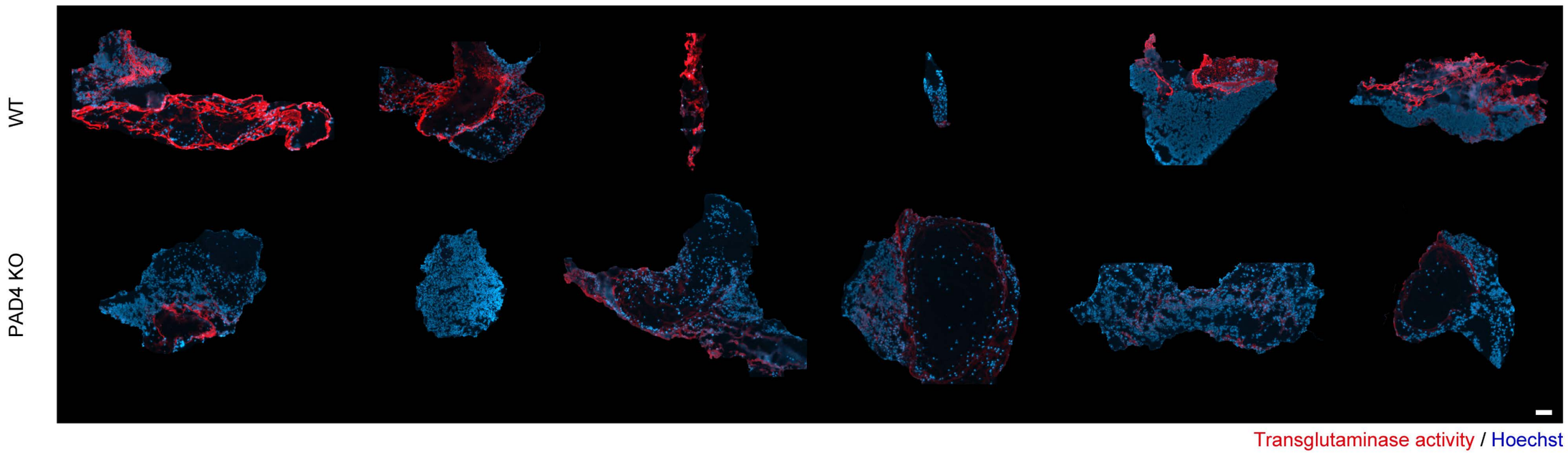
F
WT
PAD4 KO
Transglutaminase activity / Hoechst

Supplementary Figure 8: PAD4 affects the balance between coagulation and fibrinolysis via serpin inactivation and facilitates thrombus remodelling by transglutaminases

(A) A simplified model of the coagulation and fibrinolysis cascade is presented. Serine proteases interact with their respective serine protease inhibitors (serpins), numerous of which carry an arginine in their P1 reactive site (highlighted with Arg). PAD4 can suppress serpin functionality and thus impact the coagulation-fibrinolysis balance on multiple levels (tPA = tissue plasminogen activator; PAI1/2 = plasminogen activator inhibitor-1/2; AT = antithrombin; α_2-AP = α_2-antiplasmin) (modified arginine highlighted with Cit). **(B)** Active plasmin was incubated together with the fluorescent substrate N-Succinyl-Ala-Phe-Lys-AMC and α_2-antiplasmin in various dilutions at 37 °C *in vitro* in the presence or absence of PAD4. Citrullination of α_2-antiplasmin by PAD4 diminished its inhibitory activity on plasmin activity in a dose-dependent manner. One representative experiment of 5 independent experiments is shown. **(C)** D-dimer concentrations were assessed by ELISA in protein extracts of colon wounds from wild-type and PAD4$^{-/-}$ mice harvested 4–48 hours after wounding. A ratio to the wild-type mean of each time point was calculated to correct for differences in concentration over time. (N: 25–29 samples were studied, * $p < 0.05$, Student's t-test) **(D)** A simplified model of fibrin cross-linking by the thrombin-activated transglutaminase FXIIIa is presented. **(E)** Transglutaminase activity was assessed in colon wounds of wild-type and PAD4 knockout mice *in vivo* by i. p. injection of the biotin-labelled substrate biotin-amido-pentylamine (100 mg/kg) before wound induction and subsequent streptavidin-aided fluorescent detection. Relative fluorescence units were measured on tissue sections as in (F), showing significantly increased transglutaminase activity in the wounds of wild-type mice as compared to PAD4$^{-/-}$ mice (N: 6 wounds per group). **(F)** Histochemical detection of transglutaminase activity in sections of wild-type and PAD4$^{-/-}$ colon wounds reveals marked transglutaminase activity restricted to the wound bed. Wild-type wounds display a stronger increase in transglutaminase activity as compared to PAD4$^{-/-}$ samples.

Clinical Features of study cohort Active Ulcerative Colitis		
N		36
Age [mean (range)]		45.9 (19-78)
Male / Female [%]		41.4
Localization [%]	Proctitis	13.2
	Proctosigmoiditis	34.2
	Left- sided colitis	18.4
	Pancolitis	34.2
Partial Mayo Score (rectal bleeding)	0	36.1
	1	38.9
	2-3	25
Past or current therapies reported [%]	Aminosalicylates	66.7
	Steroids	86.1
	Thioguanines	33.3
	cyclosporine	11.1
	Vedolizumab	88.9
	Anti- TNF antibodies	44.4

		Improvement in rectal bleeding score	
		day 3 to 6	day 7 to 12
IBD treatment	**% of cohort**	**% of cohort**	**% of cohort**
Steroids	100 (13/13)	54 (7/13)	92 (12/13)
Ciclosporin	38 (5/13)	4 (2/5)	100 (5/5)
Infliximab	15 (2/13)	5 (1/2)	100 (2/2)
Concomitant therapy			
Ganciclovir	15 (2/13)	5 (1/2)	100 (2/2)
Heparin (prophylactic)	77 (10/13)	56 (5/9)	90 (9/10)
No Heparin	23 (3/13)	66 (2/3)	100 (3/3)

Supplementary Table 1:

The patient characteristics of the study cohort (N: 36) are depicted including age and sex distribution, localisation and extent of disease, partial Mayo score regarding rectal bleeding, as well as previous and current therapeutics used.

Supplementary Table 2:

Whenever available from clinical documentation, the relation of the improvement in rectal bleeding over time to IBD-related (steroids, ciclosporin, infliximab) and concomitant therapies (ganciclovir, heparin, no heparin) is reported.

Leppkes M, *et al. Gut* 2021;0:1–16. doi: 10.1136/gutjnl-2021-324725

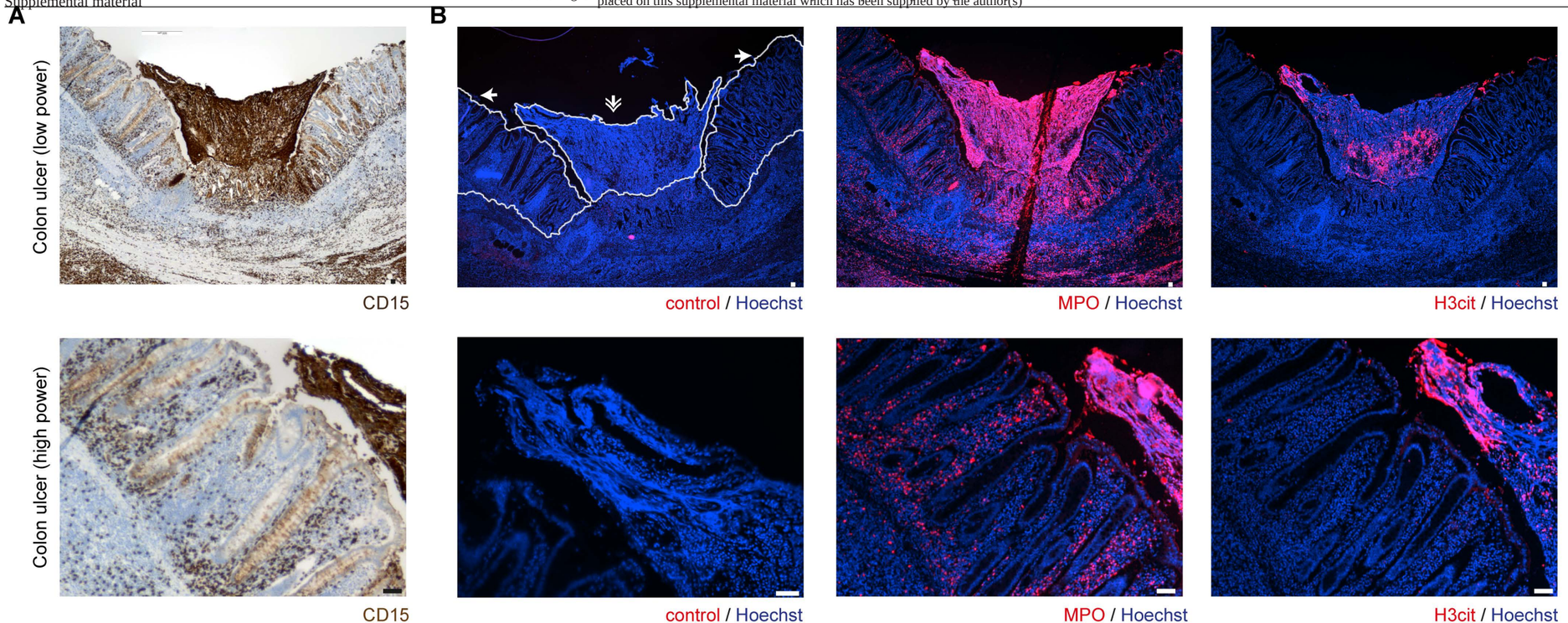

Supplementary Figure 1: Intercryptal lamina propria neutrophils mostly do not display PAD activity

(A) Low power (top) and high power (bottom) view of a human colon ulcer analysed for the presence of CD15 (DAB) and **(B)** myeloperoxidase (MPO), citrullinated histone H3 (H3cit) and. Note the broadly dispersed MPO in the fibrin layer, while MPO is also present in singly dispersed cells in the lamina propria. H3cit is strongly present in the fibrin layer whereas neutrophils in the intercryptal lamina propria are rather H3cit-negative. Please appreciate the decondensed chromatin in immunothrombi (scale bars = 100 µm) **(C)** Immunopositive cells in the intercryptal lamina propria as in (A–B) were quantified, displaying significantly less H3cit-positive cells in the intercryptal space, while MPO^+ and $CD15^+$ cells can be found in ample amounts (n = 10 samples, ** $p < 0.01$, Student's t-test).

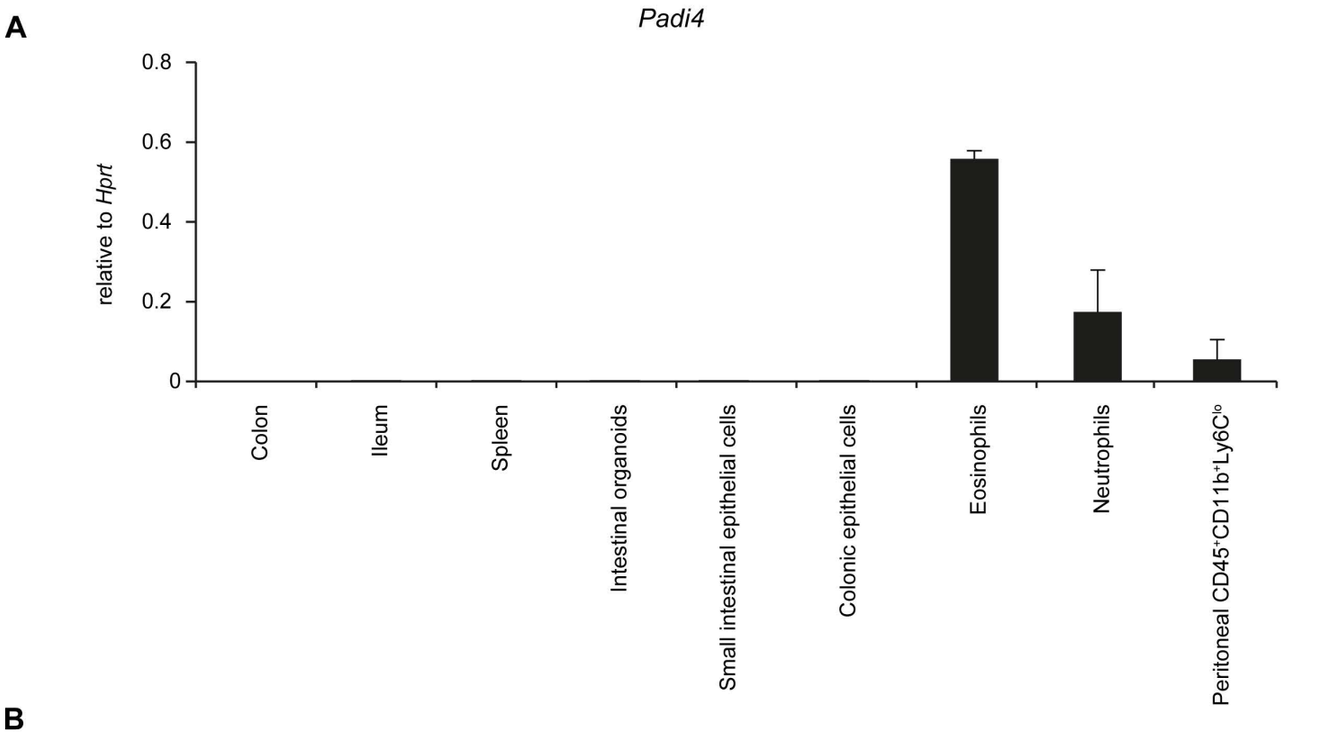
A
Padi4
relative to Hprt
0.8
0.6
0.4
0.2
0
Colon
Ileum
Spleen
Intestinal organoids
Small intestinal epithelial cells
Colonic epithelial cells
Eosinophils
Neutrophils
Peritoneal CD45+CD11b+Ly6Clo

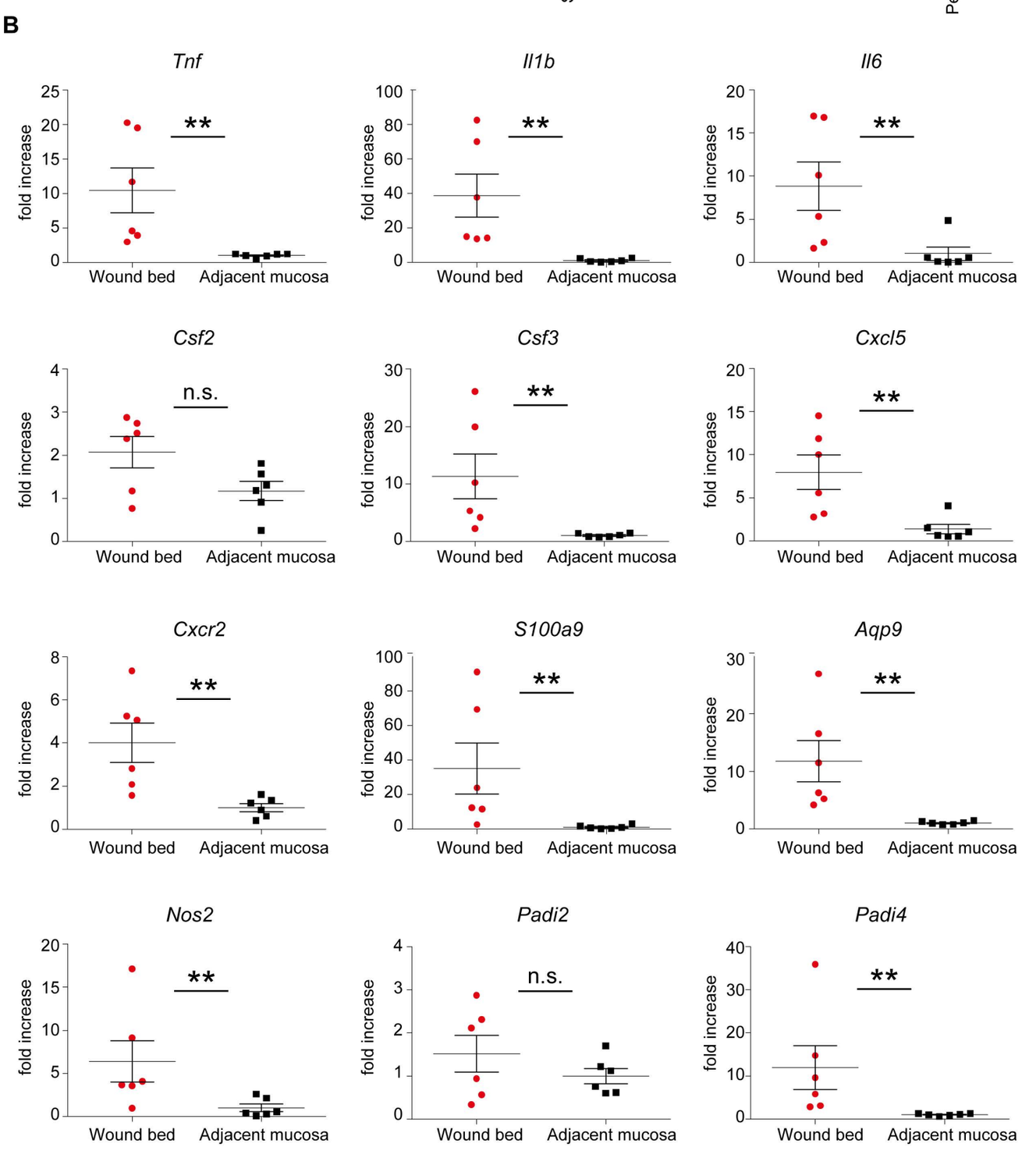
B
Tnf
Il1b
Il6
Csf2
Csf3
Cxcl5
Cxcr2
S100a9
Aqp9
Nos2
Padi2
Padi4
fold increase
Wound bed
Adjacent mucosa
**
n.s.

Supplementary Figure 2: *Padi4* is expressed in myeloid cells, predominantly granulocytes and is significantly increased in the colon wound bed

(A) RT-PCR analyses show a prevailing expression of *Padi4* in neutrophils and eosinophils and to a smaller extent in peritoneal Ly6C-low monocytes, whereas no expression of *Padi4* was detected in whole colon or ileum, isolated epithelial cells, spleen or intestinal organoids. **(B)** Analysis of mRNA expression of selected neutrophil- and inflammation-related genes in forceps-induced colonic wound beds and adjacent healthy mucosa was performed at 24 hours post-injury, displaying markedly increased abundance of neutrophil- and inflammation-related transcripts (at least n = 6 samples per group (** $p < 0.01$, Student's t-test, mean + SEM are depicted).

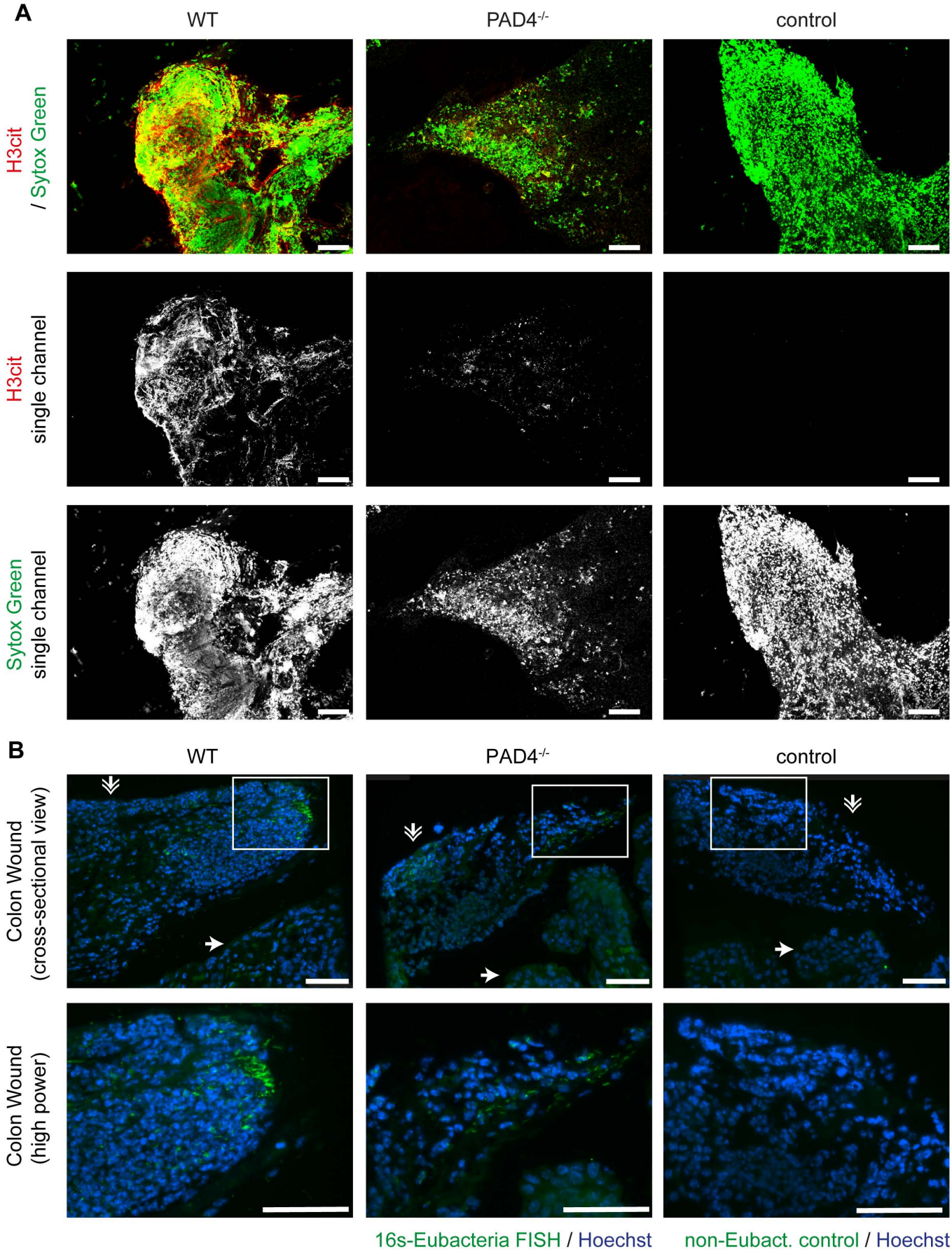
A
WT
PAD4-/-
control
H3cit / Sytox Green
H3cit single channel
Sytox Green single channel
B
WT
PAD4-/-
control
Colon Wound (cross-sectional view)
Colon Wound (high power)
16s-Eubacteria FISH / Hoechst
non-Eubact. control / Hoechst

Supplementary Figure 3: PAD4-deficient mice fail to adequately decondense neutrophil chromatin in immunothrombi on mucosal wounds

(A) Manually grasped immunothrombi from colon wounds were subjected to immunofluorescence. Decondensed chromatin is a striking feature in immunothrombi as evidenced by SYTOX Green staining. We detected H3cit throughout the immunothrombus, which is strongly diminished in fibrinoid derived from PAD4$^{-/-}$ mice. **(B)** Cross-sections of colon wounds were subjected to fluorescent *in-situ* hybridisation using 16S-rRNA-Eubacteria directed probes. The immunothrombi of both wild-type and PAD4$^{-/-}$ mice (indicated by the double-head arrow) was infiltrated by bacteria, while none were detected in deeper layers of the mucosa (the ulcer edge is highlighted by a single head arrow). Low power and high power magnification are presented. (Scale bars = 100 µm).

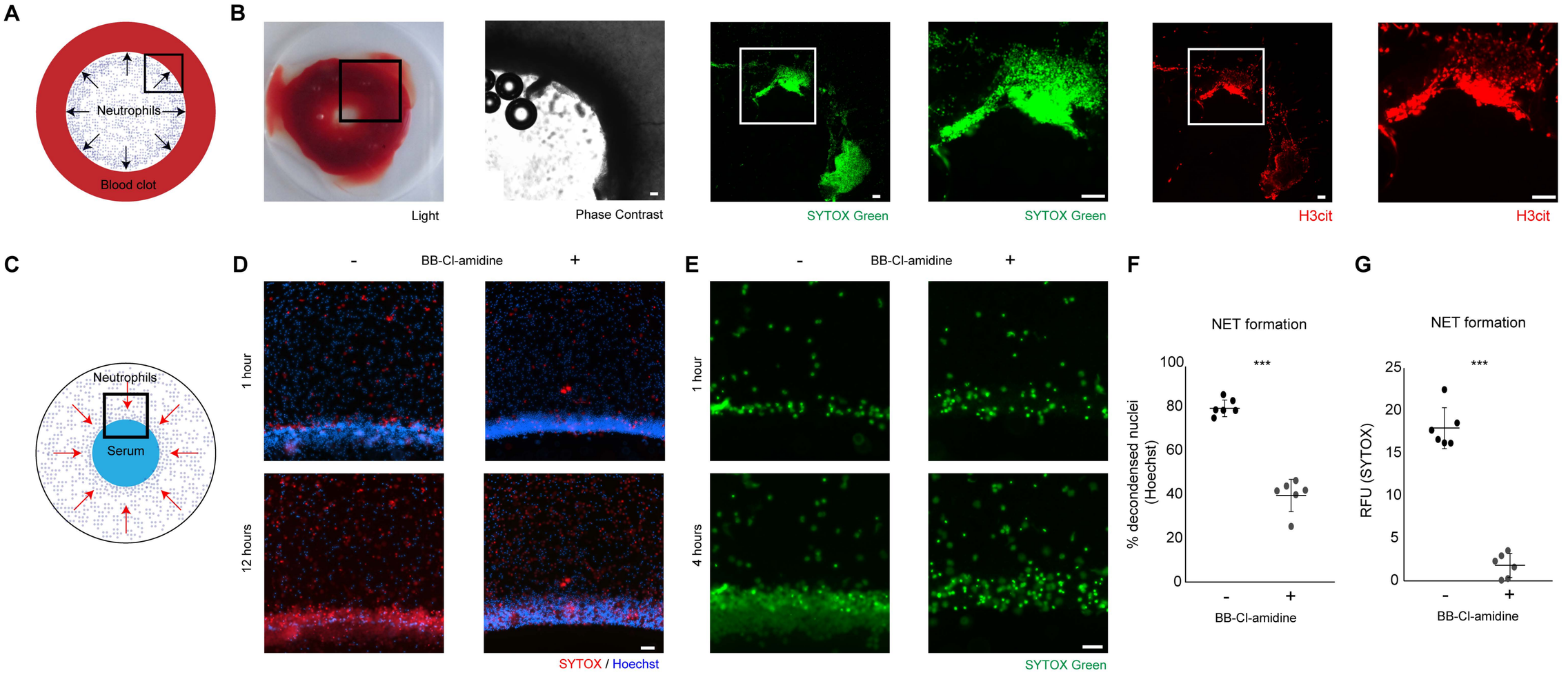

Supplementary Figure 4: PAD4-mediated NET formation is instigated in high cellular densities at the edge of a blood clot in the absence of bacteria

(A) Human citrated whole blood was clotted by recalcification. 2×10^5 isolated human neutrophils were cultured in autologous serum and added to the punched-out center of the clot (31 mm², scale bar = 2 mm). **(B)** This setup was analysed by brightfield (left) and immunofluorescence: Decondensed SYTOX Green$^+$ (center) and H3cit$^+$ chromatin (right) was preferentially formed at the edge of the blood clot as depicted in representative photomicrographs. Scale bars = 100 µm. **(C–G)** Human neutrophils were cultured in RPMI medium supplemented with 2 % autologous serum in the presence and absence of the pan-PAD inhibitor BB-Cl-amidine (20 µM) or solute control in a well prepared with an agarose gel in the center containing 20 % autologous serum. **(C)** A graphic model of this experimental setup is presented. The black box represents a typical field of view as presented in D, E. **(D)** The edge of the surrogate clot is presented at two different time points after stimulation in the presence and absence of the PAD inhibitor BB-Cl-amidine. Hoechst shows all nucleated cells in blue, while SYTOX Green staining of extracellular DNA and permeable cells is depicted in red, representative images of three independent experiments. Please appreciate the increased presence of condensed chromatin at the edge of the clot in the presence of the pan-PAD inhibitor, whereas more chromatin is decondensed in its absence. Scale bars = 100 µm. **(E)** The SYTOX Green channel of this experimental setup is displayed after 1 and 4 hours. Please appreciate the strongly reduced chromatin decondensation at the edge of the clot in the presence of BB-Cl-amidine. Scale bars = 100 µm. **(F)** NET formation was quantified in images as depicted in (D, E) by quantification of decondensed nuclei at the clot edge using the Hoechst signal and **(G)** by use of fluorescence intensity quantification of the SYTOX signal (*** $p < 0.001$, Student's t-test, three independent experiments reported). Scale bars = 100 µm.

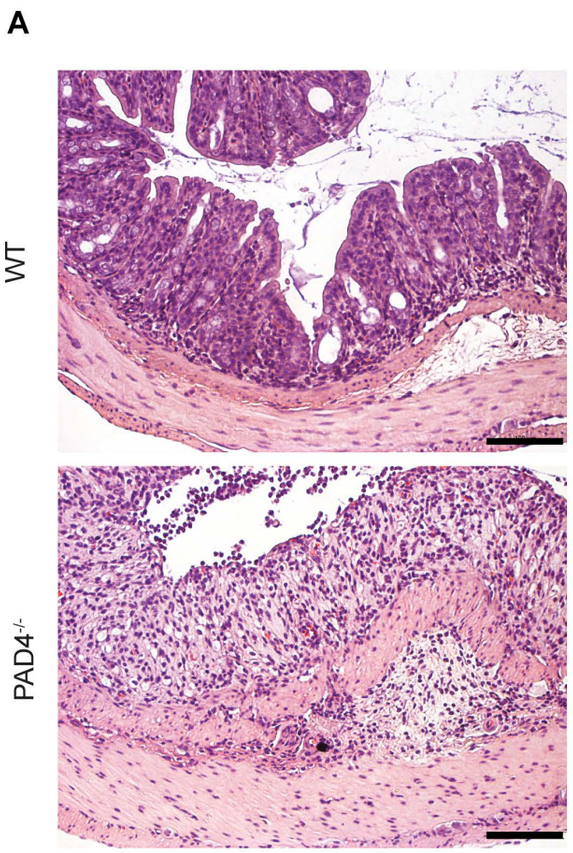
A
WT
PAD4-/-
H&E

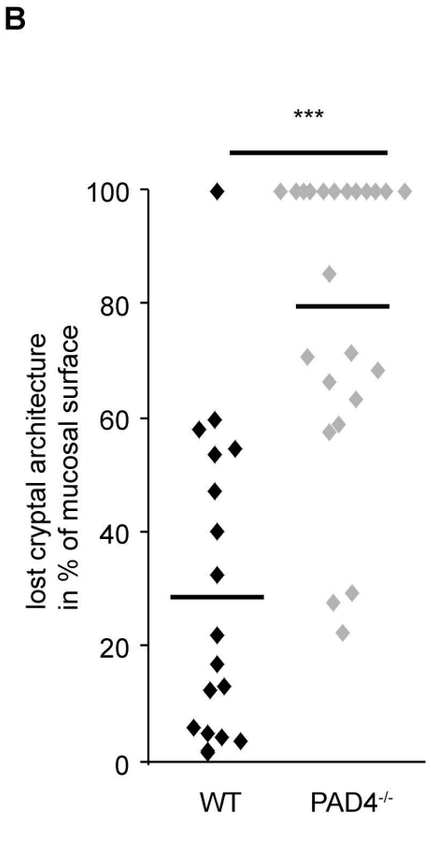
B
***
lost cryptal architecture in % of mucosal surface
100
80
60
40
20
0
WT
PAD4-/-

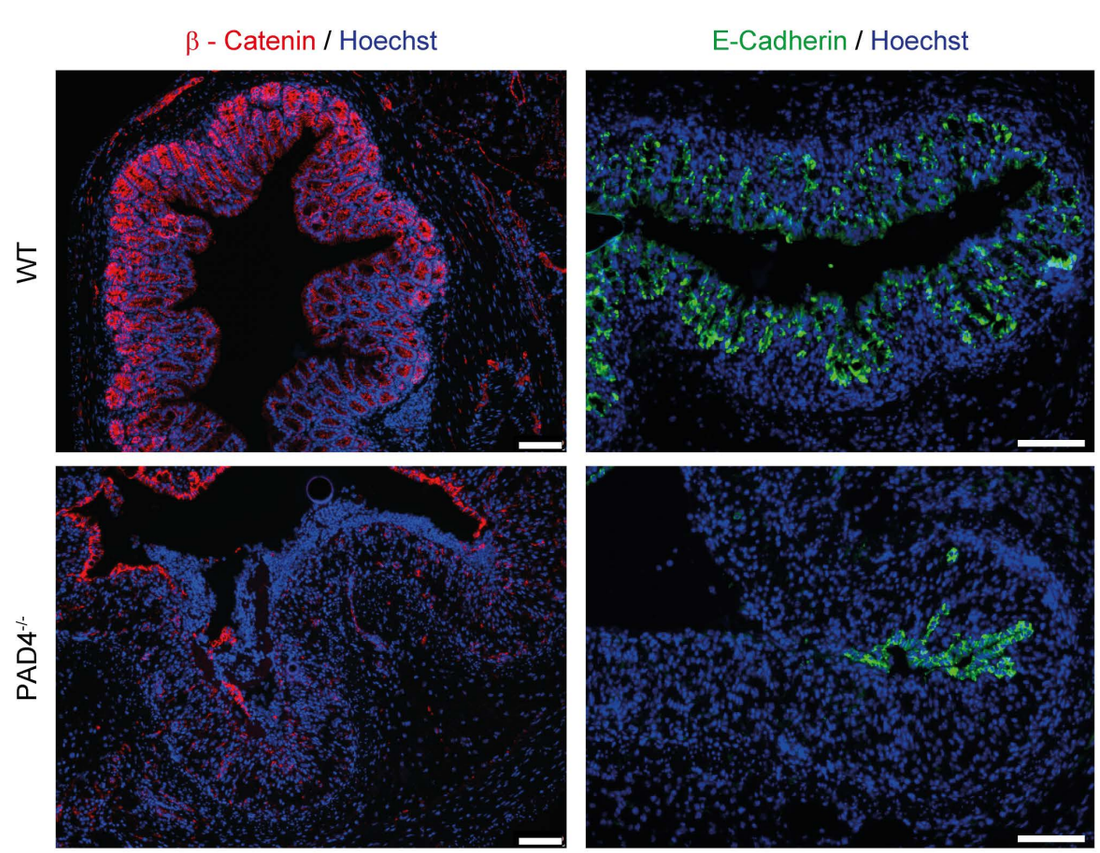
C
β - Catenin / Hoechst
E-Cadherin / Hoechst
WT
PAD4-/-

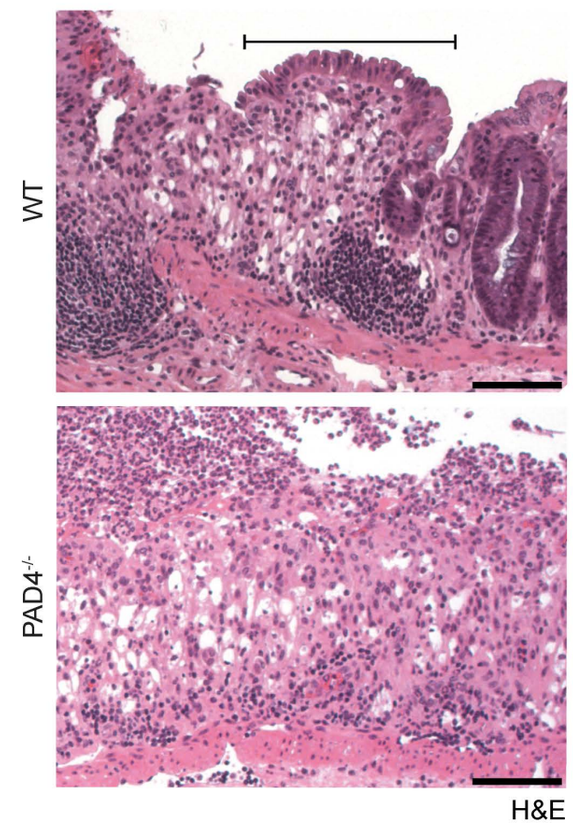
D
WT
PAD4-/-
H&E

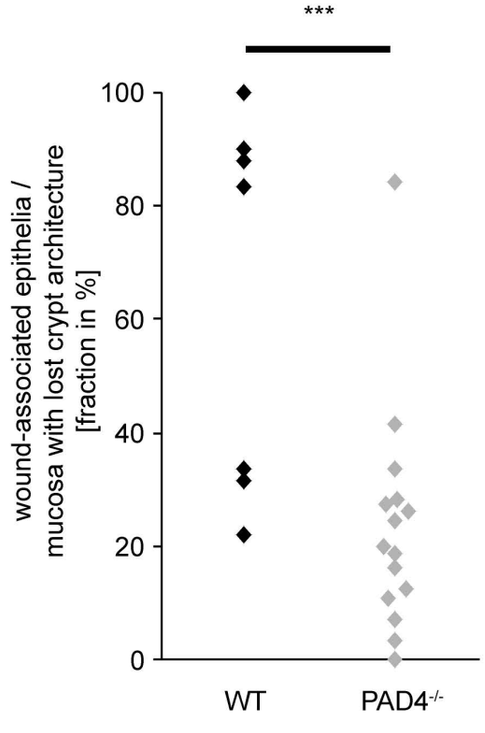
E
***
wound-associated epithelia / mucosa with lost crypt architecture [fraction in %]
100
80
60
40
20
0
WT
PAD4-/-

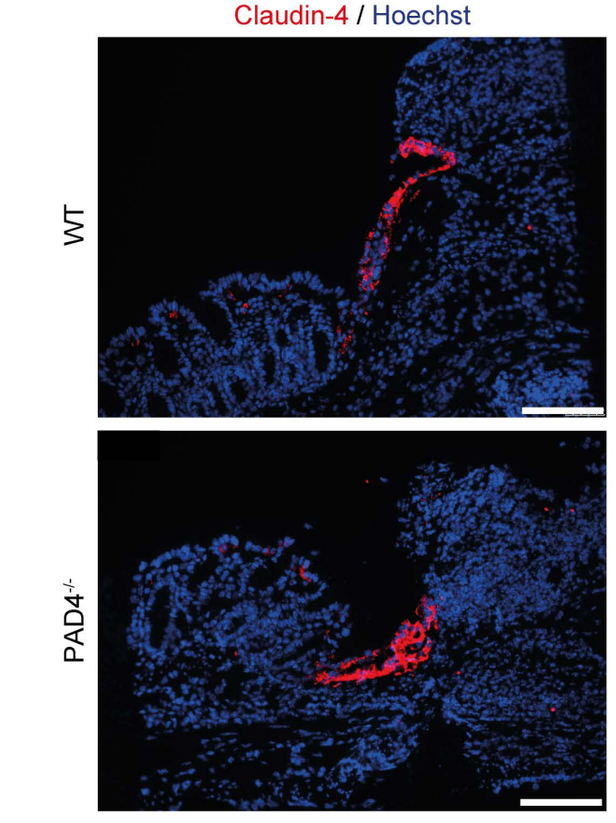
F
Claudin-4 / Hoechst
WT
PAD4-/-

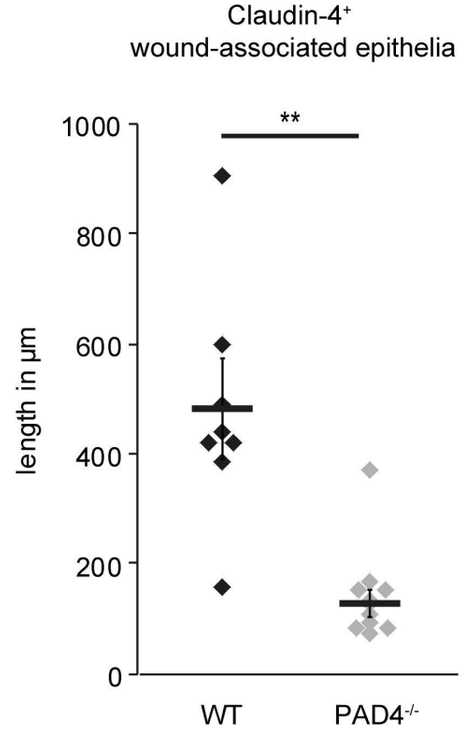
G
Claudin-4+ wound-associated epithelia
**
length in µm
1000
800
600
400
200
0
WT
PAD4-/-

Supplementary Figure 5: Epithelial restitution by wound-associated epithelial cells is improved in the presence of PAD4-dependent immunothrombi

(A) Colon sections of DSS-treated mice were stained by haematoxylin and eosin (H&E) on day 9 after DSS. Here, a completely eroded mucosa was noted in PAD4-/- mice, whereas in WT mice, the mucosa was mildly inflamed with nearly intact crypt architecture. **(B)** The eroded surface of the colon as related to the complete mucosal surface was measured on random cross-sections of the distal colon as in (A). The quantitative analysis supports the increased presence of erosions in $PAD4^{-/-}$ mice. (*** $p < 0.001$, Student's t test) **(C)** β-catenin and E-cadherin staining corroborates the increased proportion of eroded mucosa in $PAD4^{-/-}$ mice. **(D)** Colon sections of DSS-treated mice were stained by haematoxylin and eosin (H&E) as in (A). While less frequent in WT mice, areas of crypt loss were detected in both experimental groups. Please note, that in wild-type mice, adjacent wound-associated epithelia repopulate the area with a lost crypt architecture (black line), whereas this response is disturbed in $PAD4^{-/-}$ mice. (n 20–24 mice per group studied, respectively). **(E)** The fraction of the mucosal surface with lost crypt architecture, which is covered by wound-associated epithelia as in (D) was quantified (*** $p < 0.001$, Student's t test) **(F)** The edge of forceps-induced colon wounds was studied regarding the presence and length of the layer of claudin-4^{+} wound-associated epithelia employing immunofluorescence. Representative images are shown displaying a shorter layer of wound-associated epithelia in $PAD4^{-/-}$ mice. **(G)** The length of the layer of wound-associated epithelia as presented in (E) was quantified (n = 8 samples per group studied) (** $p < 0.01$ Student's t test). Scale bars equal 100 µm throughout the figure.

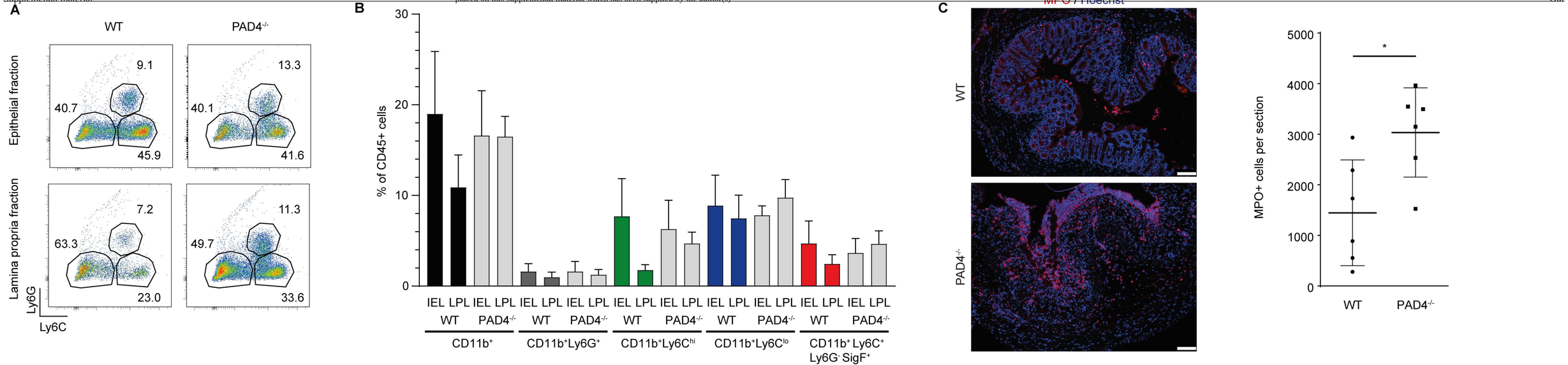

Supplementary Figure 6: Analyses of immune cell populations in colon tissue in the course of DSS-induced colitis in wild-type and PAD4$^{-/-}$ mice

(A, B) Flow cytometric analysis of colon tissue from wild-type and PAD4$^{-/-}$ mice subjected to 3 % DSS in the drinking water for 7 days. Both mouse strains exhibit ample infiltration of various myeloid cell populations to the bowel wall. Both the intraepithelial and lamina propria fraction are depicted (n = 6 samples per group), while luminal leukocytes are not represented in these analyses. **(C)** Immunofluorescence (left) of colon sections of DSS-treated mice show the marked infiltration of MPO^{+} granulocytes to the eroded mucosa in both groups. The eroded area in PAD4$^{-/-}$ mice is covered by a layer of myeloperoxidase (MPO)-positive neutrophils. Quantification (right) of MPO-positive cells in cross-sections of DSS-induced colitis reveals a significantly higher invasion of neutrophils in PAD4$^{-/-}$ mice compared to wild-type, when luminal neutrophils are accounted for (sections of n = 6 mice evaluated).

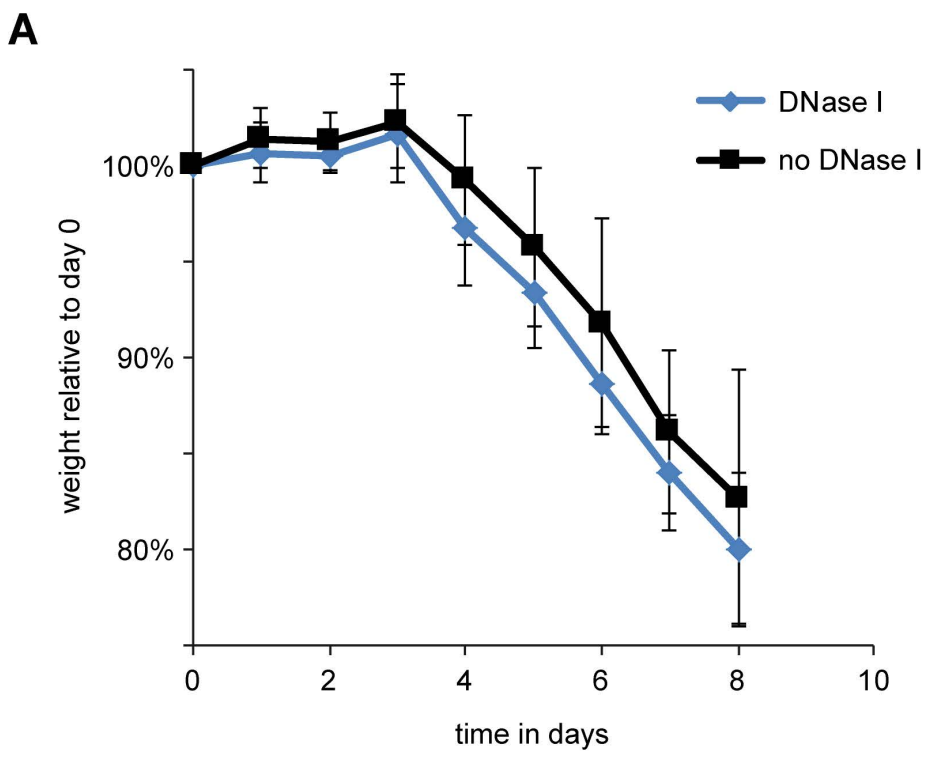
A
DNase I
no DNase I
100%
90%
80%
weight relative to day 0
0
2
4
6
8
10
time in days

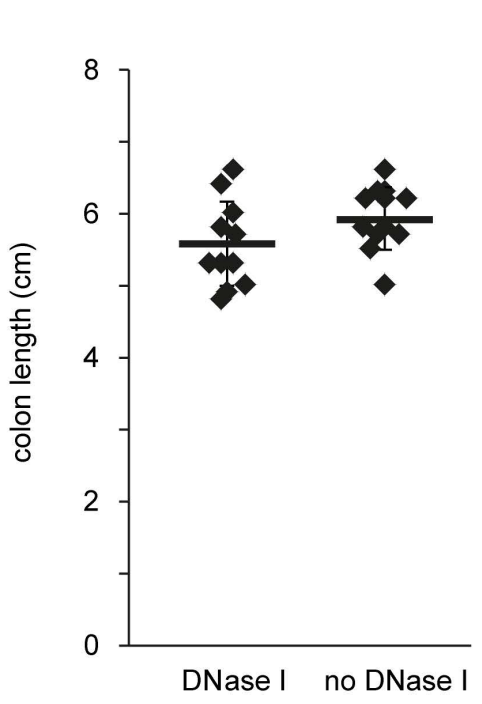
B
8
6
4
2
0
colon length (cm)
DNase I
no DNase I

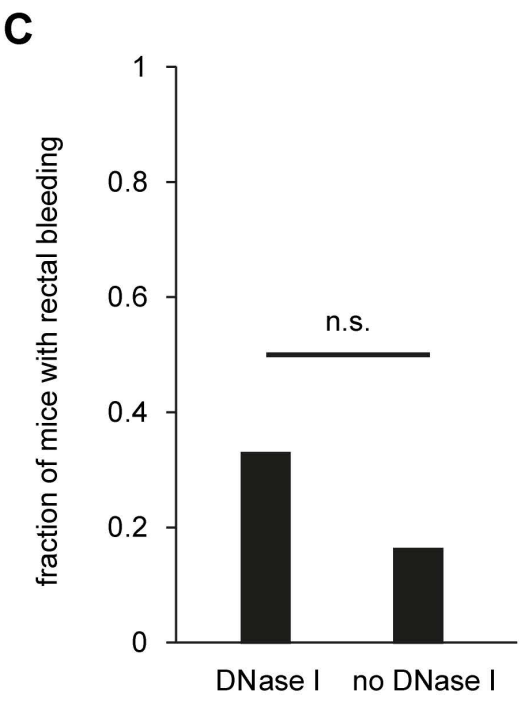
C
1
0.8
0.6
0.4
0.2
0
fraction of mice with rectal bleeding
n.s.
DNase I
no DNase I

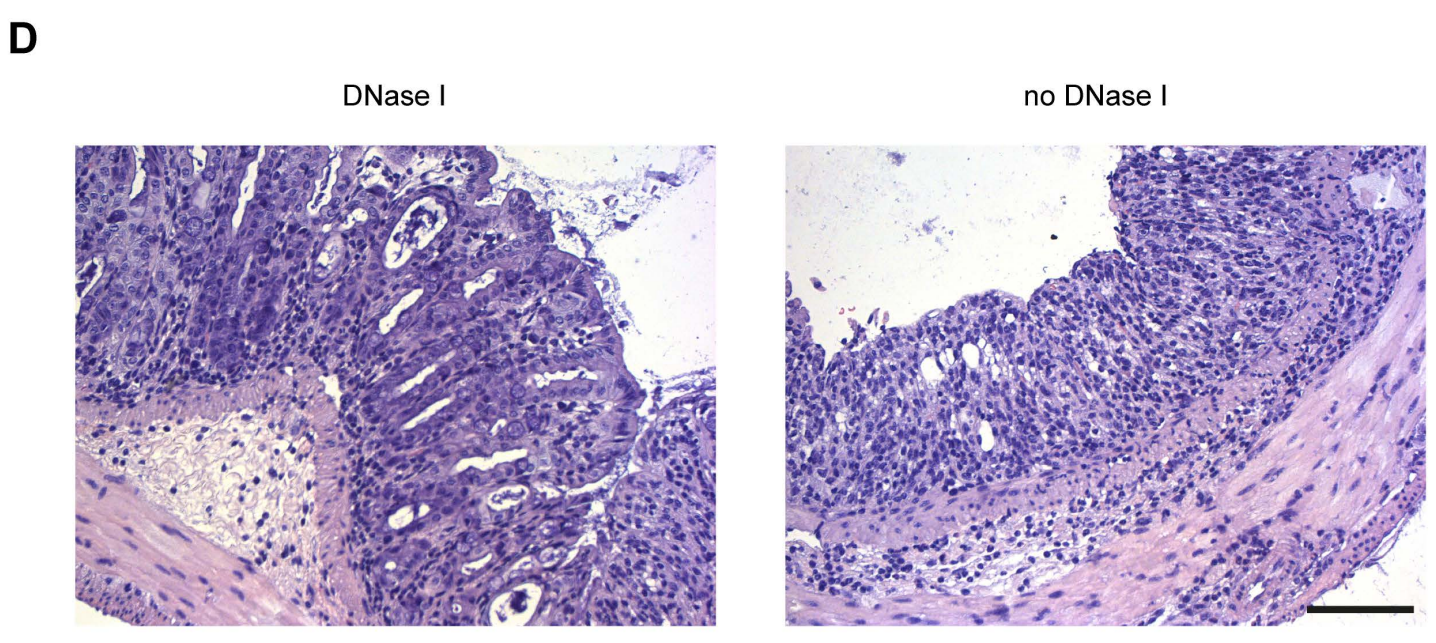
D
DNase I
no DNase I

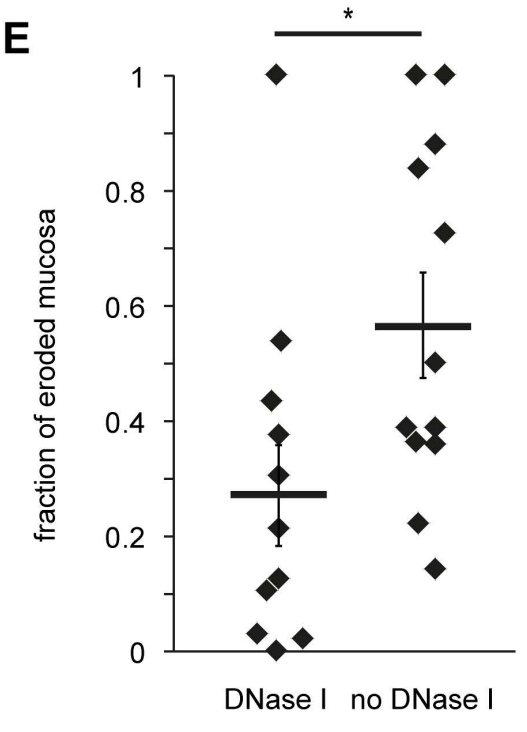
E
*
1
0.8
0.6
0.4
0.2
0
fraction of eroded mucosa
DNase I
no DNase I

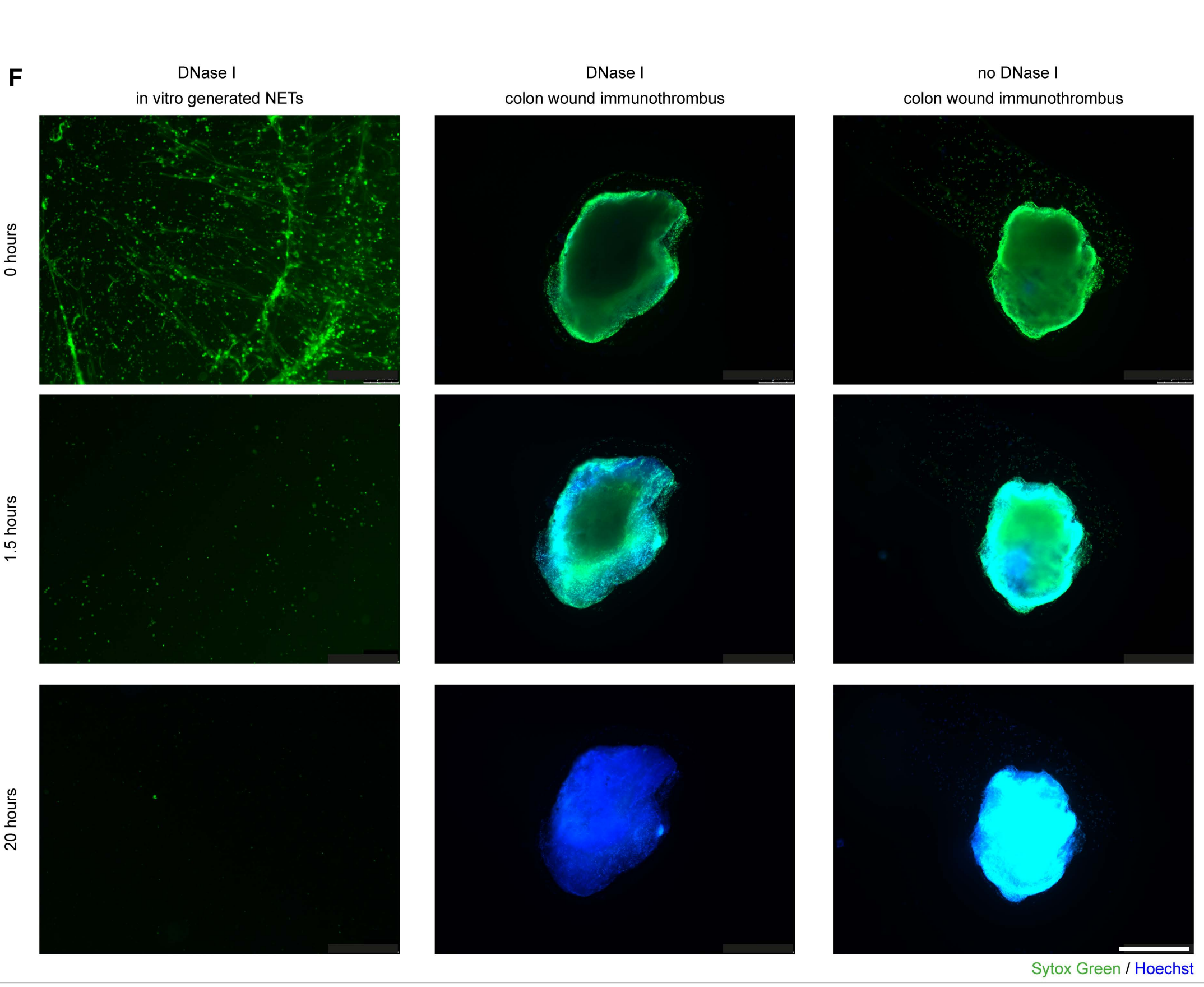
F
DNase I
in vitro generated NETs
DNase I
colon wound immunothrombus
no DNase I
colon wound immunothrombus
0 hours
1.5 hours
20 hours
Sytox Green / Hoechst

Supplementary Figure 7: DNase I does not facilitate rectal bleeding in DSS-induced colitis

Wild-type mice were treated with 3% DSS in drinking water for 7 days and injected intravenously with DNase I (5U/g) or control every day. **(A)** DNase I treatment did not affect weight loss, **(B)** colon length or **(C)** rectal bleeding frequency induced by DSS treatment. **(D)** Histological stainings of colon sections revealed reduced erosions in mice treated with DNase I (scale bar = 100 µm). **(E)** The fraction of eroded mucosa was reduced in DNase-I-treated animals as determined from images as in (D) (* $p < 0.05$, Student's t test, n: 12 mice per group). **(F)** *In-vitro* generated NETs (stimulus: 50mM $NaHCO_3$) can be effectively digested by DNase I (1U/ml). In contrast, ex-vivo colon wound immunothrombi incubated with DNase I (1U/ml) exhibit a markedly slower reduction of intercalating SYTOX Green staining over time and retained major grove-binding Hoechst signal, but are not disintegrated among enzymatic treatment (scale bar = 500 µm, representative of 3 independent experiments).

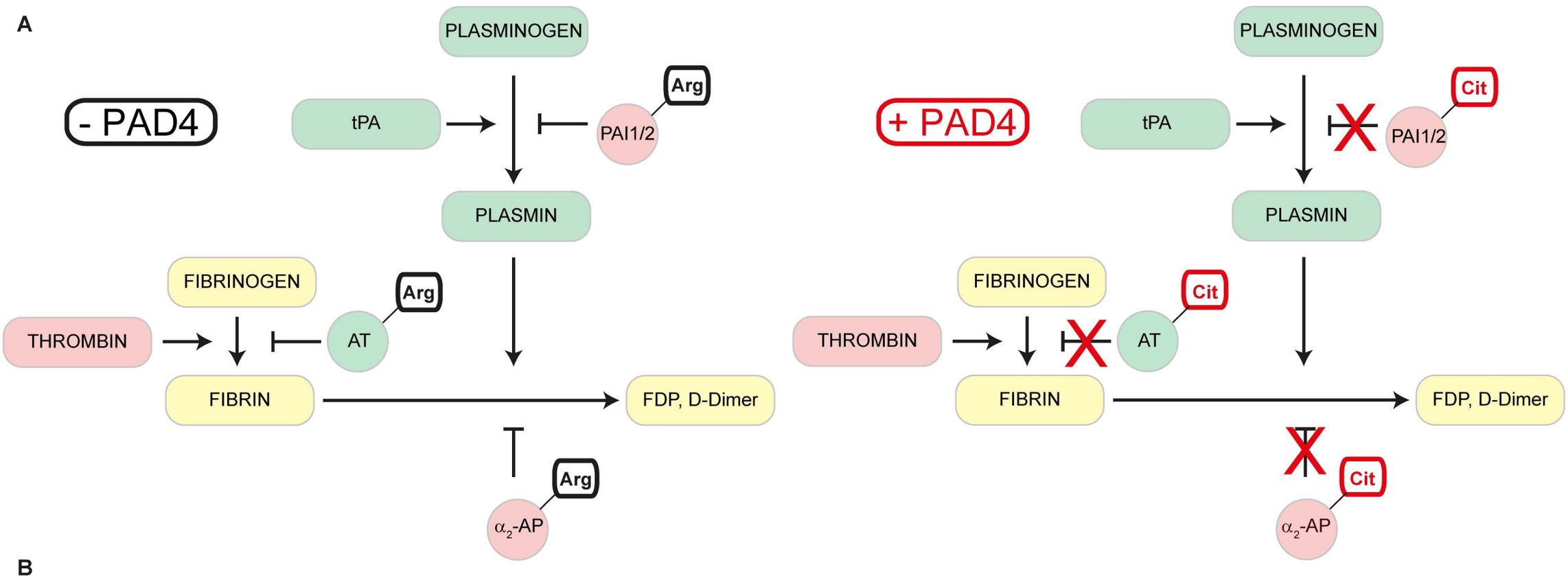
A
PLASMINOGEN
- PAD4
tPA
PAI1/2
Arg
PLASMIN
FIBRINOGEN
THROMBIN
AT
Arg
FIBRIN
FDP, D-Dimer
α2-AP
Arg
+ PAD4
PLASMINOGEN
tPA
PAI1/2
Cit
PLASMIN
FIBRINOGEN
THROMBIN
AT
Cit
FIBRIN
FDP, D-Dimer
α2-AP
Cit

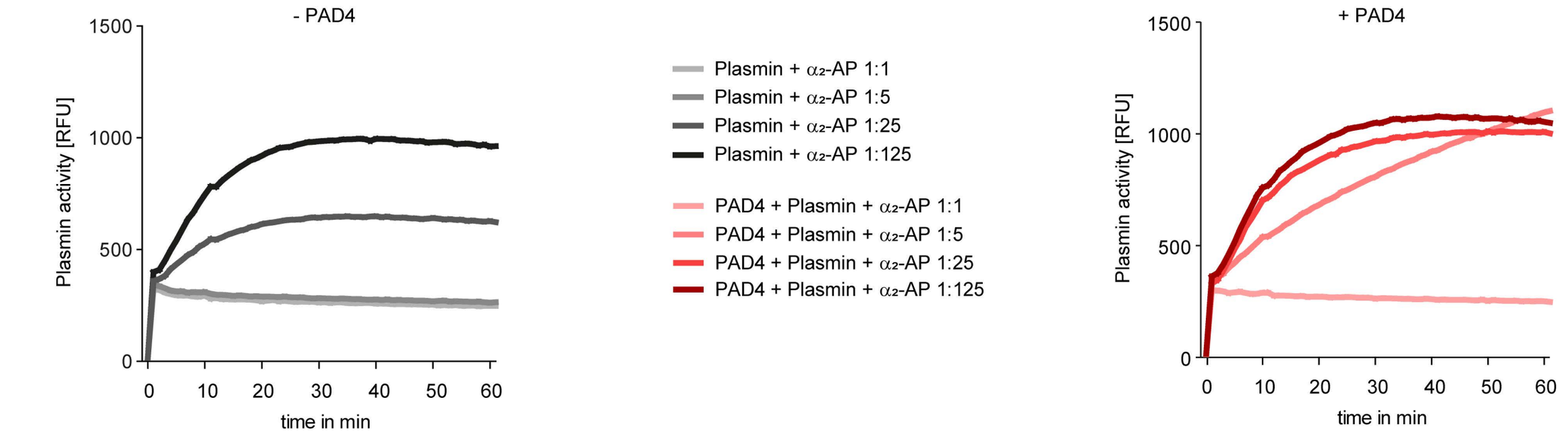
B
- PAD4
Plasmin activity [RFU]
time in min
Plasmin + α2-AP 1:1
Plasmin + α2-AP 1:5
Plasmin + α2-AP 1:25
Plasmin + α2-AP 1:125
PAD4 + Plasmin + α2-AP 1:1
PAD4 + Plasmin + α2-AP 1:5
PAD4 + Plasmin + α2-AP 1:25
PAD4 + Plasmin + α2-AP 1:125
+ PAD4
Plasmin activity [RFU]
time in min

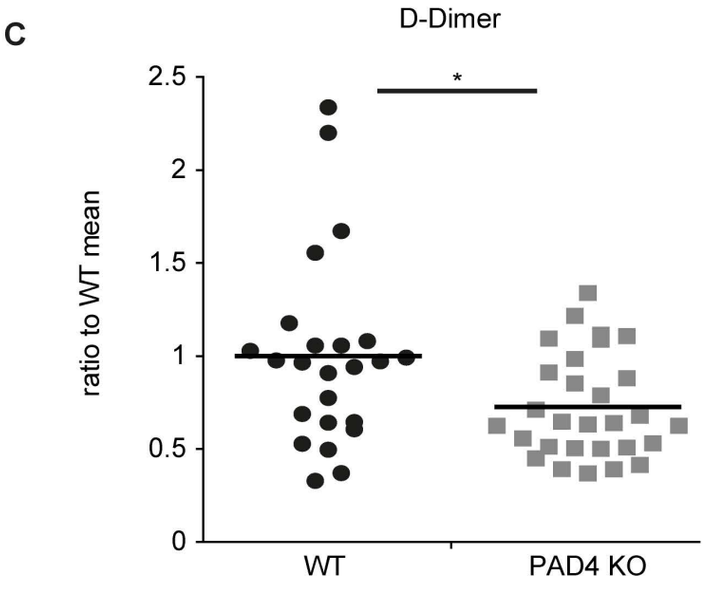
C
D-Dimer
ratio to WT mean
*
WT
PAD4 KO

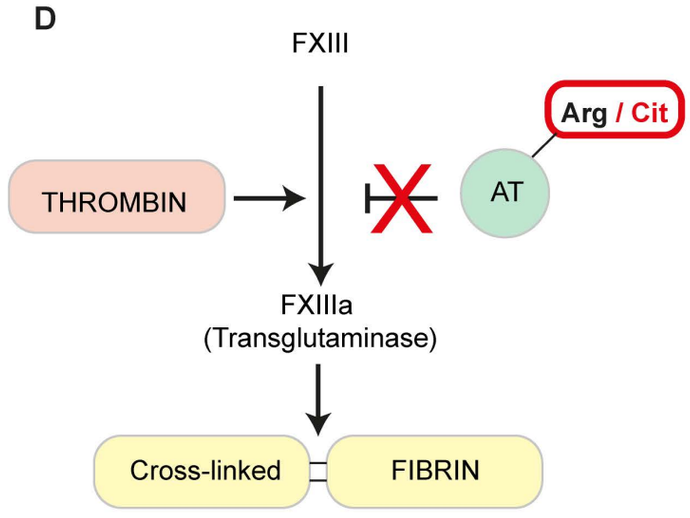
D
FXIII
THROMBIN
AT
Arg / Cit
FXIIIa
(Transglutaminase)
Cross-linked
FIBRIN

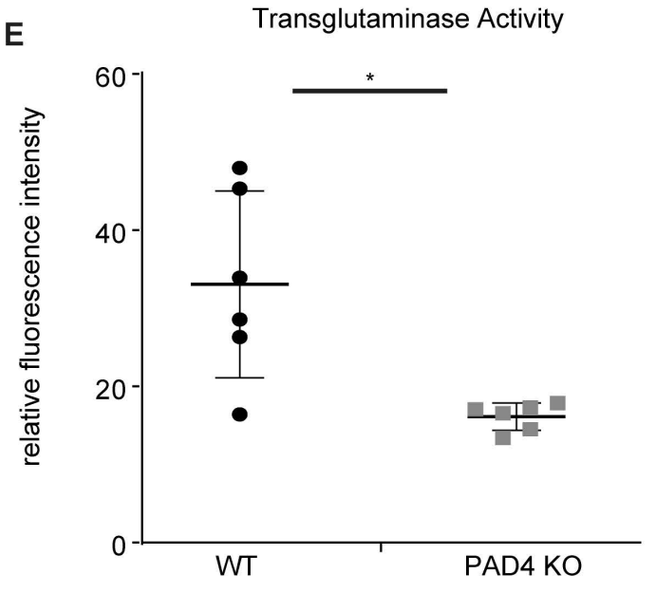
E
Transglutaminase Activity
relative fluorescence intensity
*
WT
PAD4 KO

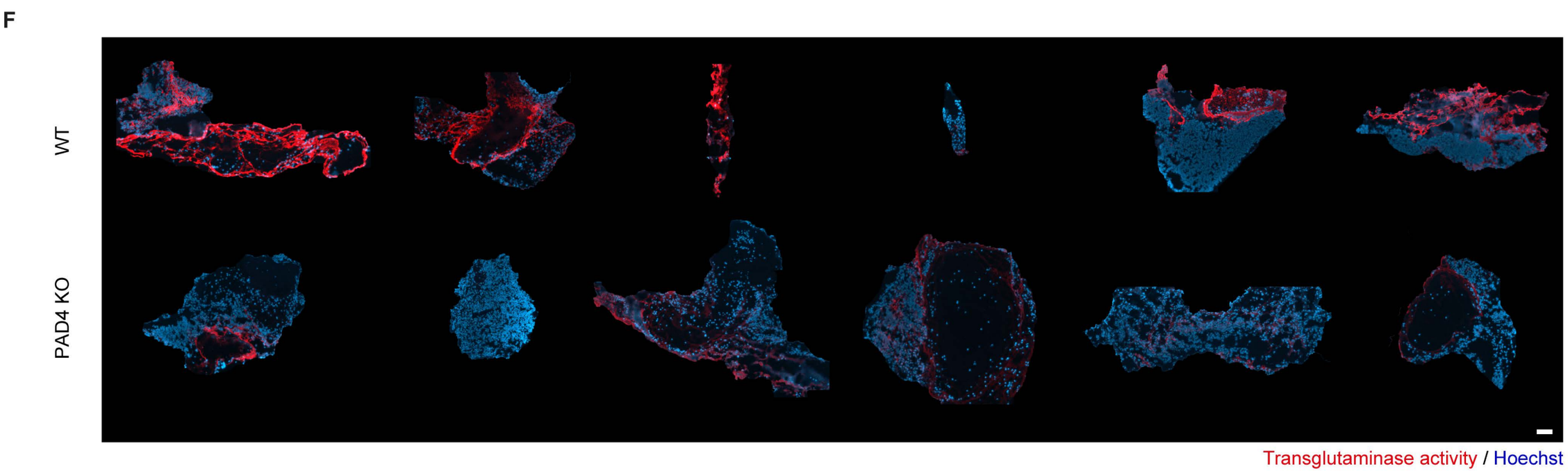
F
WT
PAD4 KO
Transglutaminase activity / Hoechst

Supplementary Figure 8: PAD4 affects the balance between coagulation and fibrinolysis via serpin inactivation and facilitates thrombus remodelling by transglutaminases

(A) A simplified model of the coagulation and fibrinolysis cascade is presented. Serine proteases interact with their respective serine protease inhibitors (serpins), numerous of which carry an arginine in their P1 reactive site (highlighted with Arg). PAD4 can suppress serpin functionality and thus impact the coagulation-fibrinolysis balance on multiple levels (tPA = tissue plasminogen activator; PAI1/2 = plasminogen activator inhibitor-1/2; AT = antithrombin; α_2-AP = α_2-antiplasmin) (modified arginine highlighted with Cit). **(B)** Active plasmin was incubated together with the fluorescent substrate N-Succinyl-Ala-Phe-Lys-AMC and α_2-antiplasmin in various dilutions at 37 °C *in vitro* in the presence or absence of PAD4. Citrullination of α_2-antiplasmin by PAD4 diminished its inhibitory activity on plasmin activity in a dose-dependent manner. One representative experiment of 5 independent experiments is shown. **(C)** D-dimer concentrations were assessed by ELISA in protein extracts of colon wounds from wild-type and PAD4$^{-/-}$ mice harvested 4–48 hours after wounding. A ratio to the wild-type mean of each time point was calculated to correct for differences in concentration over time. (N: 25–29 samples were studied, * $p < 0.05$, Student's t-test) **(D)** A simplified model of fibrin cross-linking by the thrombin-activated transglutaminase FXIIIa is presented. **(E)** Transglutaminase activity was assessed in colon wounds of wild-type and PAD4 knockout mice *in vivo* by i. p. injection of the biotin-labelled substrate biotin-amido-pentylamine (100 mg/kg) before wound induction and subsequent streptavidin-aided fluorescent detection. Relative fluorescence units were measured on tissue sections as in (F), showing significantly increased transglutaminase activity in the wounds of wild-type mice as compared to PAD4$^{-/-}$ mice (N: 6 wounds per group). **(F)** Histochemical detection of transglutaminase activity in sections of wild-type and PAD4$^{-/-}$ colon wounds reveals marked transglutaminase activity restricted to the wound bed. Wild-type wounds display a stronger increase in transglutaminase activity as compared to PAD4$^{-/-}$ samples.

Clinical Features of study cohort Active Ulcerative Colitis		
N		36
Age [mean (range)]		45.9 (19-78)
Male / Female [%]		41.4
Localization [%]	Proctitis	13.2
	Proctosigmoiditis	34.2
	Left- sided colitis	18.4
	Pancolitis	34.2
Partial Mayo Score (rectal bleeding)	0	36.1
	1	38.9
	2-3	25
Past or current therapies reported [%]	Aminosalicylates	66.7
	Steroids	86.1
	Thioguanines	33.3
	cyclosporine	11.1
	Vedolizumab	88.9
	Anti- TNF antibodies	44.4

		Improvement in rectal bleeding score	
		day 3 to 6	day 7 to 12
IBD treatment	**% of cohort**	**% of cohort**	**% of cohort**
Steroids	100 (13/13)	54 (7/13)	92 (12/13)
Ciclosporin	38 (5/13)	4 (2/5)	100 (5/5)
Infliximab	15 (2/13)	5 (1/2)	100 (2/2)
Concomitant therapy			
Ganciclovir	15 (2/13)	5 (1/2)	100 (2/2)
Heparin (prophylactic)	77 (10/13)	56 (5/9)	90 (9/10)
No Heparin	23 (3/13)	66 (2/3)	100 (3/3)

Supplementary Table 1:

The patient characteristics of the study cohort (N: 36) are depicted including age and sex distribution, localisation and extent of disease, partial Mayo score regarding rectal bleeding, as well as previous and current therapeutics used.

Supplementary Table 2:

Whenever available from clinical documentation, the relation of the improvement in rectal bleeding over time to IBD-related (steroids, ciclosporin, infliximab) and concomitant therapies (ganciclovir, heparin, no heparin) is reported.

Leppkes M, *et al. Gut* 2022;0:1–16. doi: 10.1136/gutjnl-2021-324725